GEOMETRICAL UNDERSTANDING OF THE CONSTANT MODULUS ALGORITHM: ADAPTIVE BLIND EQUALIZATION AND CROSS-POLARIZED SOURCE SEPARATION

A Thesis

Presented to the Faculty of the Graduate School

of Cornell University

in Partial Fulfillment of the Requirements for the Degree of

Master of Science

by

Wonzoo Chung

May 1999

Abstract

This thesis analyzes the multimodal structure of an adaptive algorithm called the Constant Modulus Algorithm (CMA) in the digital communication applications blind equalization and blind (cross polarized) source separation. In order to deal with the fourth order high dimensional cost function of the CMA, a geometrical approach is applied. This thesis consists of the following three main results.

First, the geometrical structure of the regions of convergence of CMA minima in the absence of noise is analyzed. The relation between the equalizer norm and the volume of the regions of convergence is studied. Second, the CMA minima locations in the presence of noise are investigated. The mechanism of the disappearance of CMA minima due to the trade-off between noise gain and inter symbol interference reduction is presented with low dimensional simulations. Finally, a specific source separation problem in digital communication systems, cross pole interference cancellation, is formulated in a fractionally spaced framework, including derivation of the zero forcing and minimum mean squared error solutions. The application of CMA to the cross pole interference cancellation is analyzed, with special attention paid to initalization strategies.

Biographical Sketch

Wonzoo Chung was born in Seoul, Korea. He finished his B.S. in mathematics at Korea University, Seoul Korea, and obtained Diplom Mathematiker at Universität Regensburg, Germany in 1989 and 1992 respectively. He is currently pursuing MS/PhD degree in Electrical Engineering at Cornell University.

Acknowledgements

Born as a human being, I have enjoyed a life of pursuing the beauty of the world, free from the struggles for the existence. This is my first metamorphosis to the useful as useful from the useful as useless. Although I have faced some bitter times, I have learned that the virtue of being useless is ultimate. Therefore, I appreciate my parents who have shown me the invisible correct way and supported me with their heart. I also deeply appreciate two persons who made this transition possible for me. Professor James P. Leblanc and my adviser Professor Richard Johnson Jr., who took me under his wing and has patiently watched the development of this work. I thank my commitee member Professor Lang Tong. Finally, I thank my research companions, Raul, Phil, Rick, and Jai, for their existence and what I have learned from them.

Table of Contents

List of Figures

Chapter 1

Introduction

1.1 Background and Problems

In this thesis we focus on a blind adaptive digital signal processing scheme dealing with the deleterious effects of multipath propagation on transmitted signals in digital communication systems, which is one of the major obstacles in modern digital communication systems. Multipath propagation of the transmitted signal causes ambiguity of the received signal, and with noise, significantly degrades bit error rate (BER) performance of the communication system. The distortion of the received signal due to multipath is referred to as *Inter Symbol Interference* (ISI), and a channel inducing ISI is called a multipath channel.

In most cases, a multipath channel is modeled as a linear, discrete-time, time invariant, finite impulse response (FIR) filter [1] and thus ISI can be formulated as the residual terms of the convolution between the source symbol sequence and a FIR channel. The removal of ISI from the received signal, or *equalization,* turns out to be a classical problem in digital signal processing, namely deconvolution. A FIR filter applied to the sampled signal to deal with ISI is called an *equalizer*, and determining the "best" equalizer given a particular communication environment is the goal of equalization. Although the concept of the "best" equalizer is a little fuzzy, considering the veriety of communication systems, an equalizer providing minimum mean squared error (MMSE) performance is generally considered as a desirable solution [22].

In many applications, in order to reduce the computational complexity of the receiver and in order to cope with possible time variation of the channel, the MMSE equalizer is implemented by the celebrated least mean square (LMS) adaptive algorithm [22]. However, in spite of its robustness and simplicity, the LMS algorithm has one critical drawback. It inherently requires training signals. Training signals unacceptably degrade efficiency in many applications (for example, mobile telephony systems), and they are not even feasible in a stringently band limited high rate communication system such as a digital TV channel [34].

The constant modulus algorithm (CMA) is perhaps the most popular adaptive equalization algorithm which does not require any training signal (so called *blind* equalization). Instead, it utilizes the higher order statistics of the source in its learning algorithm. Therefore, the CMA shows quite different features in comparison with LMS, although CMA achieves almost the same convergent performance as LMS in general [37]. One easy way to analyze the CMA is to look at its cost function in the *system space* of a fractionally spaced receiver, which is the set of all realizable system responses of the receiver by all possible equalizers.

The CMA cost function is a fourth order polynomial of a multi-dimensional variable with multimodal structure, unlike the simple quadratic LMS cost function. Depending on the initialization of the equalizer, the CMA may converge to different local minima corresponding to different system delays (and polarities, or phases). This multimodal structure makes use of CMA more difficult in that the system delay is determined by the initialization of the equalizer, and, at the same time, slows down the convergence rate.

There are some interesting but not yet clearly resolved problems related to the multimodality of CMA due to the complexity of CMA cost function. First of all, the delineation of the regions of convergence of the CMA local minima has not been resolved. Their locations, shape, and volume can potentially give us important information for designing CMA initialization as well as for completing the understanding of CMA. Furthermore, the behavior of CMA local minima with arbitrary channel noise power is not fully investigated - whether CMA local minima exist in an environment with severe noise, how and where they relocate, and whether the number of local minima is always constant for arbitrary noise power.

In this thesis we provide an intuitive and geometrical framework which allows us to address such problems and we present partial solutions which help to explain some important behavior of CMA in its fractionally spaced receiver applications.

1.2 Outline of thesis

The CMA cost function in the system space of a fractionally spaced receiver has a simple, symmetric, and even beautiful geometric representation. The basic strategy we employ in this thesis is to exploit the symmetric structure as much as possible and translate the results into an equalizer space, i.e., the real world (of course, the CMA cost function in the equalizer space is not elegant anymore, but robust and practical).

In chapter 2, we introduce basic terminology and review channel equalization in terms of the system space. The Zero Forcing (ZF) solutions and the MMSE-solutions are defined for a baud spaced receiver and a fractionally spaced receiver respectively. The structure of the channel convolution matrix is investigated, and the LMS algorithm and CMA are introduced with attention to their relationship to each other.

In chapter 3, the geometrical representation of the CMA cost function in the system space is derived. The CMA cost function is decoupled into a radial component and a spherical component, where the radial component plays a role of "norm constraint" and the radial component removes ISI. To focus on the radial component, we introduce the radial minima surface. By investigating the radial minima surface, we derive the existence of CM local minima at any channel noise power and the constraint on the output power of CM equalizers. On the other hand, the symmetric structure of the spherical term enables us to derive a closed form expression for the regions of convergence of the CMA cost function in the system space in the absence of noise.

In chapter 4, we characterize the regions of convergence of the CMA in the equalizer space in the absence of noise. We study the metamorphism of regions of convergence in the system space due to the channel convolution matrix, since the equalizer space and the system space are connected by that matrix. The metamorphism is characterized by rotation and dilation corresponding to the singular value decomposition of the channel convolution matrix. By looking at the dilation closely, we show that the regions of convergence of small noise gain exponentially expand near the origin.

In chapter 5, we attempt to explain the robustness of CMA in two ways, which suggest that CMA tends to optimize MSE performance in a severe noise environment. First, we characterize the spherical location of the CM solution, by analyzing the radial minima surface in chapter 3 more closely, and derive an equivalent model for the asymptotic location of local minima for large noise power. As a result, we show that many of the local minima with large noise gain in the absence of noise can disappear in the presence of noise. Second, we review the single (double) spike initialization technique with respect to the result of chapter 4. The result in chapter 4 tells us that it is unlikely for the CM receiver to achieve the bad local minima with the single (double) spike initialization, even if they exist. This echoes the noise-free baud-spaced result in [15].

In chapter 6, we consider a cross-pole interference (CPI) equalizer [35], which is a generalized version of a single user receiver equalizer. We derive the ZF solution and the MMSE solution for the CPI equalizer and apply CMA. The CMA CPI equalizer inherits the properties of the conventional CMA. The choice of the system delay, however, determines which signal is acquired by the CPI CMA. For a a simple case, we investigate the regions of convergence and show how to initialize the CPI CMA to obtain the desired signal.

Chapter 2

Equalization

2.1 Equalization in a System Space Viewpoint

We consider a communication system described in Figure 2.1 as a black box to which the input is the source sequence and the output is the receiver output. It turns out that the "function" of a communication system with a linear equalizer can be modeled as a linear function (the inner product of the source sequence and a vector, referred to as the *system response*, which is determined by an equalizer vector and the channel vector). The system response can be expressed as a linear transformation of the equalizer vector. We define the *system space* as the linear space of all system responses constructed by all equalizers of a given communication system.

In the system space the objective of equalization is expressed in a simple form independent of any particular channel. In this section we will introduce the terminologies related to equalization.

Let us consider a multirate digital communication system with an equalizer described in Figure 2.1. To transmit source symbols $\{s_i\}$ effectively, each symbol

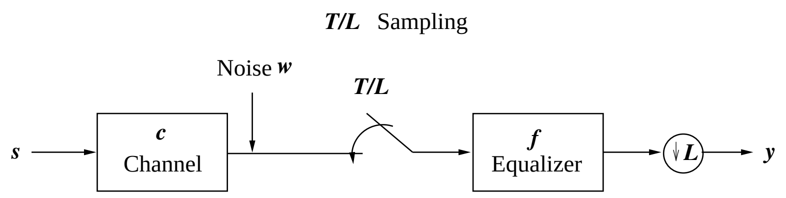

Figure 2.1: A communication system with linear equalizer receiver

is carried by an analog pulse ψ which has a finite time support and transmitted once in every baud interval T. Then the analog source signal is represented as

$$s(t) = \sum_{i=-\infty}^{\infty} s_i \psi(t - iT) \tag{2.1}$$

Assuming an absence of channel noise and that the analog channel $\mathfrak{c}$ is linear and time invariant with finite time support, the received signal r is written as

$$\begin{aligned} r(t) &= \int_{-\infty}^{\infty} s(\tau)\mathfrak{c}(t-\tau)d\tau & (2.2) \\ &= \sum_{i=-\infty}^{\infty} s_i \mathfrak{c}(t - iT) & (2.3) \end{aligned}$$

Depending on the sampling rate T/L, the output sequence of the equalizer $\{y(n)\}$ is expressed as a linear function of the source sequence, the equalizer, and the sampled channel response denoted by $\mathbf{c}$, as we will demonstrate after we define some basic terms.

Definition 1 (Equalizer Space) *Let N_f be the fixed equalizer length. We define an* equalizer space, *denoted by F, as the linear space of all equalizers with length N_f. For a complex (real) equalizer, F is isomorphic to $\mathbb{C}^{N_f}$ ($\mathbb{R}^{N_f}$).*

Definition 2 (System Space) *For an equalizer $\mathbf{f}$, we refer to the channel-equalizer system response in the absence of noise as* system response $\mathbf{h}$ *and define* system space *as the set of all possible system response of equalizers in the equalizer space* F.

Definition 3 (ZF Solution) *A zero-forcing(ZF) solution for a particular channel response* $\mathbf{c}$ *is an equalizer* $\mathbf{f}$ *whose system response is a pure delay, i.e.,* $\mathbf{h} = [0 \cdots 0\ 1\ 0 \cdots 0]$

Definition 4 (MMSE Solution) *A minimum mean squared error (MMSE) solution of delay* i *is a equalizer whose mean squared error between the output and* s_i*, the source delayed by* iT*, is minimized over* F*, i.e.,*

$$\mathbf{f}_{MMSE} = \arg\min_{\mathbf{f} \in F} E(\|y - s_i\|^2) \tag{2.4}$$

In the following sections we show the relation between system space and equalizer space, and review the ZF-solutions and the MMSE-solutions for a baud spaced system ($L = 1$) and fractionally spaced systems ($L \geq 2$) respectively.

2.1.1 Equalization in a Baud Spaced System

Let the sampling interval be the same as the baud interval T (i.e. $L = 1$), which is referred to as a *baud spaced* system. In this case the sampled signal $r(nT)$ of continuous received signal $r(t)$ in (2.3) can be written as a convolution of the discrete FIR channel $\mathbf{c}_T = [\mathfrak{c}(0)\ \mathfrak{c}(T)\ \cdots\ \mathfrak{c}((N_{\mathbf{c}_T} - 1)T)]$ and source symbol sequence $\mathbf{s}_n = \{s_n,\ s_{n-1},\ \cdots\}$.

$$\mathbf{r}_n = \mathbf{s}_n \star \mathbf{c}_T, \tag{2.5}$$

where $\star$ denotes the convolution operator. Furthermore, from the formula of the equalizer output, the system response $\mathbf{h}$ of an equalizer $\mathbf{f}$ is given by convolution with the channel $\mathbf{c}$; $\mathbf{h} = \mathbf{c} \star \mathbf{f}$.

$$\mathbf{y} = \mathbf{r}_n \star \mathbf{f} = (\mathbf{c}_T \star \mathbf{f}) \star \mathbf{s}_n = \mathbf{h} \star \mathbf{s}_n \tag{2.6}$$

Geometrically, the system space H can be visualized as an image of the equalizer space of F under the linear transformation given by the channel convolution matrix C of the channel $\mathbf{c}$.

$$H = CF \subset \mathbb{C}^{N_{\mathbf{c}_T} + N_{\mathbf{f}} - 1} \tag{2.7}$$

where

$$C = \begin{bmatrix} c_0 & & & \\ c_1 & c_0 & & \\ \vdots & c_1 & \ddots & c_0 \\ c_N & \vdots & & c_1 \\ & c_N & \ddots & \vdots \\ & & & c_N \end{bmatrix} \tag{2.8}$$

Observe that C is not an invertible matrix unless $\mathbf{c}_T$ is simply a constant, and thus H is a proper subset of $\mathbb{C}^{N_c+N_f-1}$ which does not contain the desirable system responses, namely, pure delays. This can be also checked in algebraic presentation via the z-transform of (2.6)

$$\mathbf{f}(z)\mathbf{c}(z) = 1 \tag{2.9}$$

There is no polynomial $\mathbf{f}(z)$ that satisfies the above equation for non-trivial polynomial $\mathbf{c}(z)$. Therefore, in general ZF-solutions do not exist in a baud spaced system.

The MMSE solutions in the absence of noise are the solutions of a linear optimization problem with respect to the ℓ_2 norm, which is given by the pseudo inversion of C. The MMSE solution corresponding to the i-th delay is given by

$$\mathbf{f}_{MMSE} = (C^H C)^{-1} C^H \delta_i \tag{2.10}$$

where $\cdot^H$ is the hermitian operator and $\delta_i = [0 \ \cdots \ 0 \ 1(i+1th) \ 0 \cdots \ 0]^T$.

In the presence of white Gaussian noise with noise power σ^2, the MMSE solution corresponding to the i-th delay is given by a similar form which includes the noise power term [22]

$$\mathbf{f}_{MMSE} = (C^H C + \frac{\sigma^2}{\sigma_s^2} I)^{-1} C^H \delta_i \tag{2.11}$$

where σ_s^2 is the source power.

2.1.2 Equalization in a Fractionally Spaced System

Unlike in a baud spaced system, in a *fractionally spaced* (FS) system, in which the sampling rate is set to a fraction T/L of the baud interval T (e.g. $L \geq 2$), a FIR equalizer can achieve perfect equalization in the absence of noise. The FS system was originally designed to improve sampling synchronization with the helps of the additional channel information provided by fractional sampling [36]. It turned out the fractional sampling also helps perfect equalization [31]. Without much loss of generality, we consider only $L = 2$. The $T/2$ sampled signal of $r(t)$ is written as

$$r(k\frac{T}{2}) \quad = \quad \sum_{i=0}^{N_c - 1} s_i \mathbf{c}_{T/2}(k\frac{T}{2} - iT) \tag{2.12}$$

where $\mathbf{c}_{T/2} = [\mathfrak{c}(0) \ \mathfrak{c}(T/2) \ \ \mathfrak{c}(T) \ \mathfrak{c}(T + T/2) \cdots \ \mathfrak{c}((N_{\mathbf{c}_{T/2}} - 1)T)]$ is $T/2$-sampled channel response.

Let us designate every on-baud sample (nT) as "even" and every fractional (or off-baud) sample ($nT + \frac{T}{2}$) as "odd". Observe that for even samples $k = 2n$

$$\begin{aligned} r(nT) &= \sum_{i=0}^{N_{c_{T/2}}-1} s_i \mathbf{c}((n-i)T) && (2.13) \\ &= \mathbf{s} \star \mathbf{c}_{even} && (2.14) \end{aligned}$$

and for odd samples $k = 2n + 1$

$$\begin{aligned} r(nT + \frac{T}{2}) &= \sum_{i=0}^{N_{c_{T/2}}-1} s_i \mathbf{c}((n-i)T + \frac{T}{2}) && (2.15) \\ &= \mathbf{s} \star \mathbf{c}_{odd} && (2.16) \end{aligned}$$

Meanwhile, the $T/2$-spaced output of the equalizer before decimation is

$$y(k\frac{T}{2}) = \sum_{i=0}^{N_f-1} \mathbf{f}(i\frac{T}{2}) r((k-i)\frac{T}{2}) \tag{2.17}$$

Decimation of the output y, say odd samples of y are thrown away (this choice of decimation does not affect the following result, since it is merely a matter of indexing), yields

$$\begin{aligned} y(n\frac{T}{2}) &= \sum_{i=0}^{\frac{N_f-1}{2}} \mathbf{f}(iT) r((n-i)T) + \mathbf{f}(iT + \frac{T}{2}) r((n-i)T - \frac{T}{2}) && (2.18) \\ &= \mathbf{f}_{even} \star \mathbf{r}_{even} + \mathbf{f}_{odd} \star \mathbf{r}_{odd} && (2.19) \end{aligned}$$

by combining equations (2.13), (2.17), and (2.18), we obtain a filter bank structure in the baud space with a system response $\mathbf{h} = \mathbf{c}_{even} \star \mathbf{f}_{even} + \mathbf{c}_{odd} \star \mathbf{f}_{odd}$.

Now a ZF-solution is the equalizer $\mathbf{f}$ such that

$$\mathbf{c}_{even} \star \mathbf{f}_{even} + \mathbf{c}_{odd} \star \mathbf{f}_{odd} = \delta_i, \tag{2.20}$$

or in z-transformed form

$$\mathbf{c}_{even}(z)\mathbf{f}_{even}(z) + \mathbf{c}_{odd}(z)\mathbf{f}_{odd}(z) = 1 \tag{2.21}$$

The above equation is known as the Bezout equation, a polynomial ring version of the Diophantine equation, and has a unique solution $\mathbf{f}(z)$ when $\mathbf{c}_{even}$ and $\mathbf{c}_{odd}$ are co-prime, i.e. when they do not share any common roots [see [17]].

Geometrically, the system space H is an image of F linearly transformed by a *baud spaced channel matrix* $[C_{even}\ C_{odd}]$

$$\mathbf{h} = [C_{even} C_{odd}] \begin{bmatrix} \mathbf{f}_{even} \\ \mathbf{f}_{odd} \end{bmatrix} \tag{2.22}$$

where C_{even} and C_{odd} are the convolution matrixes of $\mathbf{c}_{even}$ and $\mathbf{c}_{odd}$ respectively. Since the mapping $j : \begin{bmatrix} \mathbf{f}_{even} \\ \mathbf{f}_{odd} \end{bmatrix} \mapsto \mathbf{f}$ can be viewed as a basis permutation, j is an invertible linear map. Let J be the matrix representation of j, then we have

$$\mathbf{h} = [C_{even} C_{odd}]\, J^{-1} J \begin{bmatrix} \mathbf{f}_{even} \\ \mathbf{f}_{odd} \end{bmatrix} = [C_{even} C_{odd}]\, J^{-1}\mathbf{f} \tag{2.23}$$

by defining $C := [C_{even} C_{odd}]\, J^{-1}$ we obtain a desired relation between the equalizer and the system response.

$$\mathbf{h} = C\mathbf{f} \tag{2.24}$$

C turns out to be the row decimated convolution matrix of $\mathbf{c}_{T/2}$, and full rank when $\mathbf{c}_{even}$ and $\mathbf{c}_{odd}$ are co-prime [16], i.e.

$$C = \begin{bmatrix} c_1 & c_0 & & & & & \\ \vdots & \vdots & c_1 & c_0 & & & \\ c_{N_c-1} & c_{N_c-2} & \vdots & \vdots & \ddots & c_1 & c_0 \\ & & c_{N_c-1} & c_{N_c-2} & \ddots & \vdots & \vdots \\ & & & & & c_{N_c-1} & c_{N_c-2} \end{bmatrix} \tag{2.25}$$

With a length constraint $N_f = N_{c_{T/2}} - 2$, C can be an invertible mapping from F to H. In other words, a finite length ZF solution corresponding to the i-th delay

$$\mathbf{f}_{ZF} = C^{-1}\delta_i \tag{2.26}$$

can exist. The MMSE solution corresponding to the i-th delay for a FS system can be derived analogously to that for the baud space system [14]

$$\mathbf{f}_{MMSE} = (C^H C + \frac{\sigma^2}{\sigma_s^2} I)^{-1} C^H \delta_i \tag{2.27}$$

where σ^2 and σ_s^2 represent the power of noise and source respectively. Notice that in the absence of noise and with appropriate equalizer length, the MMSE-solutions match the ZF-solutions, i.e.,$\mathbf{f}_{MMSE} = \mathbf{f}_{ZF}$.

2.1.3 The Structure of Channel Matrix

In the previous sections we have learned that the channel matrix is directly related to the equalizer solutions. The channel matrix is generated from the channel coefficients and has a special structure. Here, we describe the structure of the channel matrix for later use in this thesis.

Baud Spaced Case

In a baud spaced case, the channel convolution matrix C displays the following features as partly mentioned in [8].

- C is a Töplitz matrix.

- For $C = U\Lambda V^H$, it can be viewed such that V and Λ contain frequency domain information, while U contains time domain information:

  Asymptotically as N (the length of a row vector of V) $\to \infty$,

- The vector $\mathbf{v}_i$ ($:=$ i-th row vector of V), which is an eigenvector of the autocorrelation matrix $C^H C$, corresponds to the sinusoid with $\omega_i = \frac{\pi i}{NT}$
- The singular value λ_i corresponds to the magnitude response of the channel to the sinusoidal input with ω_i. ($\|C\mathbf{v}_i\| = \sqrt{\mathbf{v}_i C^H C \mathbf{v}_i} = \lambda_i$).
- Let $\mathbf{u}_i$ be the i-th row vector of U, then from

$$\mathbf{u}_i = \frac{1}{\lambda_i} C\mathbf{v}_i, \tag{2.28}$$

$\mathbf{u}_i$ is the normalized channel output with respect to the input $\mathbf{v}_i$.

Fractionally Spaced Case

In a fractionally spaced case, the channel matrix C is no longer a Töplitz matrix. Instead, it can be viewed as a block matrix of Töplitz matrices by using the form $C = [C_{even}\ C_{odd}]$ in (2.22). The eigenstructure of the autocorrelation matrix $C^H C$ is investigated by Giltin and Weinstein [8].

$$C^H C = \begin{bmatrix} C_{even}^H \\ C_{odd}^H \end{bmatrix} \begin{bmatrix} C_{even} & C_{odd} \end{bmatrix} = \begin{bmatrix} C_{even}^H C_{even} & C_{even}^H C_{odd} \\ C_{odd}^H C_{even} & C_{odd}^H C_{odd} \end{bmatrix} \tag{2.29}$$

Let $\mathbf{v}$ be an eigenvector of $C^H C$ with the eigenvalue λ, i.e. $C^H C\mathbf{v} = \lambda\mathbf{v}$. Applying the Fourier transformation for each matrix in $C^H C\mathbf{v} = \lambda\mathbf{v}$ yields an approximation for all $\omega_i = \frac{2\pi i}{NT}$ for $i = 0, .., N-1$. As $N \to \infty$, we have

$$\begin{bmatrix} |\mathbf{c}_{even}(\omega)|^2 \mathbf{v}_{even}(\omega_i) + \mathbf{c}_{even}(\omega)\mathbf{c}_{odd}^*(\omega)\mathbf{v}_{odd}(\omega) \\ \mathbf{c}_{odd}(\omega)\mathbf{c}_{even}^*(\omega)\mathbf{v}_{even}(\omega) + |\mathbf{c}_{odd}(\omega)|^2 \mathbf{v}_{odd}(\omega) \end{bmatrix} = \lambda \begin{bmatrix} \mathbf{v}_{even}(\omega) \\ \mathbf{v}_{odd}(\omega) \end{bmatrix} \tag{2.30}$$

In order for (2.30) to hold for all $i = 0, .., N-1$, $\mathbf{v}_{even}(\omega)$ and $\mathbf{v}_{odd}(\omega)$ must be delta functions at ω_i. Therefore, we can write down (2.30) for each ω_i as the following

$$\begin{bmatrix} |\mathbf{c}_{even}(\omega_i)|^2 & \mathbf{c}_{even}(\omega_i)\mathbf{c}_{odd}^*(\omega_i) \\ \mathbf{c}_{odd}(\omega_i)\mathbf{c}_{even}^*(\omega_i) & |\mathbf{c}_{odd}(\omega_i)|^2 \end{bmatrix} \begin{bmatrix} \mathbf{v}_{even}(\omega_i) \\ \mathbf{v}_{odd}(\omega_i) \end{bmatrix} = \lambda_i \begin{bmatrix} \mathbf{v}_{even}(\omega_i) \\ \mathbf{v}_{odd}(\omega_i) \end{bmatrix} \tag{2.31}$$

The eigenvalues of the square matrix in the above equation are given by the solutions of the following algebraic equation

$$\det\left(\begin{bmatrix} |\mathbf{c}_{even}(\omega_i)|^2 & \mathbf{c}_{even}(\omega_i)\mathbf{c}^*_{odd}(\omega_i) \\ \mathbf{c}_{odd}(\omega_i)\mathbf{c}^*_{even}(\omega_i) & |\mathbf{c}_{odd}(\omega_i)|^2 \end{bmatrix} - \lambda_i I\right) = 0 \tag{2.32}$$

equivalently

$$\lambda_i^2 - \lambda_i(|\mathbf{c}_{even}(\omega_i)|^2 + |\mathbf{c}_{odd}(\omega_i)|^2) = 0 \tag{2.33}$$

and thus the eigenvalues are

$$\begin{aligned} \lambda_i^{(1)} &= 0 \\ \lambda_i^{(2)} &= |\mathbf{c}_{even}(\omega_i)|^2 + |\mathbf{c}_{odd}(\omega_i)|^2 \end{aligned} \tag{2.34}$$

This implies that half of the eigenvalues of $C^H C$ are zero (For the eigenvalue structure of a finite N, refer result in Z. Reznic et. al. [28]).

The eigenvector associated with the zero eigenvalue is given by [8]

$$\mathbf{v}_i(k) = \begin{cases} \mathbf{c}_{odd}(\omega_i)e^{j\omega_i k(T/2)} & k \text{ even} \\ -\mathbf{c}_{even}(\omega_i)e^{j\omega_i k(T/2)} & k \text{ odd} \end{cases} \tag{2.35}$$

while the eigenvector associated with the nonzero eigenvalue is

$$\mathbf{v}_i(k) = \begin{cases} \mathbf{c}_{even}(\omega_i)e^{j\omega_i k(T/2)} & k \text{ even} \\ \mathbf{c}_{odd}(\omega_i)e^{j\omega_i k(T/2)} & k \text{ odd} \end{cases} \tag{2.36}$$

In summary, the asymptotic features of C as $N \to \infty$ are:

- Let $C = U\Lambda V^H$. For the i-th row vector $\mathbf{v}_i$ of V, $\mathbf{v}_{ieven}$ and $\mathbf{v}_{iodd}$ correspond to the sinusoids given by (2.35) and (2.36).

- Half of the λ_i's are zero (near zero for finite N) and the nonzero λ_i's correspond to the aliased magnitude channel response at ω_i.

- The i-th row vector of U associated with a nonzero λ_i is the normalized summation of $\mathbf{c}_{even} \star \mathbf{v}_{ieven}$ and $\mathbf{c}_{odd} \star \mathbf{v}_{iodd}$.

2.2 Adaptive Equalization

In realistic situations, adaptive schemes converging to a MMSE equalizer are preferred over a direct calculation of a MMSE equalizer from channel information and estimated noise power in order to reduce the hardware complexity of a receiver or in order to cope with possible time variation of the channel. An adaptive receiver can determine an equalizer vector minimizing a certain cost function by using a stochastic descent update equation [13]. From a mathematical view point, the stochastic descent update can be viewed as an approximation of a trajectory path on the gradient system induced by the cost function.

2.2.1 Trained Adaptation : LMS Algorithm

The adaptive algorithm conventionally used is the least mean square (LMS) algorithm [27] which uses MSE as a cost function, i.e.

$$J(\mathbf{f}) = E\left\{(y - s_i)^2\right\} \tag{2.37}$$

with the update equation

$$\mathbf{f}_{new} = \mathbf{f}_{old} - \mu \frac{\partial}{\partial \mathbf{f}} J|_{\mathbf{f}=\mathbf{f}_{old}} = \mathbf{f}_{old} - \mu(y - s_i)\mathbf{r}^* \tag{2.38}$$

where μ is the step size, $\mathbf{r}^*$ is the complex conjugated regressor vector of equalizer $\mathbf{f}$, and s_i denotes i-delayed signal. Since this algorithm requires the pre-knowledge of the transmitted signal (s_i), it can be realized only in the presence of "training signals," a sequence of symbols known to both the receiver and the transmitter. At the cost of training signals, the LMS algorithm is proven to converge to a MMSE equalizer regardless of the initialization under certain broad conditions [13].

2.2.2 Blind Adaptation: Constant Modulus Algorithm

Unlike the LMS algorithm, the constant modulus algorithm is a blind algorithm that requires no training signal. CMA was originally proposed by Godard in [11] and developed independently by Treichler and Agee in [32].

Definition 5 (CM solution) *A* constant modulus (CM) solution *is an equalizer* $\mathbf{f} \in F$ *which is a local minimum of the following cost function*

$$J(\mathbf{f}) = \frac{1}{4} E\left\{(|y|^2 - \gamma)^2\right\} \tag{2.39}$$

where $\gamma := m_4/m_2$*, the ratio of the fourth moment* (m_4) *and the second moment* (m_2) *of the source, is called the dispersion constant.*

The stochastic update equation for CMA is:

$$\mathbf{f}_{new} = \mathbf{f}_{old} - \mu y(|y|^2 - \gamma)\mathbf{r}^* \tag{2.40}$$

where μ is a step size, $\mathbf{r}^*$ is the complex conjugated regressor vector of equalizer $\mathbf{f}$.

Notice that there is no training signal involved in the cost function (2.39). Instead, it utilizes the dispersion of the output from a constant, $|y|^2 - \gamma$. An intuitive justification for this cost function is that when a source sequence in digital communication is constant modulus, the equalizer recovers the modulus of the output sequence as constant, hoping that ISI would be removed.

In the absence of noise, for constant modulus sources, any ZF solution satisfies the CM criterion, and is a CM solution. As will be described in detail in Chapter

3, the CM solution is not unique and the CMA cost function has a multimodal structure. For example, for a real channel in the absence of noise there can be $2N$ CM solutions corresponding to various system delays and polarities in the absence of noise.

2.2.3 LMS vs CMA

Although CMA is a blind algorithm, it has a relatively simple update equation, and more importantly some of the CM solutions are proven to achieve performance near that of LMS. Zeng and co-authors in [37] have calibrated the boundary of a volume about a LMS solution which contains a CM solution for any LMS solution whose MSE is less than 1/3. For such cases, a CM solution can be approximately understood as a scaled version of a LMS solution. It is a remarkable result in that CMA can perform as well as the trained LMS if undesirable local minima can be avoided.

However, the multimodality of CMA due to the fourth order cost function imposes uncertainty on the choice of system delay. It implies that, for a single user case, the choice among CM solutions depends on the initialization of the equalizer. Furthermore, in multiuser applications such as the cross-pole interference equalizer or the CDMA multi user detector, the choice of system delays determines the acquisition of the desired signal [26]. Therefore, in order to reduce the uncertainty in which delay or user is obtained, detailed analysis of the multimodal structure, such as the regions of convergence, is desired. (In Chapter 4, some answers related to this question will be presented.)

Furthermore, the multimodality slows down the convergence rate of CMA dramatically [18]. The CMA cost function has an exponentially increasing number of stationary points, for example 3^N, in order to bear $2N$ local minima in the absence of noise for a real channel.

Unlike LMS, the CM solution does not have any closed form expression in the presence of noise. To gain a global understanding of the CM solution in the presence of noise, one needs to visualize the forth order high dimensional cost function in great detail. In this thesis we analyze the multimodal structure of the CMA cost function by simplifying the required computational complexity with an approximate geometrical approach at the cost of giving up an exact closed form expression.

2.2.4 Good and Bad CM Solutions

In this section we will introduce a fuzzy, but convenient, classification of the CM solutions. As a result of the singular value distribution of the channel matrix of a $T/2$ channel (Section 2.1.3), almost half of the MMSE solutions have large MSE in comparison with the other half of the MMSE solutions for a channel with sufficiently large length. The MSE of a MMSE solution given a specific delay is obtained by the following closed form expression

$$MSE_i = \sigma^2 \delta_i^T \left[I - C(C^T C + \frac{\sigma^2}{\sigma_s^2} I)^{-1} C^T \right] \delta_i, \tag{2.41}$$

and can be readily calculated as in Figure 2.2. For the LMS receiver, one can choose the optimal MMSE solution by simply searching across various delays of the training signal.

However, for the CM receiver, first of all, we do not have detailed knowledge of closed-form CM solutions for a given noise power yet. (Chapter 5 will answer some of the questions related to this problem.) Furthermore, in general we cannot

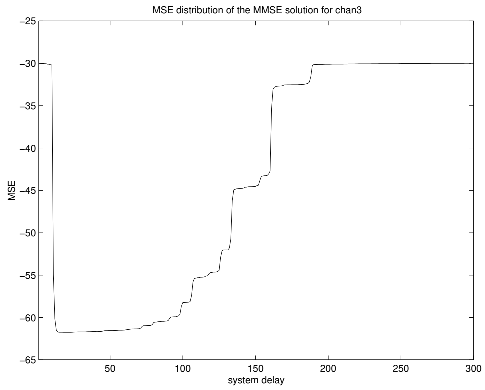

Figure 2.2: MSE distribution of MMSE solutions: -30dB

control the achieved system delay of the CM receiver without almost perfect channel information. Shortly, the uncertainty of the initialization for a desired system response is the cost we should pay for blind equalization.

Fortunately, since CMA is usually used during startup mode to achieve a MSE less than a certain threshold [27], in the application point of view it is enough to avoid some "bad" CM solutions. As Zeng et. al. in [37] have shown, we know some of the CM solutions locate near the MMSE solution with low MSE. Although simulation results suggest that the CM receiver always converges to such "good" solutions, we suspect that the noise gain (i.e. ℓ_2-norm of the equalizer) of the CM solutions may be divided into a class with relatively small values and a class with relatively large values, like LMS solutions, and refer to the CM solutions with large noise gain as bad CM solutions (which may or may not exist). At least for the noise-free case, the CM solutions can be divided into such two classes. In chapter 5, we will investigate the (non) existence of bad CM solutions.

Chapter 3

Geometrical Understanding of Fractionally Spaced Constant Modulus Algorithm

In this chapter we construct a geometrical representation of the cost function of the fractionally spaced constant modulus algorithm, and investigate the properties of the FS-CM algorithm in the system space by exploiting the structure of the geometrical representation. For a complicated multidimensional cost function such as the CM cost function it is important to construct a structural representation. We decompose the CM cost function in the system space into radial and spherical components, which are related to the parameter norm and inter symbol interference (ISI) respectively. Under this decomposition, classification of the stationary points of the CM cost function in system space and delineation of the regions of convergence can be achieved relatively easily.

3.1 CM Cost Function on the Fractionally Spaced System Space

3.1.1 Assumptions

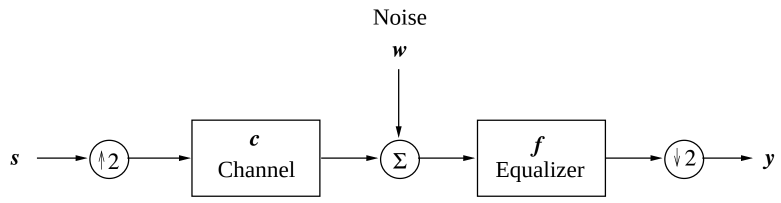

Figure 3.1: A $T/2$-spaced digital communication model

We consider a $T/2$-spaced system model as shown in Figure 3.1. There are critical assumptions on the source and the channel under which CMA has been proven to work, as formalized in the following assumption.

Assumption 1 (For general CMA)

A1. The source symbol sequence is independent and identically distributed (zero mean) sub-Gaussian.

A2. The $T/2$ spaced channel $\mathbf{c}$ has no common sub-channel roots.

By sub-Gaussian, we mean the kurtosis $(E(s^4)/E^2(s^2))$ of the source is less than that of a Gaussian source. It has been shown that violating one of above assumtions would cause failure of convergence of CMA as summarized in [16].

3.1.2 Inter Symbol Interference in the System Space

We want to formulate the Inter symbol interference (ISI) in the system space. In the system space viewpoint, ISI is caused by system responses that are not exactly pure delays. We introduce a measure of ISI due to a system response vector $\mathbf{h}$ in H:

Definition 6 *For any vector* $\mathbf{h} = [h_0 \cdots h_{N-1}]^T \in H$, the inherent ISI of $\mathbf{h}$, $I_{\mathbf{h}}$, *is a positive semi-definite real valued function on* H *defined by;*

$$I_{\mathbf{h}} := \sum_{i,j;i\neq j}^{N-1} |h_i|^2|h_j|^2 = \|\mathbf{h}\|^4 - \sum_{i=0}^{N-1} |h_i|^4, \tag{3.1}$$

where $\|\cdot\|$ *is the* ℓ_2 *norm.*

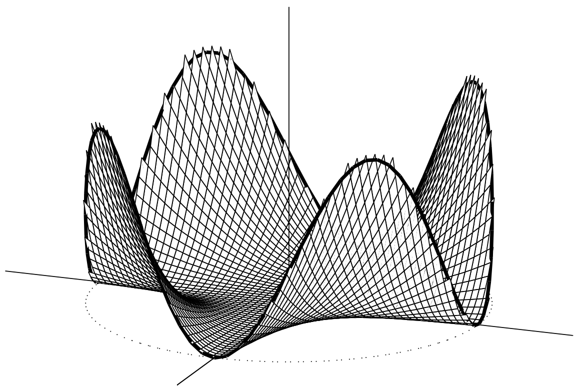

Figure 3.2: $I_{\mathbf{h}}$ in 2 dim. H-space

Remark 1 The conventionally used measure of ISI is *peak distortion* [10], defined as

$$\text{Peak distortion of } \mathbf{h} = \frac{\sum_i |h_i| - \max_i |h_i|}{\max_i |h_i|} \tag{3.2}$$

This function is also minimized at the same points where $I_{\mathbf{h}}$ are minimized.

Lemma 1 (Stationary points of $I_{\mathbf{h}}$) $I_{\mathbf{h}}$ *has the following properties;*

i) $0 \leq I_{\mathbf{h}} \leq \|\mathbf{h}\|^4 \frac{N-1}{N}$.

ii) **(Minima)** *For any fixed* $\|\mathbf{h}\| > 0$*,* $I_{\mathbf{h}} = 0$ *if and only if* h *is a pure delay, i. e.*

$$\mathbf{h} = [0 \cdots 0 \ h_i \ 0 \cdots 0]^T$$

iii) **(Maxima)** *For any fixed* $\|\mathbf{h}\| > 0$*,* $I_{\mathbf{h}} = \|\mathbf{h}\|^4 \frac{N-1}{N}$ *when* $|h_0| = |h_1| =, \cdots, = |h_{N-1}|$.

iv) **(Saddle Points)** *Let* $\frac{\partial}{\partial|\mathbf{h}|} I_{\mathbf{h}}$ *denote* $[\frac{\partial}{\partial|h_0|} I_{\mathbf{h}} \cdots \ \frac{\partial}{\partial|h_{N-1}|} I_{\mathbf{h}}]^T$*. Then* $\frac{\partial}{\partial|\mathbf{h}|} I_{\mathbf{h}} = 0$ *if and only if for an arbitrary index set* $J = \{j_1, ..., j_M\} \subset \{0, 1, ..., N-1\}$*,* $|h_{j_1}| = |h_{j_2}| =, \cdots, = |h_{j_M}|$ *and* $h_k = 0$ *for* $k \notin J$

Proof: Since $I_{r\mathbf{h}} = r^4 I_{\mathbf{h}}$, for a real r, from the definition of $I_{\mathbf{h}}$, we can assume $\|\mathbf{h}\| = 1$ without loss of generality. First we will prove *iv)*, and then *i), ii), iii)* follows from *iv)* as a special case. According to the Lagrange Multipliers method [30], we need to solve

$$\frac{\partial}{\partial|\mathbf{h}|} I_{\mathbf{h}} = \lambda \frac{\partial}{\partial|\mathbf{h}|} (\sum |h_i|^2 - 1) \tag{3.3}$$

$$\Rightarrow |h_i|(2 \sum_{j \neq i} |h_j|^2 - \lambda) = 0, \quad \text{for } \forall i \tag{3.4}$$

This yields $|h_i| = 0$ or $\lambda = 2 \sum_{j \neq i} |h_j|^2$ for $i = 0, ..., N-1$. Since we have a constraint $\sum |h_i|^2 = 1$, the solutions become $|h_i| = 0$ or $|h_i|^2 = (2-\lambda)/2$ for $i = 0, ..., N-1$. Let $J = \{j_1, ..., j_M\}$ be the index set such that $|h_k| \neq 0$ for $k \in J$. Then we have $|h_k| = 0$ for $k \notin J$ and

$$|h_{j_1}| = |h_{j_2}| = \cdots = |h_{j_M}| = \sqrt{1 - \frac{\lambda}{2}},$$

which proves *iv)*. Furthermore, for the stationary points,

$$\|\mathbf{h}\|^2 = \sum_{i=1}^{M} |h_{j_i}|^2 = M \left(1 - \frac{\lambda}{2}\right) = 1 \tag{3.5}$$

$$I_{\mathbf{h}} = \sum_{i \neq j; i,j \in J} |h_i|^2 |h_j|^2 = M(M-1) \left(1 - \frac{\lambda}{2}\right)^2 = \frac{M-1}{M} \tag{3.6}$$

If $M=1$, i.e. $J=\{k\}$, then we have pure delay and $I_{\mathbf{h}}=0$, which proves *ii*). If $M=N$, i.e. $J=\{0,1,...,N-1\}$, then we have the maximum $I_{\mathbf{h}}=(N-1)/N$ among all stationary points, which proves *iii*).

■

For a real $\mathbf{h}$ Lemma 1 implies that, for the unit sphere $S^{N-1}:=\{\|\mathbf{h}\|=1 \mid \mathbf{h}\in H\}$, the $I_{\mathbf{h}}$ restricted to the sphere, $I_{\mathbf{h}}|_{S^{N-1}}$, has $2N$ local minima (on each axis), $\{(0,..,0,\pm1,0,..,0)\}$, and 2^N local maxima (on every $|h_0|=|h_1|=,...,=|h_{N-1}|$ ray).

Remark 2 Notice that $I_{\mathbf{h}}$ is a symmetric function, i.e. $I_{\mathbf{h}}=I_{\sigma(\mathbf{h})}$ where σ is an arbitrary permutation. Thus, $I_{\mathbf{h}}$ shows a strong symmetry for arbitrary coordinate orientation in its geometrical representation. Furthermore, we can view the stationary points with the index set $J=\{j_1,...,j_M\}$ as an embedded maxima of M-dimensional I_h function. This suggests to us a recursive way to construct all N dimensional stationary points of $I_{\mathbf{h}}$.

3.1.3 CMA cost function on the system space

In this subsection, the CMA cost function is expressed in a simple and intuitive form in the system space. The CMA cost function has a strong symmetry inherited from the $I_{\mathbf{h}}$ function and thus is easy to analyze in the absence of noise.

Lemma 2 (CM cost function in the absence of noise) *W.l.o.g, we assume the source is zero mean, and further we assume circular ($E(s_n^2)=0$) if complex. Then the CMA cost function can be expressed as*

$$4J_H(\mathbf{h})=m_4(\|\mathbf{h}\|^2-1)^2+\eta_s I_{\mathbf{h}}+\gamma^2-m_4, \tag{3.7}$$

where η_s is defined as the deviation of the source kurtosis from the Gaussian kurtosis κ_w (with normalized kurtosis $\kappa_s := m_4/m_2^2$)

$$\eta_s := \kappa_w m_2^2 - m_4 = m_2^2(\kappa_w - \kappa_s) \tag{3.8}$$

From Assumption A1, we have $\eta_s > 0$.

Proof: First, consider the expected value of the output power and the square of the output power of the CMA equalizer: From $y_n = \mathbf{h}^T\mathbf{s}$

$$\begin{aligned}
E(|y_n|^2) &= E(\sum h_i h_i^* s_i s_i^* + \sum_{i \neq j} h_i h_j^* s_i s_j^*) && (3.9)\\
&= \sum |h_i|^2 E(|s_i|^2) = m_2 ||\mathbf{h}||^2, \text{ and similarly} && (3.10)\\
E(|y_n|^4) &= m_4 \sum |h_i|^4 + 2m_2^2 \sum_{i \neq j} |h_i|^2 |h_j|^2 + |E(s_n^2)|^2 \sum_{i \neq j} h_i^2 (h_j^*)^2 && (3.11)\\
&= m_4 \left((\sum |h_i|^2)^2 - \sum_{i \neq j} |h_i|^2 |h_j|^2 \right) && (3.12)\\
&\quad +2m_2^2 \sum_{i \neq j} |h_i|^2 |h_j|^2 + |E(s_n^2)|^2 \sum_{i \neq j} h_i^2 (h_j^*)^2 && (3.13)\\
&= m_4 ||\mathbf{h}||^4 + m_2^2(\kappa_\omega - \kappa_s) \sum_{i \neq j}^{N\text{-}1} |h_i|^2 |h_j|^2 && (3.14)\\
&= m_4 ||\mathbf{h}||^4 + \eta_s I_{\mathbf{h}} && (3.15)
\end{aligned}$$

Recall $I_{\mathbf{h}}$ from (3.1). In (3.13), notice that if $\mathbf{s}$ is circular complex, then $|(s_n^2)|^2 = 0$, and if $\mathbf{s}$ is real, then $|E(s_n^2)|^2 \sum_{i \neq j} h_i^2 (h_j^*)^2 = m_2^2 \sum_{i \neq j} |h_i|^2 |h_j|^2$. Recall that $k_\omega = 2$ when complex and 3 when real. The CMA cost function is written as a function of $\mathbf{h}$:

$$\begin{aligned}
4J_H &= E\{(|y_n|^2 - \gamma)^2\} && (3.16)\\
&= E(|y_n|^4) - 2\gamma E(|y_n|^2) + \gamma^2 && (3.17)\\
&= m_4 ||\mathbf{h}||^4 + \eta_s I_{\mathbf{h}} - 2\gamma m_2 ||\mathbf{h}||^2 + \gamma^2 && (3.18)
\end{aligned}$$

$$= \quad m_4\|\mathbf{h}\|^4 - 2m_4\|\mathbf{h}\|^2 + \eta_s I_{\mathbf{h}} + \gamma^2 \tag{3.19}$$

$$= \quad m_4(\|\mathbf{h}\|^2 - 1)^2 + \gamma^2 - m_4 + \eta_s I_{\mathbf{h}}. \tag{3.20}$$

Recall $\gamma := m_4/m_2$ in Definition 5 in Chapter 2. ■

We refer to $m_4(\|\mathbf{h}\|^2 - 1)^2$ as a radial term of J_H, since it only depends on the radial change of $\mathbf{h}$, while we refer to $\eta_s I_{\mathbf{h}}$ as a spherical term. The following example clarifies the intuition behind this decomposition.

Example 1 For a BPSK source and a real channel $\gamma^2 = m_4 = 1$ and the cost function is simplified to

$$4J_H(\mathbf{h}) = \underbrace{(\|\mathbf{h}\|^2 - 1)^2}_{\text{Radial term}} \quad + \quad \underbrace{\eta_s I_{\mathbf{h}}}_{\text{Spherical term}} \tag{3.21}$$

where η_s becomes $3-1 = 2$. Figure 3.3 illustrates an example of this decomposition for two-dimensional H space.

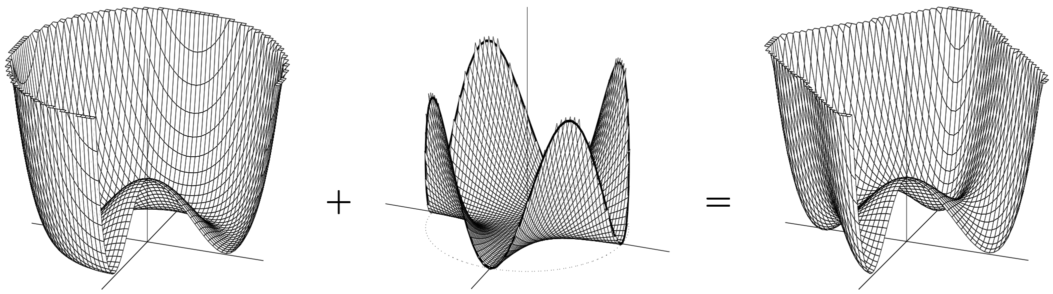

a) Radial $(\|\mathbf{h}\|^2 - 1)^2$

b) Spherical $\eta_s I_{\mathbf{h}}$

c) FS-CMA $(\|\mathbf{h}\|^2 - 1)^2 + \eta_s I_{\mathbf{h}}$

Figure 3.3: Decomposition of CM cost function

Remark 3 Notice that this decomposition of the CMA cost function provides a simple explanation of the effect of the source statistics on the performance of the CMA analyzed in [21]:

- If the source is Gaussian, then $\eta_s = m_2^2(\kappa_w - \kappa_s) = 0$. The spherical term $I_{\mathbf{h}}$ disappears, and there is no equalization (system parameters are wandering along $\|\mathbf{h}\| = 1$).
- If the source is super Gaussian, then $\eta_s = m_2^2(\kappa_w - \kappa_s) < 0$. Instead of minimizing $I_{\mathbf{h}}$, CMA maximizes $I_{\mathbf{h}}$, which results in maximizing ISI.

In the presence of noise, the CMA cost function becomes a bit complicated, since the additional $\mathbf{f}$ term is involved with the noise term. In order to express it in terms of $\mathbf{h}$, we use the system model described in Figure 3.4, which is equivalent to our original system model in Figure 3.1. Furthermore, we request further assumptions

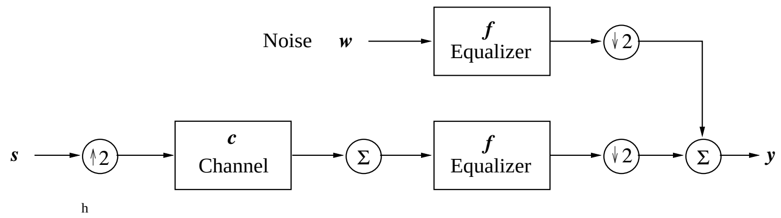

Figure 3.4: A $T/2$-spaced digital communication model equivalent to Figure 3.1

in order to construct an ideal mathematical model.

Assumption 2

A3. The equalizer length $N_f = N_c - 2$, where N_c is the length of the channel.

A4. The noise is white, Gaussian, and uncorrelated with the source.

One may argue that knowing exact channel length in the assumption 3 is unrealistic. However, like many assumptions in digital signal processing theory, this assumption allows us to have a clearly focused mathematical picture for an ideal case, which helps us understand less ideal but realistic situations.

Under the assumptions A2-A3, the channel convolution matrix C of the $T/2$ spaced channel $\mathbf{c}$ is invertible. Therefore, any equalizer parameter vector $\mathbf{f}$ uniquely determines a noise-free system response $\mathbf{h}$ and vice versa via the following equation.

$$\mathbf{h} = C\mathbf{f}. \tag{3.22}$$

Thus we have an isomorphism between the system space and the equalizer space.

Lemma 3 (FS-CM cost function in the presence of noise) *Without loss of generality, assume zero mean source with $m_2 = 1$ (then $\gamma = m_4$) and circular if comlex. The FS-CMA cost function in the presence of noise is expressed as*

$$\begin{aligned} 4J_H &= \gamma\|\mathbf{h}\|^4 + 2\kappa_w\sigma^2\|\mathbf{h}\|^2\|C^{-1}\mathbf{h}\|^2 + \kappa_w\sigma^4\|C^{-1}\mathbf{h}\|^4 \\ &\quad -2\gamma(\|\mathbf{h}\|^2 + \sigma^2\|C^{-1}\mathbf{h}\|^2) + \gamma^2 \\ &\quad +\eta_s I_{\mathbf{h}}. \end{aligned} \tag{3.23}$$

Proof: Let $\mathbf{w}$ be Gaussian white noise and $\mathbf{z}$ be the down sampled noise of $\mathbf{w}$ with variance σ^2, i. e. $z_n = w_{2n-1}$ (refer to Figure 3.4). Then $y_n = \mathbf{h}^T\mathbf{s} + \mathbf{f}^T\mathbf{z}$. Since the noise and the source are uncorrelated:

$$E(|y|^2) = \|\mathbf{h}\|^2 + \sigma^2\|\mathbf{f}\|^2 \tag{3.24}$$

$$E(|y|^4) = E\left\{|\mathbf{h}^T\mathbf{s}|^4\right\} + 4E\left\{|\mathbf{h}^T\mathbf{s}|^2|\mathbf{f}^T\mathbf{z}|^2\right\} + E\left\{|\mathbf{f}^T\mathbf{z}|^4\right\} \tag{3.25}$$

$$+E\left\{((\mathbf{h}^T\mathbf{s})^*)^2(\mathbf{f}^T\mathbf{z})^2\right\} + E\left\{(\mathbf{h}^T\mathbf{s})^2((\mathbf{f}^T\mathbf{z})^*)^2\right\} \tag{3.26}$$

$$= \gamma\|\mathbf{h}\|^4 + \kappa_w\sigma^2\|\mathbf{h}\|^2\|\mathbf{f}\|^2 + E\left\{|\mathbf{z}|^4\right\}\|\mathbf{f}\|^4 \tag{3.27}$$

$$+\eta_s I_{\mathbf{h}} + \eta_{\mathbf{z}} I_{\mathbf{f}}. \tag{3.28}$$

Since $\mathbf{z}$ is Gaussian, $\eta_{\mathbf{z}} = 0$ and $E\{|\mathbf{z}|^4\} = \kappa_w\sigma^4$. Furthermore, since $\left\{\mathbf{h}^T\mathbf{s}\right\}$ and $\left\{\mathbf{f}^T\mathbf{z}\right\}$ are uncorrelated and circularly complex (i.e. $\mathbf{s}$ and $\mathbf{w}$ are uncorrelated and circularly complex), we have $E\left\{((\mathbf{h}^T\mathbf{s})^*)^2(\mathbf{f}^T\mathbf{z})^2\right\} = E\left\{(\mathbf{h}^T\mathbf{s})^2((\mathbf{f}^T\mathbf{z})^*)^2\right\} = 0$ for complex case. By developing the FS-CMA cost function with the above formulae we obtain (3.23)

■

3.2 Radial Minima Surface View

3.2.1 Radial Minima Surface

Since the radial term of CM cost function plays the role of bringing the system response vector to near the unit sphere, the CM cost function is almost characterized by the spherical term I_h. This idea can be rigorously expressed by defining a sphere-like manifold, *the Radial Minima Surface* Φ, which contains all stationary points of FS-CMA except the origin. The concept of the radial minima surface of the CM cost function was introduced by Benveniste [2] and developed by Leblanc [21] in the absence of noise. Here, we extend this idea for the noisy case.

Lemma 4 *For every ray on H-space,* $\mathbb{R}^+\mathbf{h} := \{r\mathbf{h} | r > 0\}$ *(for a given* $\mathbf{h} \in S^{N-1}$*), the CM cost function restricted on the ray,* $J_H|_{\mathbb{R}^+\mathbf{h}}$ *has a unique minimum. Furthermore, the minimum is located in the range of* $(0, 1]$.

Proof: The noisy FS-CM cost function (3.23) restricted on a ray $\mathbb{R}^+\mathbf{h}$ becomes

$$\begin{aligned} 4J_H(r\mathbf{h}) &= (\kappa_w\sigma^4\|C^{-1}\mathbf{h}\|^4 + 2\kappa_w\sigma^2\|C^{-1}\mathbf{h}\|^2 + \gamma + \eta_s I_{\mathbf{h}})r^4 \\ &\quad -2\gamma(1+\sigma^2\|C^{-1}\mathbf{h}\|^2)r^2 + \gamma^2. \end{aligned} \tag{3.29}$$

This is a quadratic function of r^2. By solving this quadratic function, we have $r_{\min}$ satisfying $\frac{\partial J_H}{\partial r}|_{\mathbb{R}^+\mathbf{h}} = 0$ for a ray $\mathbb{R}^+\mathbf{h}$

$$r^2_{\min} = \frac{\gamma(1+\sigma^2\|C^{-1}\mathbf{h}\|^2)}{\kappa_w(1+\sigma^2\|C^{-1}\mathbf{h}\|^2)^2 - \eta_s(1-I_{\mathbf{h}})}. \tag{3.30}$$

Since $\eta_s/N \leq \eta_s(1-I_h) \leq \eta_s = \kappa_w - \kappa_s = \kappa_w - \gamma$,

$$\frac{\gamma(1+\sigma^2\|C^{-1}\mathbf{h}\|^2)}{\kappa_w(1+\sigma^2\|C^{-1}\mathbf{h}\|^2)^2} < r_{\min}^2 \leq \frac{\gamma(1+\sigma^2\|C^{-1}\mathbf{h}\|^2)}{\kappa_w(1+\sigma^2\|C^{-1}\mathbf{h}\|^2)^2 - \eta_s} \leq \frac{\gamma}{\kappa_w - \eta_s} = 1 \quad (3.31)$$

On the other hand,

$$0 < \frac{\gamma(1+\sigma^2\|C^{-1}\mathbf{h}\|^2)}{\kappa_w(1+\sigma^2\|C^{-1}\mathbf{h}\|^2)^2} \quad (3.32)$$

This shows $0 < r_{\min}^2 \leq 1$. ■

Definition 7 (Radial Minima Surface) *Let φ denote the mapping from $\mathbf{h} \in S^{N-1} \subset H$ to the scalar $r_{\min}$;*

$$\begin{aligned} \varphi : S^{N-1} &\rightarrow \mathbb{R} \\ \mathbf{h} &\mapsto r_{\min} \end{aligned} \quad (3.33)$$

We define the radial minima surface Φ *as the union of all minima in Lemma 4,*

$$\Phi := \{\varphi(\mathbf{h})\mathbf{h} | \mathbf{h} \in S^{N-1}\}. \quad (3.34)$$

Remark 4 Since $r_{\min}$ is a differentiable function of $\mathbf{h}$, φ is also differentiable, and thus Φ is a differentiable manifold homeomorphic to S^{N-1}.

In the absence of noise (i.e. $\sigma^2 = 0$), the radial minima surface is simplified as a function of $I_{\mathbf{h}}$.

$$\Phi = \left\{ \sqrt{\frac{\gamma}{\gamma + \eta_s I_{\mathbf{h}}}}\mathbf{h} \mid \mathbf{h} \in S^{N\text{-}1} \right\} \quad (3.35)$$

In this case, Φ inherits the symmetric structure of $I_{\mathbf{h}}$ as the following example shows.

Example 2 Assume a BPSK source in the absence of channel noise. Then the radial minima surface becomes

$$\Phi = \left\{ \sqrt{\frac{1}{1+\eta_s I_{\mathbf{h}}}}\mathbf{h} \mid \mathbf{h} \in S^{N\text{-}1} \right\} \tag{3.36}$$

Φ is symmetrical to arbitrary coordinate permutation, and an M-dimensional Φ is embedded into an N-dimensional Φ $(M < N)$ (Figure 3.5).

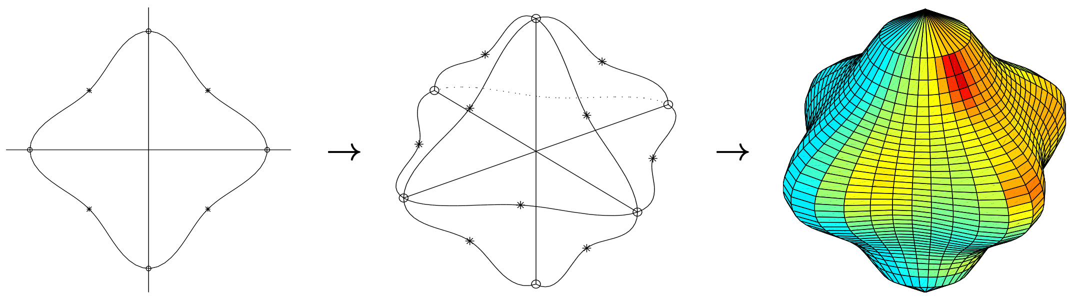

a) 2-dim. b) 3-dim

Figure 3.5: Radial Minima Surface Φ in the absence of noise

3.2.2 Radial minima surface and CM solution

Every point on Φ is a candidate for a CM solution, and CM solutions should locate on Φ, if there are any. By examining only Φ instead of the entire H, we can determine all CM solutions on H.

Theorem 1 (The existence of a CM solution) *J_H has at least one pair of local minima at any given noise power.*

Proof: Since Φ is a compact space (homeomorphic to a sphere), J_H has a minimum on Φ, which is also a local minimum of J_H on H. Since $J_H(h) = J_H(-h)$, we have a pair of local minima. ∎

Let $\rho(\mathbf{h})$ denote the output power of the receiver at $\mathbf{h}$;

$$\rho(\mathbf{h}) = E(y^2)|_{\mathbf{h}} \tag{3.37}$$

From (3.24), for all $\varphi(\mathbf{h})\mathbf{h} \in \Phi$ we have

$$\begin{aligned} \rho(\varphi(\mathbf{h})\mathbf{h}) &= (1+\sigma^2\|C^{-1}\mathbf{h}\|^2)\varphi^2(\mathbf{h}) \\ &= \frac{\gamma(1+\sigma^2\|C^{-1}\mathbf{h}\|^2)^2}{\kappa_w(1+\sigma^2\|C^{-1}\mathbf{h}\|^2)^2 - \eta_s(1-I_{\mathbf{h}})}. \end{aligned} \tag{3.38}$$

Theorem 2 *On the radial minima surface Φ, every local maximum with respect to the output power ρ is a CM solution and vice versa.*

Proof: From a direct calculation we have

$$4J_H(\varphi(\mathbf{h})\mathbf{h}) = \gamma^2 - \frac{\gamma^2(1+\sigma^2\|C^{-1}\mathbf{h}\|^2)^2}{\kappa_w(1+\sigma^2\|C^{-1}\mathbf{h}\|^2)^2 - \eta_s(1-I_{\mathbf{h}})} \tag{3.39}$$

$$= \gamma^2 - \gamma\rho(\varphi(\mathbf{h})\mathbf{h}). \tag{3.40}$$

Since $\gamma > 0$, J_H is minimized when ρ is maximized.

■

Corollary 1 *In the absence of noise, the CM solutions are the local maxima of the ℓ_2 norm on the radial minima surface Φ.*

Proof:

$$\|\varphi(\mathbf{h})\mathbf{h}\|^2 = \varphi(\mathbf{h})^2 = \frac{\gamma}{\gamma + \eta_s I_{\mathbf{h}}} = \rho(\varphi(\mathbf{h})\mathbf{h}) \tag{3.41}$$

■

Corollary 2 (Output Power Constraint of FS-CMA) *For arbitrary noise power, the output power of any CM solution lies on $(\gamma/\kappa_w,\ \gamma/\kappa_s]$, i.e., for a CM solution* $\mathbf{h}$

$$\frac{\gamma}{\kappa_w} < \rho(\mathbf{h}) \le \frac{\gamma}{\kappa_s} \tag{3.42}$$

Proof: From (3.38), we have

$$\rho(\mathbf{h}) = \frac{\gamma\zeta}{\kappa_w\zeta - \eta_s\xi} \tag{3.43}$$

where $1 \leq \zeta < \infty$ and $0 < \xi \leq 1$. $\rho(\mathbf{h})$ is maximized when $\zeta = 1$ and $\xi = 1$ with $\rho(\mathbf{h}) = \gamma/\kappa_s$, and minimized when $\zeta \to \infty$ and $\xi \to 0$ with $\rho(\mathbf{h}) \to \gamma/\kappa_w$.

■

Remark 5 Corollary 2 provides an independent proof of the generalized version of the CM norm constraint Theorem appearing in Zeng et. al. [37]

3.3 CM solutions in the system space in the absence of noise

In this section we will classify all stationary points of the CM cost function in the H space. In order to simplify the classification, we assume the source to be real. We do not lose much generality by this assumption, since the CMA cost function is invariant under the phase change of a complex source. The classification of CM stationary points in the absence of noise has been done by Leblanc in [20] with great detail, which is an extension of Johnson and Anderson's work in [15]. Here we derive the same results by utilizing the properties of the spherical component $I_{\mathbf{h}}$.

In the absence of noise, the radial minima surface Φ is given by

$$\Phi = \varphi(\mathbf{h})\mathbf{h} = \left\{ \sqrt{\frac{\gamma}{\gamma + \eta_s I_{\mathbf{h}}}}\mathbf{h} \mid \mathbf{h} \in S^{N\text{-}1} \right\} \tag{3.44}$$

From Corollary 1, the CM solutions are the maximum of $\varphi(\mathbf{h})$. Since $\varphi(\mathbf{h})$ is a function of $I_{\mathbf{h}}$, the CM solutions are φ evaluated at the minima of $I_{\mathbf{h}}$. We summarize the results as follows:

Lemma 5 (Stationary Points of J_H) *Let H be a N-dimensional real vector space. The stationary points of J_H consist of*

i) **(CM solutions)** $2N$ *local minima on every axis,*

$$\delta_i = [0 \cdots 0\ 1(i\text{-th place})\ \ 0 \cdots 0],\ \textit{for } i = 0, ...N\text{-}1 \textit{ and } \{-\delta_i\}$$

ii) **(Maxima)** *One local maxima* $\mathbf{h} = 0$.

iii) **(Saddle points)** $3^N - 2N - 1$ *saddle points: for any distinct index subset* $J = \{j_1, ..., j_M\}$,

$$\{\alpha(M)\mathbf{h} \mid |h_k| = 1 \textit{ for } k \in J \textit{ and } h_k = 0 \textit{ otherwise } \}$$

where

$$\alpha(M) = \left(\frac{1}{M} + \eta_s \frac{M-1}{M^2}\right)^{-\frac{1}{2}}$$

Proof: Let's restrict $\mathbf{h}$ to $S^{N\text{-}1}$. From $\varphi = \sqrt{\frac{\gamma}{\gamma + \eta_s I_{\mathbf{h}}}}$,

$$\frac{\partial}{\partial \mathbf{h}} \varphi|_{\mathbf{h}=\mathbf{h}'} = 0 \Leftrightarrow \frac{\partial}{\partial \mathbf{h}} I_{\mathbf{h}}|_{\mathbf{h}=\mathbf{h}'} = 0. \tag{3.45}$$

Furthermore, on Φ, $\frac{\partial}{\partial \mathbf{h}}\varphi|_{\mathbf{h}=\mathbf{h}'} = 0$ implies $\mathbf{h}'$ is a stationary point of the CM cost function in polar coordinates, since $\frac{\partial}{\partial r} J|_{\varphi(\mathbf{h}')\mathbf{h}'} = 0$ already. Therefore, the CM solutions are $\varphi(\mathbf{h})\mathbf{h}$ evaluated at the local minima of $I_{\mathbf{h}}$, and the saddle points of the CMA cost function are $\varphi(\mathbf{h})\mathbf{h}$ evaluated at the other stationary points.

By Lemma 1, $\{\pm\delta_i\}$ are minima of $I_{\mathbf{h}}$ and $\varphi(\pm\delta_i) = 1$, which proves i). Also one gets iii) by evaluating φ at the other stationary points in Lemma 1. To prove ii) one needs to evaluate the Hessian of the CM cost function J_H at the origin. The number of all stationary points of J_H, 3^N, comes from the N choices of $\{-1,\ 0,\ 1\}$ used to construct an N-dimensional stationary point of $I_{\mathbf{h}}$ given $\|\mathbf{h}\| = 1$.

$\blacksquare$

Definition 8 *We define the 2^N saddle points of the CM cost function for the index set $J = \{0, ..., N\text{-}1\}$ as* spherical maxima *and denote them as $\{\mathbf{m}_i\}$. i.e.,*

$$\mathbf{m}_i = \alpha(N)[(-1)^{i_0} \cdots (-1)^{i_k} \cdots (-1)^{i_{N\text{-}1}}]^T \tag{3.46}$$

where $i = 0, ..., 2^N$ and $i = (i_0, ..., i_{N\text{-}1})_2$ is a binary representation of i. (For example, $3 = (11)_2$.)

3.4 Regions of Convergence of CM solutions in the System Space

In this section we present a closed form expression for the regions of convergence of FS-CM solutions in the system space. As the geometrical representation of the decomposition of the CM cost function shows (Figure 3.3), the regions of convergence are determined mainly by the spherical term $I_{\mathbf{h}}$. Due to the symmetrical structure of $I_{\mathbf{h}}$, the regions of convergence turn out to be identical.

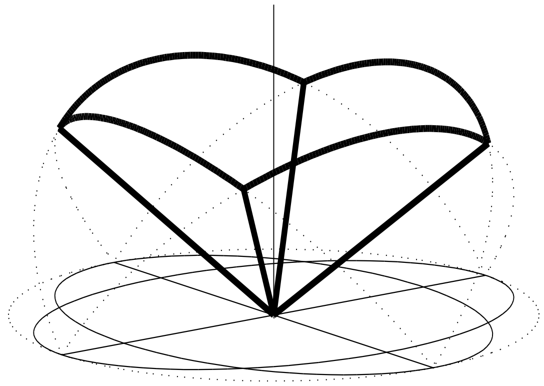

Figure 3.6: Regions of convergence in the system space

Theorem 3 (Regions of Convergence on H) *Let $\mathcal{R}(\delta_i)$ denote the regions of convergence of the CM solution δ_i, Then $\mathcal{R}(\delta_i)$ is a hypercone defined by*

$$\mathcal{R}(\delta_i) = \{\mathbf{h} \in H \mid h_i > 0, \quad |h_i| > |h_k| \text{ for all } k \neq i\}, \tag{3.47}$$

$$\text{and } \mathcal{R}(-\delta_i) = -\mathcal{R}(\delta_i). \tag{3.48}$$

Geometrically $\mathcal{R}(\delta_i)$ is a hyper-cone whose edges are spherical maxima around δ_i (Figure 3.6),

$$\{\mathbf{m}_k \mid \mathbf{m}_k \text{ are the spherical maxima with its } i\text{-th entry } (\mathbf{m}_k)_i = 1\}.$$

Proof: W.l.o.g., it is sufficient to show for $\mathcal{R}(\delta_0)$, since the proof for other CM-solutions are identical. To determine $\mathcal{R}(\delta_0)$, we introduce a local coordinate on H: Let H_0^+ denote the upper half space of H in δ_0 direction, i.e.

$$H_0^+ = \{\mathbf{h} \in H \mid h_0 > 0\} \tag{3.49}$$

For arbitrary $\mathbf{h} \in H_0^+$ we represent $\mathbf{h}$ with its norm and a vector in a $N-1$ dimensional disk.

$$\mathbf{h} \mapsto (r, \hat{\mathbf{h}}), \quad \text{where } r = ||\mathbf{h}|| \text{ and } \hat{\mathbf{h}} = \frac{1}{r}[h_1 \ \cdots h_{N\text{-}1}]^T \tag{3.50}$$

(notice that $||\hat{\mathbf{h}}|| < 1$). This local coordinate on H_0^+ is well defined, since we have an inverse identification

$$(r, [\hat{h}_1 \cdots \hat{h}_{N\text{-}1}]^T) \mapsto r[\sqrt{1 - \sum_{i=1}^{N\text{-}1} h_i^2} \ h_1 \cdots h_{N\text{-}1}^T] \tag{3.51}$$

By using this identification we can express $I_{\mathbf{h}}$ as a function of $\hat{\mathbf{h}}$.

$$I_{\mathbf{h}} = r^4(I_{\hat{\mathbf{h}}} + 2(1 - ||\hat{\mathbf{h}}||^2)||\hat{\mathbf{h}}||^2) \tag{3.52}$$

Denote $(I_{\hat{\mathbf{h}}} + 2(1 - ||\hat{\mathbf{h}}||^2)||\hat{\mathbf{h}}||^2)$ as $\hat{I}_{\hat{\mathbf{h}}}$. Then J_H is expressed as

$$4J_H = (r^2 - 1)^2 + \eta_s r^4 \hat{I}_{\hat{\mathbf{h}}} \tag{3.53}$$

and the derivative on this coordinate is

$$\begin{bmatrix} \frac{\partial}{\partial r} \\ \frac{\partial}{\partial \hat{\mathbf{h}}} \end{bmatrix} 4J_H = \begin{bmatrix} \left\{4(r^2 - 1) + 4r^2 \hat{I}_{\hat{\mathbf{h}}}\right\} r \\ r^4 \eta_s \frac{\partial}{\partial \hat{\mathbf{h}}} I_{\hat{\mathbf{h}}} \end{bmatrix} \tag{3.54}$$

with

$$\frac{\partial}{\partial \hat{\mathbf{h}}} \hat{I}_{\hat{\mathbf{h}}} = 4 \begin{bmatrix} (1 - ||\hat{\mathbf{h}}||^2 - \hat{h}_1^2)\hat{h}_1 \\ \vdots \\ (1 - ||\hat{\mathbf{h}}||^2 - \hat{h}_{N\text{-}1}^2)\hat{h}_{N\text{-}1} \end{bmatrix} \tag{3.55}$$

On the other hand, we can rewrite the CM update equation in terms of $(r, \hat{\mathbf{h}})$. Recognize that r always converges to a point (radial minima), and the movement direction of $\hat{\mathbf{h}}$ is independent of r. Since $\delta_0 = (1, \vec{0})$ in this coordinate, it is sufficient to determine the convergence region of $\vec{0}$ for $I_{\mathbf{h}}$. Consider the update equation of $I_{\mathbf{h}}$ in component wise form

$$[\hat{\mathbf{h}}\text{new}]_i = \hat{h}_i - \mu \hat{h}_i (1 - ||\hat{\mathbf{h}}||^2 - \hat{h}_i^2) \tag{3.56}$$

From the cubic nature of $\hat{h}_i(1 - ||\hat{\mathbf{h}}||^2 - \hat{h}_i^2)$ as a function of $\hat{h}_i$, each h_i converges to 0 if and only if

$$(1 - ||\hat{\mathbf{h}}||^2 - \hat{h}_i^2) > 0 \tag{3.57}$$

This defines a hyperellipse on the $N - 1$ dimensional disk

$$2\hat{h}_i^2 + \sum_{j \neq i} \hat{h}_j^2 < 1 \tag{3.58}$$

The region of convergence for δ_i on the $N-1$ dimensional disk is the intersection of the inner area of the hyperellipse for $i = 1, ..., N$-1. Eq (3.57) also can be expressed in the coordinate on $S^{N\text{-}1}$

$$(h_i^2 - h_0^2) = (h_i + h_0)(h_i - h_0) < 0 \tag{3.59}$$

Therefore,

$$\begin{aligned} \mathcal{R}(\delta_0) &= \left\{ r\mathbf{h} \mid h_0 > 0 \text{ and } |h_0| > |h_i| \text{ for all } i, \text{ where } r > 0, \mathbf{h} \in S^{N\text{-}1} \right\} && (3.60) \\ &= \{ \mathbf{h} \in H \mid h_0 > 0 \text{ and } |h_0| > |h_i| \text{ for all } i \} && (3.61) \end{aligned}$$

Also one can confirm that $H_0^- = \{h \in H \mid h_0 < 0\}$ does not intersect $\mathcal{R}(\delta_0)$. Similarly, it can be shown that $\mathcal{R}(-\delta_0) = -\mathcal{R}(\delta_0)$.

■

The hyper-cone in Theorem 3 was first introduced by Y. Li and Z. Ding to prove global convergence of CMA [23] and the equivalent result with an independent aproach appeared in [12].

The regions of convergence in system space does not have significant meaning by itself, since the adaptation occurs in equalizer space. However, in the following chapter this information will be utilized to delineate regions of convergence in equalizer space.

Chapter 4

Regions of Convergence of FS-CM Solutions in Equalizer Space in the Absence of Noise

In this chapter, we start talking about the equalizer space of a particular channel. The main goal of this chapter is to delineate the regions of convergence of the fractionally spaced CM solutions in the equalizer space. The analysis tool applied here, however, is not an explicit analytical method which can provide all details about the ROC of every individual CM solution, but a qualitative method which enables us to observe the structure of ROCs of the FS-CM solutions of a particular channel. To simplify the analysis we assume a BPSK source.

4.1 FS-CM solutions in the Equalizer Space

Denote J_F as the FS-CM cost function on the equalizer space F under a channel $\mathbf{c}$ with the channel convolution matrix C. J_F is given by the equalizer−system space relation, $\mathbf{h} = C\mathbf{f}$;

$$J_F(\mathbf{f}) = J_H(C\mathbf{f}) = (\|C\mathbf{f}\|^2 - 1)^2 + \eta_s I_{C\mathbf{f}} \tag{4.1}$$

Due to the channel convolution matrix C, J_F has lost the symmetry which enabled us to analyze stationary points and their regions of convergence of J_H in Chapter 3. However, we observe that J_F is a coordinate-transformed version of J_H via the $T/2$ channel convolution matrix, and

$$\begin{aligned}
\frac{\partial}{\partial \mathbf{f}} J_F(\mathbf{f})|_{\mathbf{f}=\mathbf{f}'} &= \frac{\partial}{\partial \mathbf{f}} J_H(C\mathbf{f})|_{\mathbf{f}=\mathbf{f}'} \\
&= \left[\frac{\partial}{\partial \mathbf{f}_i} J_H(\mathbf{h})|_{\mathbf{h}=C\mathbf{f}'} \right]_{i=0,..,N\text{-}1} \\
&= \left[\sum_{j=0}^{N\text{-}1} \frac{\partial \mathbf{h}_j}{\partial \mathbf{f}_i} \frac{\partial}{\partial \mathbf{h}_j} J_H(\mathbf{h})|_{\mathbf{h}=C\mathbf{f}'} \right]_{i=0,..,N\text{-}1} \\
&= \left[\sum_{j=0}^{N\text{-}1} C_{ij} \frac{\partial}{\partial \mathbf{h}_j} J_H(\mathbf{h})|_{\mathbf{h}=C\mathbf{f}'} \right]_{i=0,..,N\text{-}1} \\
&= C^T \frac{\partial}{\partial \mathbf{h}} J_H(\mathbf{h})|_{\mathbf{h}=C\mathbf{f}'}
\end{aligned} \tag{4.2}$$

where the notation $[\ \cdot\ ]_{i=0,..,N\text{-}1}$ represents a column vector. Similarly

$$\begin{aligned}
\frac{\partial^2}{\partial \mathbf{f}^T \partial \mathbf{f}} J_F(\mathbf{f})|_{\mathbf{f}=\mathbf{f}'} &= \frac{\partial^2}{\partial \mathbf{f}^T \partial \mathbf{f}} J_H(C\mathbf{f})|_{\mathbf{f}=\mathbf{f}'} \\
&= \frac{\partial}{\partial \mathbf{f}^T} \frac{\partial}{\partial \mathbf{f}} J_H(C\mathbf{f})|_{\mathbf{f}=\mathbf{f}'} \\
&= \frac{\partial}{\partial \mathbf{f}^T} C^T \frac{\partial}{\partial \mathbf{h}} J_H(\mathbf{h})|_{\mathbf{h}=C\mathbf{f}'} \\
&= C^T \frac{\partial^2}{\partial \mathbf{h}^T \partial \mathbf{h}} J_H(\mathbf{h}) C|_{\mathbf{h}=C\mathbf{f}'}
\end{aligned} \tag{4.3}$$

The stationary points of the J_F are given by the above relations as Theorem 4 summarizes.

Theorem 4 (Stationary points on F) *Let* $\dim(F) = N$. *The stationary points of J_F consist of* *i)* **(CM solutions)** $2N$ *local minima* $\mathbf{d}_i = C^{-1}\delta_i$ *(where* δ_i *are the local minima of* J_H*) and* $\{-\mathbf{d}_i\}$

ii) **(Maxima)** *One local maximum* $\vec{0}$*,*

iii) **(Saddle points)** $3^N - 2N - 1$ *saddle points:* $\{C^{-1}\mathbf{h} | \mathbf{h}$ *is saddle point of* $J_H\}$

Proof: Let $\mathbf{h} = C\mathbf{f}$ be the system response corresponding $\mathbf{f}$. From (4.2)

$$\frac{\partial}{\partial \mathbf{f}} J_F(\mathbf{f})|_{\mathbf{f}=\mathbf{f}'} = C^T \frac{\partial}{\partial \mathbf{h}} J_H(\mathbf{h})|_{\mathbf{h}=C\mathbf{f}'}. \tag{4.4}$$

Since C is invertible, $\mathbf{f}$ is a stationary point of J_F if and only if $C\mathbf{f}$ is a stationary point of J_H. On the other hand, the Hessian matrix of J_F at $\mathbf{f}$ is positive definite (negative definite) if and only if that of J_H is positive definite (negative definite).

$$\mathbf{f}^T \left[\frac{\partial^2}{\partial \mathbf{f}^T \partial \mathbf{f}} J_F(\mathbf{f})|_{\mathbf{f}=\mathbf{f}'} \right] \mathbf{f} = (C\mathbf{f})^T \left[\frac{\partial^2}{\partial \mathbf{h}^T \partial \mathbf{h}} J_H(\mathbf{h})|_{\mathbf{h}=C\mathbf{f}'} \right] (C\mathbf{f}) \tag{4.5}$$

Since C is invertible, $\mathbf{f}$ is a maximum (saddle, or minimum) of J_F if and only if $C\mathbf{f}$ is a maximum (saddle, or minimum) of J_H.

■

Definition 9 *We define the* 2^N *saddle points of* J_F*,*

$$\left\{ \mathbf{v}_i = C^{-1}\mathbf{m}_i \mid \mathbf{m}_i \text{ is a spherical maximum of } J_H \right\} \tag{4.6}$$

as the spherical maxima of J_F*.*

4.2 Regions of Convergence in Equalizer Space in the Absence of Noise

As stationary points on F have been simply obtained from those on H via the channel matrix C, one may expect the regions of convergence can be also obtained from the hyper-cones in Theorem 3 via the channel matrix C. This is true. However, the details are not straightforward, and we are limited to describing the qualitative effects of the transform from the hyper-cones. The transform consists of *rotation* and *dilation*, and the dilation parts contribute the most interesting features of the regions of convergence in equalizer space. In order to study the transformation of regions of convergence, first we need to study vector fields of the equalizer space.

4.2.1 The Relation between the System Space Vector Field and the Equalizer Space Vector Field

In the previous section, we have shown that the stationary points of J_F and J_H have a linear relation. However, a linear relationship is not retained for the regions of convergence, since the cost function is non-linear. Generally, describing the change of trajectory due to a coordinate change of a non-linear cost function is quite difficult. Since a trajectory is determined by the update equation $\mathbf{f}^{(n+1)} = \mathbf{f}^{(n)} - \mu\frac{\partial}{\partial \mathbf{f}}J_F|_{f(n)}$, we look at (4.2) (rewriten here as (4.7)) closely.

$$\frac{\partial}{\partial \mathbf{f}}J_F(\mathbf{f})|_{\mathbf{f}=\mathbf{f}'} = C^T\frac{\partial}{\partial \mathbf{h}}J_H(\mathbf{h})|_{\mathbf{h}=C\mathbf{f}'}. \tag{4.7}$$

Eq (4.7) shows that for each update, $\mathbf{f}$ goes to H space by C and gets the $\frac{\partial}{\partial \mathbf{h}}J_H(\mathbf{h})$ on H and returns to F space by C^T (Figure 4.1). To develop this idea in detail, we introduce a convenient terminology.

Definition 10 (Vector Field) *A vector field on a n-dimensional differentiable manifold X, denoted by ∇^X is a smooth mapping from X to a n-dimensional vector space $T(X)$.*

$$\nabla^X : X \to T(X). \tag{4.8}$$

$\nabla^X_{\mathbf{x}}$ denotes the vector in $T(X)$ corresponding to $\mathbf{x} \in X$ by ∇^X. (see [3])

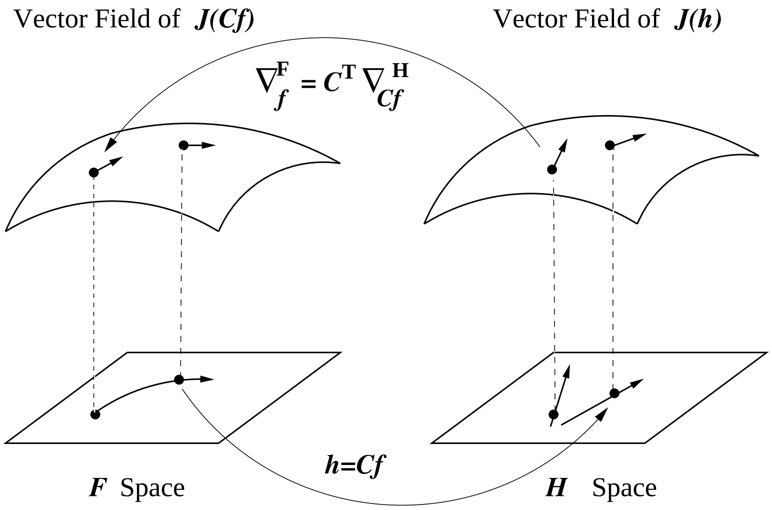

Figure 4.1: The relation between the vector field on F and H

Example 3 (Gradient System) Let J be a cost function on X, i.e. $J : X \to \mathbb{R}$. Then J induces a vector field on X

$$\nabla^X_{\mathbf{x}'} := -\frac{\partial}{\partial \mathbf{x}} J(\mathbf{x})|_{\mathbf{x}=\mathbf{x}'} \tag{4.9}$$

Now we can write down equation (4.7)

$$\frac{\partial}{\partial \mathbf{f}} J_F(\mathbf{f})|_{\mathbf{f}=\mathbf{f}'} = C^T \frac{\partial}{\partial \mathbf{h}} J_H(\mathbf{h})|_{\mathbf{h}=C\mathbf{f}'}$$

simply as

$$\nabla^F_{\mathbf{f}'} = C^T \nabla^H_{C\mathbf{f}'} \tag{4.10}$$

or equivalently,

$$\nabla^F_{C^{-1}\mathbf{h}'} = C^T \nabla^H_{\mathbf{h}'}, \tag{4.11}$$

where $\mathbf{h}' = C\mathbf{f}'$. In these equations, notice that the point $\mathbf{f}$ is transformed by C^{-1} from H,

$$\mathbf{f} = C^{-1}\mathbf{h},$$

while the vector field on that point is transformed by C^T from H,

$$\nabla^F_{\mathbf{f}} = C^T \nabla^H_{\mathbf{h}}.$$

The difference between C^T and C^{-1} causes difficulty in establishing a simple relation between the trajectories in F under ∇^F and those in H under ∇^H. If $C^T = C^{-1}$, i.e. C is a unitary matrix, we have a nice result that the trajectories in F under ∇^F are given by the linear transformation, C^T, from the trajectories in H under ∇^H (Lemma 6 in this chapter). Motivated by this result we decompose C into unitary matrices and a diagonal matrix.

Let $C = U\Lambda V$ be the singular decomposition of C.

- U and V are unitary matrices
- $\Lambda = \mathrm{diag}(\lambda_0, ..., \lambda_{\mathrm{N-1}})$ with $\lambda_0 > \cdots > \lambda_{N-1} > 0$.

(4.10) can be rewritten as

$$\nabla^F_{\mathbf{f}} = V^T \Lambda^T U^T \nabla^H_{U\Lambda V\mathbf{f}}. \tag{4.12}$$

To appreciate the meaning of (4.12), we consider the following intermediate vector spaces between H and F with the corresponding vector fields:

1) $H = X_1$ with $\nabla^{X_1} = \nabla^H$

2) $X_2 = U^{-1}X_1$ with $\nabla^{X_2}_{\mathbf{x}} = U^T \nabla^{X_1}_{U\mathbf{x}}$ (rotation)

3) $X_3 = \Lambda^{-1}X_2$ with $\nabla^{X_3}_{\mathbf{x}} = \Lambda^T \nabla^{X_2}_{\Lambda\mathbf{x}}$ (dilation)

4) $F = X_4 = V^{-1}X_3$ with $\nabla^{X_4}_{\mathbf{x}} = V^T \nabla^{X_3}_{V\mathbf{x}}$ (rotation)

The relation of vector fields on H and F in (4.12) can be viewed as the concatenation of the relations between $X_1 = H$ and X_2, X_2 and X_3, and X_3 and $X_4 = F$.

In the following sections, we will show that any trajectory in X_2 (X_4) is indeed a trajectory on X_1 (X_3) rotated by U^T (V^T). The following diagram labelled as equation (4.13) summarizes this observation.

$$
\begin{array}{ccccccc}
\text{Space} & & \text{Vector Field} & & \text{Local minima} & & \text{R.O.C.} \\
H = X_1 & \cdots & \nabla^H & \cdots & U\Lambda V\mathbf{d}_i & \cdots & \mathcal{R} \\
\Big\downarrow U^{-1} & & \Big\downarrow U^T & & \Big\downarrow U^{-1} & & \Big\downarrow U^T \\
X_2 & \cdots & \nabla^H & \cdots & \Lambda V\mathbf{d}_i & \cdots & U^T(\mathcal{R}) \\
\Big\downarrow \Lambda^{-1} & & \Big\downarrow \Lambda^T & & \Big\downarrow \Lambda^{-1} & & \Big\downarrow \Lambda \\
X_3 & \cdots & \Lambda U^T\nabla^H & \cdots & V\mathbf{d}_i & \cdots & \mathcal{S} \\
\Big\downarrow V^{-1} & & \Big\downarrow V^T & & \Big\downarrow V^{-1} & & \Big\downarrow V^T \\
F = X_4 & \cdots & V^T\Lambda U^T\nabla^H & \cdots & \mathbf{d}_i & \cdots & V(\mathcal{S})
\end{array}
\tag{4.13}
$$

where $\mathcal{R}$ denotes the region of convergence of δ_i.

To provide a feeling for the above diagram (4.13), we present a two-dimensional example.

Example 4 Consider a $T/2$-spaced channel $c = [0.11,\ 0.8779,\ 0.3762,\ 0.2751]$. Then

$$
C = \begin{bmatrix} 0.8779 & 0.11 \\ 0.2751 & 0.3762 \end{bmatrix} = U\Lambda V \tag{4.14}
$$

where

$$
U = \begin{bmatrix} \cos(\pi/8) & -\sin(\pi/8) \\ \sin(\pi/8) & \cos(\pi/8) \end{bmatrix} \tag{4.15}
$$

$$
\Lambda = \begin{bmatrix} 0.9487 & 0 \\ 0 & 0.3162 \end{bmatrix} \tag{4.16}
$$

$$V = \begin{bmatrix} \cos(\pi/12) & \sin(\pi/12) \\ -\sin(\pi/12) & \cos(\pi/12) \end{bmatrix} \tag{4.17}$$

and the process in (4.13) above unfolds as shown in Figure 4.2.

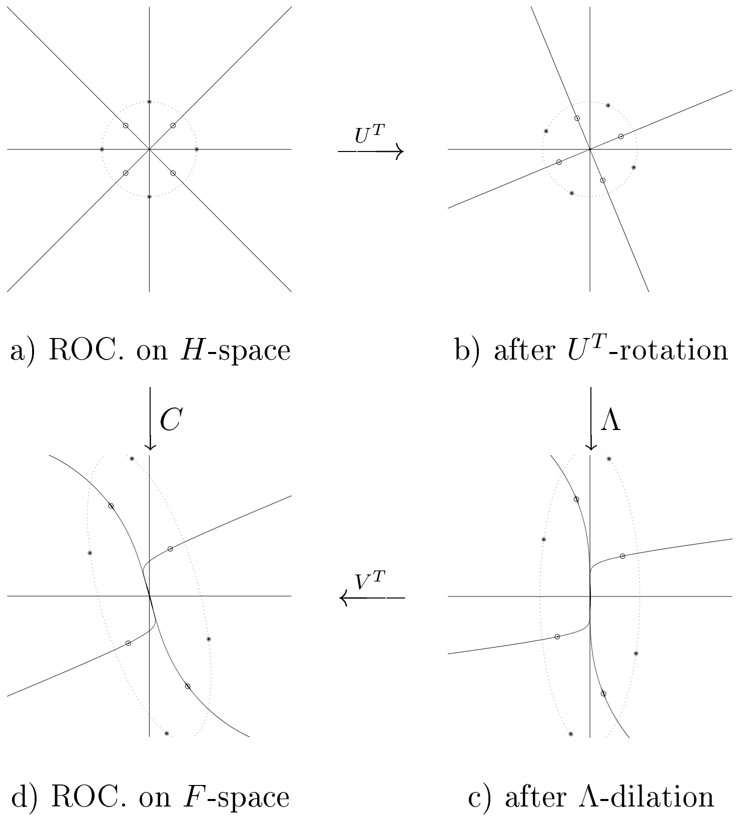

Figure 4.2: Regions of convergence of FS-CMA: ROC in Equalizer space from those in System space

4.2.2 Rotation

Since $U^T = U^{-1}$ for a unitary matrix, the rotation process can be expressed by a linear transform between the trajectory in X_1 and X_2, namely the trajectory on X_2 is given by the U^T-rotation from that on X_1.

Lemma 6 (Rotation) *Let ∇^{X_1} be a vector field on X_1 and U be a unitary matrix. Define a vector field ∇^{X_2} on X_2 as*

$$\nabla^{X_2}_{\mathbf{x}} := U^T \nabla^{X_1}_{U\mathbf{x}} \tag{4.18}$$

Then, for a local minima $\mathbf{x}_1$ under ∇^{X_1}, $\mathbf{x}_2 = U^{-1}\mathbf{x}_1$ is a local minima under ∇^{X_2}. Denote the regions of convergence $\mathbf{x}_i$ as $\mathcal{R}(\mathbf{x}_i)$ for $i = 1, 2$. It holds that

$$\mathcal{R}(\mathbf{x}_2) = U^T \mathcal{R}(\mathbf{x}_1) \tag{4.19}$$

Proof: For a given $\mathbf{x} \in \mathcal{R}(\mathbf{x}_1)$, let $\mathbf{y} = U^{-1}\mathbf{x}$. For an arbitrary small step size μ, the trajectory of $\mathbf{y}$ under ∇^{X_2} consists of:

$$\begin{aligned}
\mathbf{y}_{\text{new}} &= \mathbf{y} + \mu \nabla^{X_2}_{\mathbf{y}} && (4.20)\\
&= U^{-1}\mathbf{x} + \mu U^T \nabla^{X_1}_{UU^{-1}\mathbf{x}} && (4.21)\\
&= U^{-1}\mathbf{x} + \mu U^T \nabla^{X_1}_{\mathbf{x}} && (4.22)\\
&= U^T(\mathbf{x} + \mu \nabla^{X_1}_{\mathbf{x}}) && (4.23)\\
&= U^T(\mathbf{x}_{\text{new}}) && (4.24)
\end{aligned}$$

This implies the trajectory of $\mathbf{y}$ under ∇^{X_2} is a U^T-transformed trajectory of $\mathbf{x}$ under ∇^{X_1}, which proves the lemma. ■

This result also applies for V^T-rotation. Since a unitary matrix preserves geometrical properties such as distance and volume, the rotation part does not change the characteristics of ROCs except for their location. The most significant structural change from the multiple-replica hyper-cone structure is due to Λ-dilation along each axis. However, the contribution of U^T-rotation cannot be ignored, since the first rotation by U^T determines which ROCs will be shrunk or expanded.

4.3 Dilation

Unfortunately, the Λ-dilation part does not allow any closed form expression. We are limited to sketching a general trend by using an approximate model. Even with this simplified model, explicit and, at the same time, general description of the high dimensional deformation of ROC is not an easy task, since our naive 3-dimensional intuition doesn't work. To proceed further with the analysis, we need an assumption on U.

Assumption 3 After U^T rotation, the regions of convergence in X_2 are the rotated version of hyper-cones $\{\mathcal{R}_k\}$. We assume that for each $U^T R_k$ there is a unique upper half space $X_2^i = \{\mathbf{x} \in X_2 \mid x_i > 0\}$ such that X_2^i contains most of $U^T\mathcal{R}_k$. Under this assumption we reindex $\left\{U^T\mathcal{R}_k\right\}$ with i, i.e., $\mathcal{S}_i = U^T\mathcal{R}_k$ and X_i contains most of $\mathcal{S}_i$.

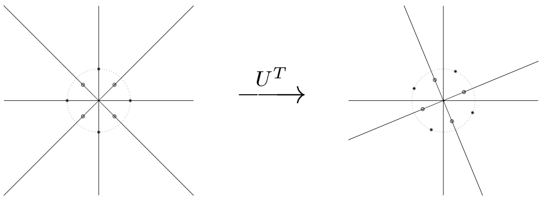

Figure 4.3: After U^T-rotation, each ROC is contained in a upper (or under) half plane

This assumption sounds obvious for $N = 2$ (Figure 4.3), but it may be too strong as $N \to \infty$. For example, consider a maximum distance d_{max} among vertices of a hyper cone on $S^{N\text{-}1}$, $d_{max} = 2\sqrt{(N-1)/N}$. As $N \to \infty$ $d_{max} \to 2$, while a minimum distance among axes on $S^{N\text{-}1}$ remains $\sqrt{2}$ (Figure 4.4). However, without this assumption further analysis becomes too complicated.

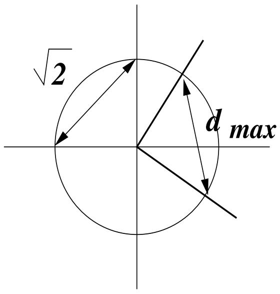

Figure 4.4: A ROC and d_{max} for 2-dimensional case

4.3.1 Simplified Vector Field Model for FS-CMA on the System Space

Now we propose a simplified vector field model which extends the idea of decomposing FS-CMA into spherical and radial terms. In the derivative

$$\frac{\partial}{\partial \mathbf{h}} J_H = (\|\mathbf{h}\|^2 - 1)\mathbf{h} + \eta_s(\|\mathbf{h}\|^2 \vec{1} - \mathbf{h}^2)\mathbf{h}, \tag{4.25}$$

where $\vec{1} = [1 \cdots 1]^T$ and $\mathbf{h}^2 = [h_0^2 \cdots h_{N\text{-}1}^2]$, we treat the radial term, $(\|\mathbf{h}\|^2 - 1)\mathbf{h}$, and the spherical term, $\eta_s(\|\mathbf{h}\|^2 \vec{1} - \mathbf{h}^2)\mathbf{h}$ separately by considering the spherical term only on the radial minima surface Φ defined in Chapter 3. This is a reasonable approach, since the spherical term remains essentially the same (except for the positive scale factor $\|\mathbf{h}\|^3$ for arbitrary radius $\|\mathbf{h}\|$). For further simplification, we replace the radial minima surface with unit sphere $S^{N\text{-}1}$. For the radial term, we ignore the magnitude of the scale factor $|\|\mathbf{h}\|^2 - 1|$, since the vector field $a\mathbf{h}$ and $\mathrm{sgn}(a)\mathbf{h}$ describe the same trajectory (the speed of a trajectory is not our concern here). In summary we define a simplified vector field model of FS-CM on the system space as

$$\nabla^H_{\mathbf{h}} = \begin{cases} \nabla^{S^{N\text{-}1}}_{\mathbf{h}} & \text{for } \|\mathbf{h}\| = 1 \\ -\mathbf{h} & \text{for } \|\mathbf{h}\| < 1 \\ \mathbf{h} & \text{for } \|\mathbf{h}\| > 1 \end{cases} \tag{4.26}$$

where $\nabla^{S^{N\text{-}1}}$ denotes the vector field on $S^{N\text{-}1}$, derived from the cost function $I_{\mathbf{h}}|_{S^{N\text{-}1}}$:

$$\nabla^{S^{N\text{-}1}}_{\mathbf{h}} = -\frac{\partial}{\partial \mathbf{h}} I_{\mathbf{h}}|_{S^{N\text{-}1}} \tag{4.27}$$

This model approximates the original one quite well, especially for $\|\mathbf{h}\| < 1$. Notice that ∇^H is not itself a vector field, since it is not smooth near $S^{N\text{-}1}$. Figure 4.5 provides a two dimensional comparison of the original vector field (a) and the proposed model (b)

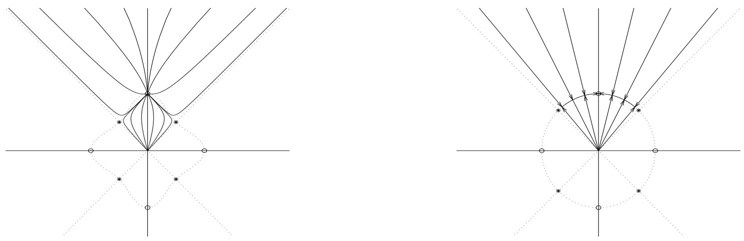

a) Trajectories of FS-CMA   b) Trajectories of simplified model

Figure 4.5: Trajectories of FS-CMA and simplified model

The benefits of this simplified vector field model are

- $S^{N\text{-}1}$, a measure zero subset of H, can be viewed as a set of initial conditions which can reach any point on H under ∇^H.

- Outside of $S^{N\text{-}1}$, ∇^H is a linear system. By a linear system we mean $\nabla^H_{\mathbf{x}} = A\mathbf{x}$ for a square matrix A [25].

Shortly, we will treat ∇^H as a linear system on most of H except for a measure zero set ($S^{N\text{-}1}$), which defines the initial conditions. In other words, ∇^H is decomposed into a spherical part (set of initial conditions with a non-linear vector field) and a radial part (linear system). For a linear system a simple expression for trajectories is possible.

Remark 6 (Trajectories of a linear system) For a linear system defined by a square matrix A, a trajectory with an initial value $\mathbf{x}_0$ at $t = 0$ is given by a simple form. Let

$$e^{tA} := \sum_{k=0}^{\infty} \frac{t^k A^k}{k!} \tag{4.28}$$

Then the trajectory of $\mathbf{x}_0$ at t under the linear system is given by

$$\mathbf{x}(t) = e^{tA}\mathbf{x}_0 \tag{4.29}$$

In particular, when $A = \Lambda$ is a diagonal matrix with $\Lambda = \mathrm{diag}(\lambda_0, ..., \lambda_{\mathrm{N\text{-}1}})$,

$$e^{t\Lambda} = \mathrm{diag}(\mathrm{e}^{\mathrm{t}\lambda_0}, ..., \mathrm{e}^{\mathrm{t}\lambda_{\mathrm{N\text{-}1}}}) \tag{4.30}$$

[see [25]]

From the above properties of ∇^H, the regions of convergence on H under ∇^H are determined by the spherical part $\nabla^{S^{N\text{-}1}}$ on $S^{N\text{-}1}$. For example, let $\mathcal{BR}_i$ be a region of convergence on $S^{N\text{-}1}$ under $\nabla^{S^{N\text{-}1}}$. By a part of the proof of Theorem 3 in Chapter 3, we know the $\{BR_i\}$ equally divide $S^{N\text{-}1}$, i.e. $\mathcal{BR}_i = S^{N\text{-}1} \cap \mathcal{R}_i$, where $\mathcal{R}_i$ is the hyper-cone defined in Theorem 3. The region of convergence under ∇^H with the set of initial conditions $\mathcal{BR}_i$ is given by

$$\left\{ e^{tI}\mathbf{b} = (e^t b_0, ..., e^t b_{N\text{-}1}) \mid \mathbf{b} \in \mathcal{BR}_i,\ t \in (-\infty, \infty) \right\} \tag{4.31}$$

which is the hyper-cone $\mathcal{R}_i$.

Under this model the U^T-rotated vector field on $X_2 = U^{-1}H$ is given as

i) For $\|\mathbf{x}\| = 1$, $\nabla_{\mathbf{x}}^{X_2} = U^T \nabla_{U\mathbf{x}}^{S^{N-1}}$

ii) For $\|\mathbf{x}\| < 1$, $\nabla_{\mathbf{x}}^{X_2} = -U^T U\mathbf{x} = -\mathbf{x}$

iii) For $\|\mathbf{x}\| > 1$, $\nabla_{\mathbf{x}}^{X_2} = U^T U\mathbf{x} = \mathbf{x}$

Or compactly,

$$\nabla_{\mathbf{x}}^{X_2} = \begin{cases} \nabla_{\mathbf{x}}^{U^{-1}S^{N-1}} & \text{for } \|\mathbf{x}\| = 1 \\ -\mathbf{x} & \text{for } \|\mathbf{x}\| < 1 \\ \mathbf{x} & \text{for } \|\mathbf{x}\| > 1 \end{cases} \tag{4.32}$$

where we denote $\nabla_{\mathbf{x}}^{U^{-1}S^{N-1}} := U^T \nabla_{U\mathbf{x}}^{H}$. One can check that the regions of convergence under ∇^{X_2} are the U^T-rotated version of hyper-cones $\{\mathcal{R}_i\}$ as shown in Lemma 6 in this chapter.

Now consider the Λ-dilated vector field ∇^{X_3} on $X_3 = \Lambda^{-1}X_2$. ∇^{X_3} is given as

i) For $\|\mathbf{x}\| = 1$, $\nabla_{\mathbf{x}}^{X_3} = \Lambda^T \nabla_{\Lambda\mathbf{x}}^{X_2}$

ii) For $\|\mathbf{x}\| < 1$, $\nabla_{\mathbf{x}}^{X_3} = -\Lambda^T \Lambda\mathbf{x} = -\Lambda^2\mathbf{x}$

iii) For $\|\mathbf{x}\| > 1$, $\nabla_{\mathbf{x}}^{X_2} = \Lambda^T \Lambda\mathbf{x} = \Lambda^2\mathbf{x}$

(For a diagonal matrix $\Lambda^T = \Lambda$.) Or compactly,

$$\nabla_{\mathbf{x}}^{X_3} = \begin{cases} \nabla_{\mathbf{x}}^{\Lambda^{-1}X_2} & \text{for } \|\Lambda^{-1}\mathbf{x}\| = 1 \\ -\Lambda^2\mathbf{x} & \text{for } \|\Lambda^{-1}\mathbf{x}\| < 1 \\ \Lambda^2\mathbf{x} & \text{for } \|\Lambda^{-1}\mathbf{x}\| > 1 \end{cases} \tag{4.33}$$

where we denote $\nabla_{\mathbf{x}}^{\Lambda^{-1}X_2} := \Lambda^T \nabla_{\Lambda\mathbf{x}}^{S^{N-1}}$. Similarly to the ∇^H, ∇^{X_3} is a linear system outside of the measure zero set $\Lambda^{-1}S^{N-1}$ which can be viewed as a set of initial conditions of the linear system, and the regions of convergence under ∇^{X_3} are well determined by the regions of convergence on the $\Lambda^{-1}S^{N-1}$ under $\nabla^{\Lambda^{-1}X_2}$.

Let $\mathcal{BS}_i$ denote a region of convergence on $\Lambda^{-1}S^{N-1}$ and $\mathcal{S}_i$ denote the region of convergence containing $\mathcal{BS}_i$. Then by Remark 6 in this chapter $\mathcal{S}_i$ is given as

$$\mathcal{S}_i = \left\{ e^{t\Lambda^2}\mathbf{b} \mid \mathbf{b} \in \mathcal{BS}_i,\ t \in (-\infty, \infty) \right\}, \tag{4.34}$$

where $e^{t\Lambda^2} = \mathrm{diag}(\mathrm{e}^{\mathrm{t}\lambda_0^2}, ..., \mathrm{e}^{\mathrm{t}\lambda_{\mathrm{N-1}}^2})$.

In order to characterize the regions of convergence $\{\mathcal{S}_i\}$, we need to figure out the structure of $\mathcal{BS}_i$, which will be referred to as the *spherical effect of dilation*, and the properties of the trajectories $\left\{ e^{t\Lambda^2}\mathbf{b} \right\}$, which will be referred to as the *radial effect of dilation*. In the following sections we will investigate these effects separately. The most interesting result on the regions of convergence comes from the radial effect.

4.3.2 Spherical Effect of Dilation

In this section we attempt to understand the structure of $\mathcal{BS}_i$ on $\Lambda^{-1}S^{N-1}$. If we can develop a closed form expression for $\mathcal{BS}_i$, a quite explicit approximation for ROC will follow. However, since $\nabla^{\Lambda^{-1}S^{N-1}}$ is a non-linear system, defining $\mathcal{BS}_i$ with a closed form is hopeless. In this section we will trace the deformation of $\mathcal{BS}_i$ from $U^T\mathcal{BR}_i$ and present a low dimensional example.

In order to delineate $\mathcal{BS}_i$, which is obtained from $U^T\mathcal{BR}_i$ on S^{N-1} via Λ-dilation, we need to manipulate a function (and its derivative) between manifolds, i.e. $\Lambda^{-1}: S^{N-1} \to \Lambda^{-1}S^{N-1}$ and the Λ-dilation $\nabla^{S^{N-1}} \to \nabla^{\Lambda^{-1}S^{N-1}}$. In differential geometry, this task has been achieved by a set of local coordinates which patches together a manifold [3]. For example, define a set of local coordinates on $S^{N\text{-}1}$ as

$$S_i^{N\text{-}1} = \left\{\mathbf{h} \in S^{N\text{-}1} \mid h_i > 0\right\} \text{ for } i = 0, ..., N\text{-}1, \tag{4.35}$$

$$\pi_i(\mathbf{x}) = (x_0, ..., x_{i-1}, x_{i+1}, ..., x_{N\text{-}1}) \text{ is a projection map} \tag{4.36}$$

Then $S^{N\text{-}1} = \cup_i S_i^{N\text{-}1}$, and each $S_i^{N\text{-}1}$ is identified with a open set of $\mathbb{R}^{N\text{-}1}$ via the local coordinate π_i on $S_i^{N\text{-}1}$. Similarly, we consider the following set of local coordinates on $\Lambda^{\text{-}1}S^{N\text{-}1}$

$$\Lambda^{\text{-}1}S_i^{N\text{-}1} \qquad \text{for } i = 0, ..., N\text{-}1, \tag{4.37}$$

$$\pi_i(\mathbf{x}) = (x_0, ..., x_{i-1}, x_{i+1}, ..., x_{N\text{-}1}) \text{ is a projection map} \tag{4.38}$$

Define $\Lambda_i := \Lambda \circ \pi_i$, i.e.

$$\Lambda_i = \text{diag}(\lambda_0, .., \lambda_{\text{i}-1}, \lambda_{\text{i}+1}, .., \lambda_{\text{N-1}}) \tag{4.39}$$

Then $\Lambda^{\text{-}1} : S^{N\text{-}1} \to \Lambda^{\text{-}1}S^{N\text{-}1}$ is represented by $\Lambda_i^{\text{-}1} : \mathbb{R}^{N\text{-}1} \to \mathbb{R}^{N\text{-}1}$ for $i = 0, ..., N\text{-}1$.

$$\begin{array}{ccc} S^{N\text{-}1} & \xrightarrow{\Lambda^{\text{-}1}} & \Lambda^{\text{-}1}S^{N\text{-}1} \\ \Big\downarrow \pi_i & & \Big\downarrow \pi_i \\ \mathbb{R}^{N\text{-}1} & \xrightarrow{\Lambda_i^{\text{-}1}} & \mathbb{R}^{N\text{-}1} \end{array} \tag{4.40}$$

Furthermore, the Λ-dilation $\nabla^{S^{N\text{-}1}} \to \nabla^{\Lambda^{\text{-}1}S^{N\text{-}1}}$ on $S^{N\text{-}1}$ is also represented by Λ_i-dilation $\nabla^{\mathbb{R}^{N\text{-}1}} \to \nabla^{\Lambda^{\text{-}1}\mathbb{R}^{N\text{-}1}}$ on $\mathbb{R}^{N\text{-}1}$ for $i = 0, ..., N\text{-}1$.

$$\begin{array}{ccc} \nabla^{S^{N\text{-}1}} & \xrightarrow{\Lambda} & \nabla^{\Lambda^{\text{-}1}S^{N\text{-}1}} \\ \Big\downarrow d\pi_i & & \Big\downarrow d\pi_i \\ \nabla^{\mathbb{R}^{N\text{-}1}} & \xrightarrow{\Lambda_i} & \nabla^{\Lambda_i^{\text{-}1}\mathbb{R}^{N\text{-}1}} \end{array} \tag{4.41}$$

where $\nabla^{\mathbb{R}^{N-1}}$ is given by $d\pi_i(\nabla^{S^{N-1}})$, i.e.

$$\nabla_{\hat{\mathbf{h}}}^{\mathbb{R}^{N-1}} = -\frac{\partial}{\partial \hat{\mathbf{h}}}(I_{\mathbf{h}} \circ \pi_i) = -\frac{\partial}{\partial \hat{\mathbf{h}}} I_{\hat{\mathbf{h}}} \tag{4.42}$$

($\frac{\partial}{\partial \hat{\mathbf{h}}} I_{\hat{\mathbf{h}}}$ was defined in Theorem 3 in Chapter 3.) In order to investigate the structure of $\mathcal{BS}_i$, we examine $\pi_j(\mathcal{BS}_i)$ for $j = 0, .., N$-1, which is obtained from $\pi_j(U^T \mathcal{BR}_i)$ via Λ_j-dilation.

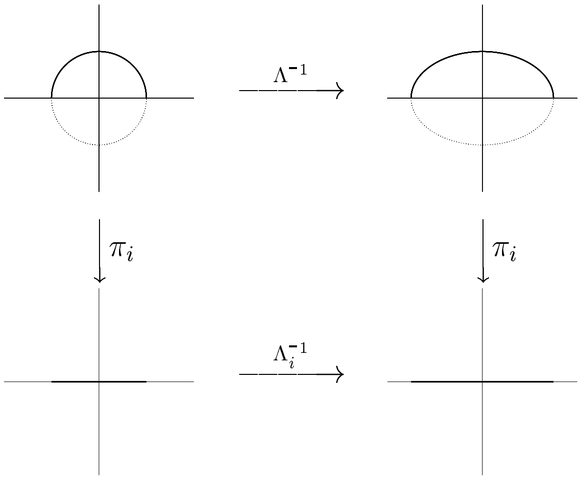

Figure 4.6: Example of local coordinates

Now let us examine the Λ_i-dilation effects on $\mathbb{R}^{N-1}$ closely. Let $\mathbf{x} \in \mathbb{R}^{N-1}$ and $\mathbf{y} = \Lambda_i^{-1}\mathbf{x}$. The trajectory of $\mathbf{y}$ under $\nabla^{\Lambda_i^{-1}\mathbb{R}^{N-1}}$ consists of:

$$\begin{aligned}
\mathbf{y}\text{new} &= \mathbf{y} + \mu \nabla_{\mathbf{y}}^{\Lambda_i^{-1}\mathbb{R}^{N-1}} && (4.43)\\
&= \Lambda_i^{-1}\mathbf{x} + \mu \Lambda_i^T \nabla_{\Lambda_i \Lambda_i^{-1}\mathbf{x}}^{\mathbb{R}^{N-1}} && (4.44)\\
&= \Lambda_i^{-1}\mathbf{x} + \mu \Lambda_i^T \nabla_{\mathbf{x}}^{\mathbb{R}^{N-1}} && (4.45)\\
&= \Lambda_i^{-1}(\mathbf{x} + \mu \Lambda_i \Lambda_i^T \nabla_{\mathbf{x}}^{\mathbb{R}^{N-1}}) && (4.46)\\
&= \Lambda_i^{-1}(\mathbf{x} + \mu \Lambda_i^2 \nabla_{\mathbf{x}}^{\mathbb{R}^{N-1}}) && (4.47)
\end{aligned}$$

Since $\Lambda_i^T\Lambda_i \neq I$, Λ_i-dilation can be viewed as a concatenation of the following two processes.

- Non-linear deformation ($\Lambda_i^2\nabla_{\mathbf{x}}^{\mathbb{R}^{N-1}}$)
- Linear transformation (Λ_i^{-1})

Unfortunately, a closed form description of the non-linear deformation is not feasible even for simple 2 and 3 dimensional cases. We can only describe some topological characteristics of this deformation: First, since $\lambda_i^2 > 0$ for $i = 0, .., N$-1, the stationary points under $\Lambda_i^2\nabla^{\mathbb{R}^{N-1}}$ and $\nabla^{\mathbb{R}^{N-1}}$ are the same. Second, a trajectory under $\Lambda_i^2\nabla^{\mathbb{R}^{N-1}}$ is similar to the trajectory under $\nabla^{\mathbb{R}^{N-1}}$, but becomes more convex. Figure 4.7 illustrates these properties.

On the other hand, the effect of Λ_i^{-1} transformation is straightforward. Let A be a region in $\mathbb{R}^{N-1}$. Then for the volume of $\Lambda_i^{-1}A$, the following holds

$$\mathrm{Vol}\,(\Lambda_i^{-1}A) = \det\Lambda_i \mathrm{Vol}\,(A) = \lambda_i \det\Lambda^{-1}\mathrm{Vol}\,(A) \tag{4.48}$$

This implies that any region in S_i^{N-1} confined by the trajectories of $\nabla^{S^{N-1}}$ is deformed (non-linearly) and expended proportional to the λ_i.

In summary, $\mathcal{BS}_i$ is a connected partition of $\Lambda^{-1}S^{N-1}$, and Vol $\pi_i(\mathcal{BS}_j)$ is expanded from Vol$\pi_i(\mathcal{BR}_j)$ proportional to λ_i, if we can ignore the Λ_i^2-deformation. In particular, when each $\mathcal{BR}_j$ is contained in S_i^{N-1} for some i, we can say $\mathrm{Vol}\,\pi_i\mathcal{BS}_i > \mathrm{Vol}\,\pi_j\mathcal{BS}_j$ for $\lambda_i > \lambda_j$.

Example 5 Let

$$U = \begin{bmatrix} \cos(\pi/8) & -\sin(\pi/8) & 0 \\ \sin(\pi/8) & \cos(\pi/8) & 0 \\ 0 & 0 & 1 \end{bmatrix}, \quad \Lambda = \begin{bmatrix} \lambda & 0 & 0 \\ 0 & 1 & 0 \\ 0 & 0 & 1 \end{bmatrix} \tag{4.49}$$

We focus on the region of convergence of $(0, 0, 1)$ on $S^{N\text{-}1}$. Figure 4.7-a) shows the region of convergence on $S^{N\text{-}1}$ in H and b) shows the U^T-rotated version. Figure c) shows $\pi_3(\mathcal{BS}_3)$ under $\nabla^{\mathbb{R}^2}$, and Figure d) and e) show the regions of convergence under $\Lambda_3^2\nabla^{\mathbb{R}^2}$ for different λ values.

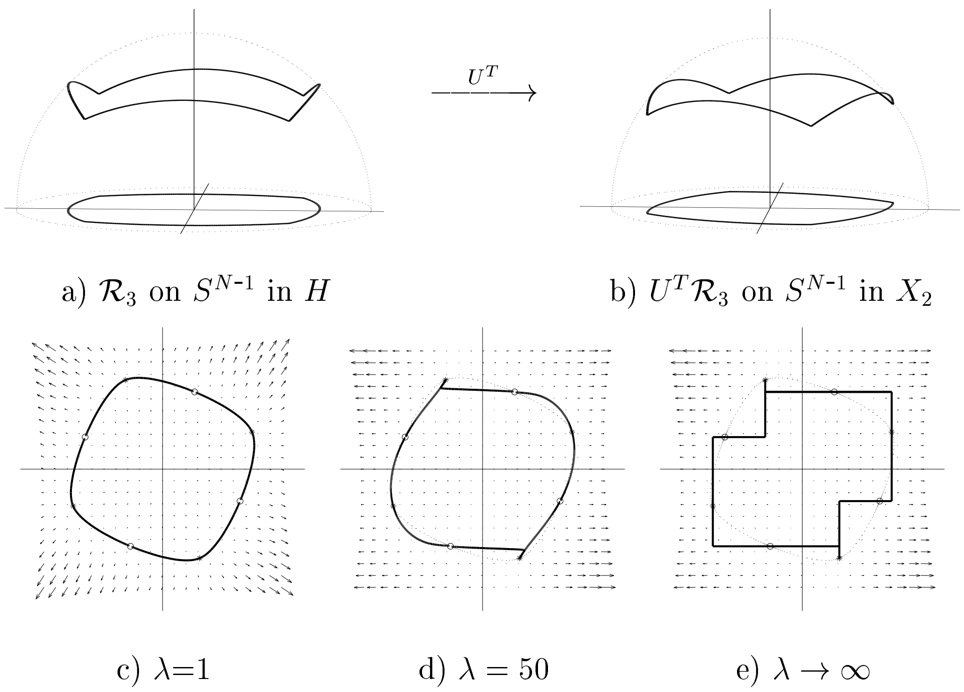

Figure 4.7: Deformation of trajectory due to $\Lambda_i^2\nabla^{\mathbb{R}^{N\text{-}1}}$ with various Λ

4.3.3 Radial Effect of Dilation

We are interested in the asymptotic structure of $\mathcal{S}_i$ near the origin and far from the origin. $\mathcal{S}_i$ consists of the trajectories

$$\mathbf{b}(t) = [e^{t\lambda_0^2}b_0 \cdots e^{t\lambda_{N\text{-}1}^2}b_{N\text{-}1}], \quad \mathbf{b}(0) = \mathbf{b} \in \mathcal{BS}_i \tag{4.50}$$

As $t \to -\infty$ (i.e. near the origin) or $t \to \infty$ (i.e. far from the origin), the disparity of the singular values $(\lambda_0, ..., \lambda_i)$ dominates the behavior of $\mathbf{b}(t)$, and the actual value of $\mathbf{b}$ becomes less important: as $t \to -\infty$,

$$e^{t\lambda_0^2} \ll e^{t\lambda_1^2} \ll \cdots \ll e^{t\lambda_{N\text{-}2}^2} \ll e^{t\lambda_{N\text{-}1}^2} \tag{4.51}$$

For a fixed t', the set $\{\mathbf{b}(t')|\mathbf{b} \in \mathcal{BS}_i\}$ can be viewed as a set spanned by $\mathcal{BS}_i$ with the basis

$$[e^{t'\lambda_0^2}, \cdots, e^{t'\lambda_i^2}, \cdots, e^{t'\lambda_{N\text{-}1}^2}] \tag{4.52}$$

Since $\mathcal{BS}_i$ is a connected subset of a hyper-ellipse ($\Lambda^{\text{-}1}S^{N\text{-}1}$), $\{\mathbf{b}(t')|\mathbf{b} \in \mathcal{BS}_i\}$ is also a connected subset of a hyper-ellipse, and the i-th coordinate shrinks much more due to $e^{t'\lambda_i^2}$ than the j-th coordinate for $i < j$. Define $\mathcal{S}_i(t) = \{\mathbf{b}(t) \mid \mathbf{b} \in \mathcal{BS}_i\}$. Then $\mathcal{S}_i(t) \subset S_i^{N\text{-}1}$ if $\mathcal{S}_i \subset {S^{N\text{-}1}}_i$, and

$$\mathrm{Vol}\,\pi_i(\mathcal{S}_i(t)) = e^{-t\lambda_i^2} \prod_{k=0}^{N\text{-}1} e^{t\lambda_k^2} c_i \tag{4.53}$$

where $\mathbf{c}_i > 0$ is a constant depending on $\mathcal{BS}_i$ bounded by $\prod_{k \neq i}[\max(b_k) - \min(b_k)]_{\mathbf{b} \in \mathcal{BS}_i}$. For a small enough t' the difference of $\{c_i\}$ term can be ignored, and it holds for all $t < t'$ that

$$\mathrm{Vol}\,\pi_1(\mathcal{S}_1(t)) \gg \mathrm{Vol}\,\pi_2(\mathcal{S}_2(t)) \gg \cdots \gg \mathrm{Vol}\,\pi_{N\text{-}1}(\mathcal{S}_{N\text{-}1}(t)) \tag{4.54}$$

Furthermore, $\mathrm{Vol}\,\pi_i(\mathcal{S}_i(t)) \gg \mathrm{Vol}\,\pi_i(\mathcal{S}_i(t'))$ for $t > t'$, and by choosing a proper t we can make the relative difference $\mathrm{Vol}\,\pi_i(\mathcal{S}_i(t))/\mathrm{Vol}\,\pi_j(\mathcal{S}_j(t))$ as large as we want. Figure 4.8 illustrates (4.54).

Denote $\alpha S^{N\text{-}1}$ as a sphere with radius α, $\{\mathbf{x} \mid \|\mathbf{x}\| = \alpha\}$, and $\mathcal{DS}_i^\alpha$ as the intersection of $\mathcal{S}_i$ with $\alpha S^{N\text{-}1}$, i.e.

$$\mathcal{DS}_i^\alpha := \mathcal{S}_i \cap \alpha S^{N\text{-}1} \tag{4.55}$$

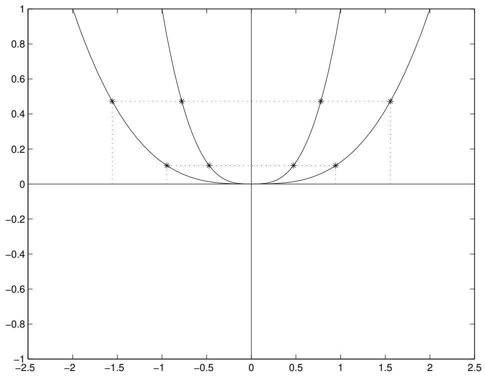

Figure 4.8: Radial effect of Dilation

From our assumption that $\mathcal{S}_i \subset S_i^{N\text{-}1}$, $\mathrm{Vol}\,\pi_i(\mathcal{S}_i(t))$ is proportional to the volume of $\mathcal{DS}_i^\alpha$ with $\alpha = \min\{\mathbf{b}(t)_i \mid \mathbf{b} \in \mathcal{BS}_i\}$. From (4.51) we have $\mathrm{Vol}\,\mathcal{DS}_i^\alpha : \mathrm{Vol}\,\mathcal{DS}_j^\alpha = \mathrm{Vol}\,\pi(\mathcal{S}_i(t)) : \mathrm{Vol}\,\pi(\mathcal{S}_j(t'))$ with $t > t'$. Therefore, finally we have

$$\mathrm{Vol}\,\mathcal{DS}_0^\alpha \gg \mathrm{Vol}\,\mathcal{DS}_1^\alpha \gg \cdots \gg \mathrm{Vol}\,\mathcal{DS}_{N\text{-}1}^\alpha \tag{4.56}$$

as $\alpha \to 0$. Similarly, we can show as $\alpha \to \infty$

$$\mathrm{Vol}\,\mathcal{DS}_0^\alpha \ll \mathrm{Vol}\,\mathcal{DS}_1^\alpha \ll \cdots \ll \mathrm{Vol}\,\mathcal{DS}_{N\text{-}1}^\alpha \tag{4.57}$$

We summarize this result as a theorem.

Theorem 5 (Regions of Convergence of FS-CMA) Let the channel convolution matrix C of a $T/2$ spaced channel $\mathbf{c}$ satisfy Assumption 3 in this chapter, and have strict singular value disparity, i.e. $\lambda_0 > \lambda_1 > \cdots > \lambda_{N\text{-}1}$. Then there are $2N$ regions of convergence $\{\pm\mathcal{S}_i\}$ for the $2N$ local minima, where $-\mathcal{S}_i := \{-\mathbf{x} \mid \mathbf{x} \in \mathcal{S}_i\}$. Each $\mathcal{S}_i$ is an exponential hyper-cone containing a local minimum in the sense of (4.34). Let $\mathcal{DS}_i^\alpha$ denote the intersection of $\mathcal{S}_i$ and a sphere of radius α. Then, we can label $\{\mathcal{S}_i\}$ such that as $\alpha \to 0$ (near the origin)

$$\mathrm{Vol}\,\mathcal{DS}_0^\alpha > \mathrm{Vol}\,\mathcal{DS}_1^\alpha > \cdots > \mathrm{Vol}\,\mathcal{DS}_{N\text{-}1}^\alpha \tag{4.58}$$

and as $\alpha \to \infty$ (far from the origin)

$$\mathrm{Vol}\, \mathcal{DS}_0^\alpha < \mathrm{Vol}\, \mathcal{DS}_1^\alpha < \cdots < \mathrm{Vol}\, \mathcal{DS}_{N\text{-}1}^\alpha \tag{4.59}$$

4.3.4 Equalizer Norm and Singular Value Disparity

In this section we try to associate the norm of a CM solution with the asymptotic property of the volume of its region of convergence in Theorem 5.

Case I (Ideal Case)

The local minima after U^T-rotation are given by $\left\{\mathbf{u}_i = U^T \delta_i\right\}$, i.e. the row vectors of U^T. If for each $\mathbf{u}_i$, one of the coefficients, say $k(\mathbf{u}_i)$, dominates other coefficients, and $\mathcal{R}(\mathbf{u}_i) \subset S_k^{N\text{-}1}$, for example $U = I$, then we can apply Theorem 5 with $\|\Lambda^{\text{-}1}\mathbf{u}_i\| < \|\Lambda^{\text{-}1}\mathbf{u}_j\|$ for $\lambda_{k(\mathbf{u}_i)} > \lambda_{k(\mathbf{u}_j)}$. This assumption was implicitly used in [6]. In this case we have:

Property 1 (Noise gain and Region of Convergence)

- Near the origin, the region of convergence of a CM solution with small equalizer norm (or noise gain) expands exponentially, while that of the CM solution with large noise gain shrinks.
- Far from the origin, the region of convergence of the CM solution with large equalizer norm (or noise gain) expands exponentially, while that of the CM solution with small noise gain shrinks.

However, this result relies on a possibly too strong assumption. For example, if U is a Hadamard matrix, where every coefficient of $\mathbf{u}_i$ is one of $\left\{1/\sqrt{N}, -1/\sqrt{N}\right\}$, we have $\|\Lambda^{\text{-}1}\mathbf{u}_i\| = \|\Lambda^{\text{-}1}\mathbf{u}_j\| = \sum \lambda_i^{-2}/N$ for all i, j. Therefore, the relation between the equalizer norm and the eigenvalue disparity is somewhere between the two extreme cases, identity matrix and Hadamard matrix, depending on U. As shown in Chapter 2, the structure of U is determined by the channel response in the time domain (therefore, the two extreme cases are very unlikely).

Case II ($T/2$-spaced Model)

Let us consider a special case of U and Λ:

$$U = \begin{pmatrix} U_0 & 0 \\ 0 & U_1 \end{pmatrix}, \quad \Lambda = \begin{pmatrix} \lambda_0 I_0 & 0 \\ 0 & \lambda_1 I_1 \end{pmatrix} \tag{4.60}$$

where U_0 and U_1 are $n \times n$ and $N-n \times N-n$ unitary matrixes respectively, I_0 and I_1 are $n \times n$ and $N-n \times N-n$ identity matrixes, and $\lambda_0 > \lambda_1$. Let $H = H_0 \oplus H_1$, where $H_0 \cong \mathbb{R}^n$ and $H_1 \cong \mathbb{R}^{N-n}$. A region of convergence $\mathcal{R}(\delta_i)$ for $i \leq n$ is a subset of $H_0^i \oplus H_1$, where $H_0^i = \{\mathbf{h} \in H_0 \mid h_i > 0\}$. After U^T transformation, $U^T\mathcal{R}(\delta_i) \subset U^T(H_0^i \oplus H_1) = U_0^T(H_0^i) \oplus H_1$. Thus, we have

$$U^T\mathcal{R}(\delta_i) \subset H_0^{k_1} \oplus H_1, \quad \text{or} \quad U^T\mathcal{R}(\delta_i) \subset \bigcup_{k_i=k_1}^{k_m} H_0^{k_i} \oplus H_1 \tag{4.61}$$

Denote $\mathcal{S}_i$ as the region of convergence of $\mathbf{d}_i = \Lambda^{-1}U^T\delta_i$ after Λ-dilation, and $\mathcal{DS}_i^\alpha = \mathcal{S}_i \cap \alpha S^{N-1}$. (4.61) implies that $\mathrm{Vol}\,\pi_k(\mathcal{S}_i(t))$ for $k = k_1, ..., k_m$ represent the volume of $\mathcal{S}_i(t)$ for $i \leq n$. Since $\lambda_i = \lambda_j$ for $i, j \leq n$ and $\lambda_i > \lambda_j$ for $i \leq n$, and $j > n$, by applying the argument of Theorem 5 we have for $i \leq n$ and $j > n$

$$\mathrm{Vol}\,(\mathcal{DS}_i^\alpha) < \mathrm{Vol}\,(\mathcal{DS}_j^\alpha), \quad \text{as } \alpha \to 0 \tag{4.62}$$

$$\mathrm{Vol}\,(\mathcal{DS}_i^\alpha) > \mathrm{Vol}\,(\mathcal{DS}_j^\alpha), \quad \text{as } \alpha \to \infty \tag{4.63}$$

Furthermore, the noise gain of the CM solution is given by

$$\|\mathbf{d}_i\| = \|\Lambda^{-1}U^T\delta_i\| = \begin{cases} \lambda_0^{-1} & \text{for } i \leq n \\ \lambda_1^{-1} & \text{for } i > n \end{cases} \tag{4.64}$$

Therefore, we have the same result of Property 1.

This U and Λ model reflects the the structure of $T/2$-spaced channel matrix C quite well, especially for the SPIB database provided on the Rice University web site (http://spib.rice.edu/spib/select_comm.html). As shown in Chapter 2, when N is large, half of the singular values of $C = U\Lambda V^T$ are almost zero and each row vector of U is given by the normalized summation of $\mathbf{c}_{even} \star \mathbf{v}_{ieven}$ and $\mathbf{c}_{odd} \star \mathbf{v}_{iodd}$, where $\mathbf{v}_i$ is the i-th row vector of V. We can approximate $\Lambda = \mathrm{diag}(\lambda_0 \mathrm{I_n}, \lambda_1 \mathrm{I_{N-n}})$. If $\mathbf{c}$ has a particular structure with delays and some peaks and small post cursor values as in Figure 4.9 a), each u_i has a structure determined by $\mathbf{c}$ and $\mathbf{v}_i$. Since $\mathbf{c}_{odd} \approx \mathbf{c}_{even}$ and $\mathbf{v}_{ieven} \approx \mathbf{v}_{iodd}$ for $i = 0, ...n$, $\mathbf{u}_i = k_i(\mathbf{c}_{even} \star \mathbf{v}_{ieven} + \mathbf{c}_{odd} \star \mathbf{v}_{iodd})$ must have also small precursor values and small post cursor values for $i = 0, ..., n$, i.e., U can be approximated by a unitary matrix of the form:

$$\left(\begin{array}{c|c} 0 & \\ A & B \\ 0 & \end{array}\right) \tag{4.65}$$

By rearranging the coordinates of H, we can locate A on the top of the matrix without rearranging Λ, and finally we have

$$U \approx \begin{pmatrix} U_0 & 0 \\ 0 & U_1 \end{pmatrix} \tag{4.66}$$

where U_0 and U_1 are unitary, and U_0 is an $m \times m$ matrix with $m \approx n$.

Example 6 In this example we provide a simulation result supporting the above argument. The $T/2$-spaced channel $\mathbf{c}$ is the down-sampled (factor 5) real part of the SPIB microwave channel 3 (chan3.mat.bin). Figure 4.9-a) shows the channel response in the time domain. The singular value distribution is shown in Figure b). Figure c) shows the noise gain of CM solution $\|\mathbf{d}_i\|$, $\mathbf{d}_i = C^{-1}\delta_i = V\Lambda^{-1}U^T\delta_i$, in dB scale. In Figure d), where the noise gain is plotted in magnitude scale, we zoom the CM solution with small noise gain, and we can observe that the distribution of noise gain corresponds to the singular value distribution. Figure e) shows the structure of U.

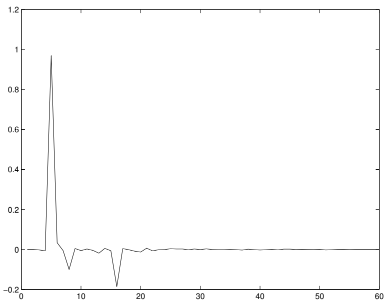

a) channel response

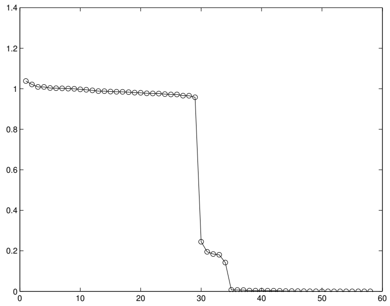

b) Singular value

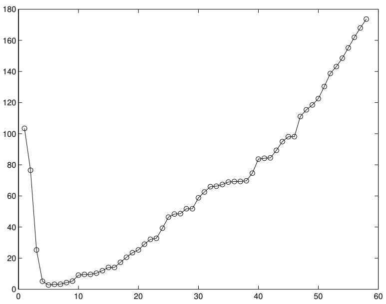

c) Noise gain (dB scale)

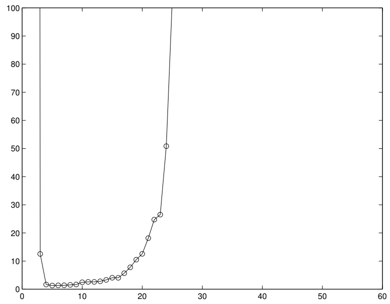

d) Noise gain (zoomed and magnitude scale)

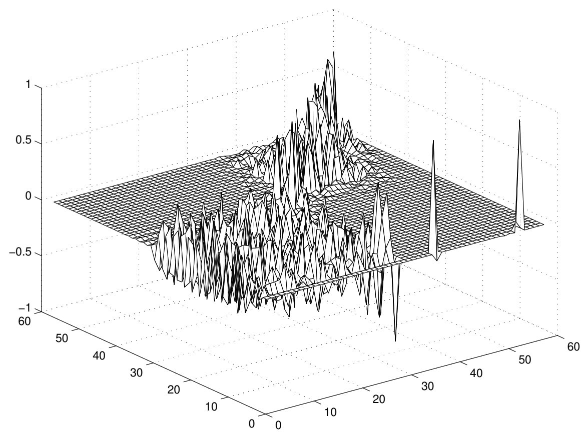

e) The structure of U

Figure 4.9: Structure of a $T/2$-spaced channel

Chapter 5

Analysis of the Robustness of Fractionally Spaced CMA

In this chapter we attempt to analyze the robustness properties of CMA. It has been observed that the performance of CMA is insensitive to the initialization with a certain technique called "spike initialization", and still performs satisfactorily in severe environments including undermodelling and channel noise. Due to mathematical difficulty, we focus on only the perfectly modeled case and show that all bad local minima can disappear as noise increases. On the other hand, we provide heuristic arguments validating the performance of the spike initialization with simulation results showing that spike initialization tends to achieve only good local minima in the absence of noise. These two results together explain the robustness of CMA under noise and spike initialization.

5.1 CMA Local Minima Location in the Presence of Noise

The previous studies on CM solutions in the presence of noise have been restricted to a local analysis, as in [37], or for small noise power such that a first order approximation is feasible [7]. The main reason for these partial analyses is the complexity of the CMA cost function. Here we present a global analysis on the CM solution location, for which the main idea was presented in [4]. Although we do not describe the exact location of CM solutions, we establish a trade-off between noise gain and ISI reduction.

5.1.1 Noise gain and ISI

The CMA cost function in the presence of noise is given by Lemma 3:

$$\begin{aligned} 4J_H &= \gamma\|\mathbf{h}\|^4 + 2\kappa_w\sigma^2\|\mathbf{h}\|^2\|C^{-1}\mathbf{h}\|^2 + \kappa_w\sigma^4\|C^{-1}\mathbf{h}\|^4 \\ &\quad -2\gamma(\|\mathbf{h}\|^2 + \sigma^2\|C^{-1}\mathbf{h}\|^2) + \gamma^2 \\ &\quad +\eta_s I_{\mathbf{h}}. \end{aligned} \tag{5.1}$$

For non-zero σ^2 the radial term ($\|\mathbf{h}\|$) suffers from a spherical disturbance due to C^{-1}, while the spherical term $I_{\mathbf{h}}$ remains unchanged. As σ^2 increases, the $\|C^{-1}\mathbf{h}\|$ ($= \|\mathbf{f}\|$) terms dominate, and the radial term is no longer symmetrical (Figure 5.1-a)). In Figure 5.1-c), we can observe that $\|C^{-1}\mathbf{h}\|$, which is the noise gain of equalizer $\|\mathbf{f}\|$, dominates over the ISI term $I_{\mathbf{h}}$, and the CMA cost function has only two local minima essentially in the location where the noise gain is minimized.

Figure 5.1 suggests that the equation of the CM solution contains a trade-off between the noise gain ($\|C^{-1}\mathbf{h}\|$) and ISI ($I_{\mathbf{h}}$). In this section, we will investigate the relation between the noise gain of the CM solution and ISI.

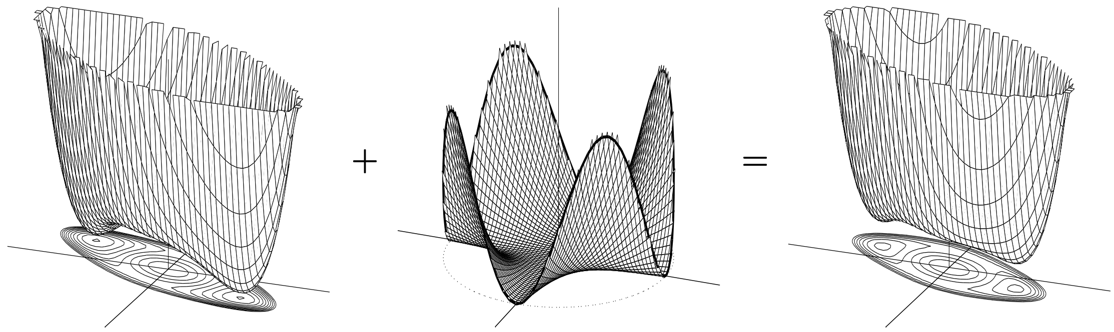

a) radial term b) spherical term c) cost function

Figure 5.1: CMA cost function in the presence of noise

Let us consider the CM cost function restricted to $\|\mathbf{h}\| = r$ for a fixed $r > 0$.

$$J|_{rS^{N\text{-}1}} = 2\sigma^2 r^2(\kappa_w r^2 - \gamma)\|C^{\text{-}1}\mathbf{h}\|^2_{S^{N\text{-}1}} + \kappa_w \sigma^4 r^4 \|C^{\text{-}1}\mathbf{h}\|^4_{S^{N\text{-}1}} + r^4 \eta_s I_{\mathbf{h}}|_{S^{N\text{-}1}} + c \tag{5.2}$$

where c is a constant depending on r. $J|_{rS^{N\text{-}1}}$ can be viewed as a function on the unit sphere $S^{N\text{-}1}$. Let $C^{\text{-}1} = V\Lambda^{\text{-}1}U^T$, then for $\mathbf{x} = U\mathbf{h}$, $\|C^{\text{-}1}\mathbf{h}\| = \sum \lambda_i^{\text{-}2} x_i^2$. With this coordinate change,

$$J|_{rS^{N\text{-}1}} = 2\sigma^2 r^2(\kappa_w r^2 \text{-} \gamma)\|\Lambda^{\text{-}1}\mathbf{x}\|^2_{S^{N\text{-}1}} + \kappa_w \sigma^4 r^4 \|\Lambda^{\text{-}1}\mathbf{x}\|^4_{S^{N\text{-}1}} + r^4 \eta_s I_{U^T\mathbf{x}}|_{S^{N\text{-}1}} + c \tag{5.3}$$

The differential property (minima or maxima) of $J|_{rS^{N\text{-}1}}$ is completely determined by the set of N local coordinates $\{\mathbf{x}^i\}$ on $\mathbb{R}^{N\text{-}1}$ for $i = 0, ..., N\text{-}1$: we can view $J_{rS^{N\text{-}1}}$ as a set of cost functions $\{J(\mathbf{x}^i)\}$ with the following identification

$$\mathbf{x}^i := [x_0, ..., x_{i-1}, x_{i+1}, ..., x_{N\text{-}1}] \mapsto [x_0, .., x_{i-1}, \sqrt{1 \text{-} \sum_{k \neq i} x_k^2},\ x_{i+1}, ..., x_{N\text{-}1}]^T \tag{5.4}$$

(Since $J(\mathbf{x}) = J(-\mathbf{x})$, it is enough to consider only the half upper sphere for each $\mathbf{x}^i$.) Notice that

$$\|\Lambda^{\text{-}1}\mathbf{x}^i\|^2 = \lambda_i^{\text{-}2} + \sum_{i \neq k} (\lambda_k^{\text{-}2} - \lambda_i^{\text{-}2}) x_k^2 \tag{5.5}$$

Furthermore, $J(\mathbf{x})$ has a stationary point, if and only if one of the $J(\mathbf{x}_i)$ has a stationary point. $\frac{\partial}{\partial \mathbf{x}^i} J|_{rS^{N-1}}$ is given by

$$\frac{\partial}{\partial \mathbf{x}^i} J|_{rS^{N-1}} = 4\sigma^2 r^2 \left(\kappa_w r^2 (1 + \sigma^2 \|\Lambda^{-1}\mathbf{x}^i\|^2) - \gamma\right) \Lambda_i^{-1}\mathbf{x}^i + r^4 \eta_s \frac{\partial}{\partial \mathbf{x}^i} I_{U^T\mathbf{x}^i} \tag{5.6}$$

where

$$\Lambda_i^{-1} = \begin{pmatrix} \lambda_0^{-2} - \lambda_i^{-2} & & 0 \\ & \ddots & \\ 0 & & \lambda_{N-1}^{-2} - \lambda_i^{-2} \end{pmatrix} \tag{5.7}$$

Setting (5.6) to zero yields

$$4\sigma^2 \left((\kappa_w (1 + \sigma^2 \|\Lambda^{-1}\mathbf{x}^i\|^2) - \frac{\gamma}{r^2} \right) \Lambda_i^{-1}\mathbf{x}^i + \eta_s \frac{\partial}{\partial \mathbf{x}^i} I_{U^T\mathbf{x}^i} = 0 \tag{5.8}$$

Since $\eta_s \frac{\partial}{\partial \mathbf{x}^i} I_{U^T\mathbf{x}^i}$ is a bounded function, for relatively large r^2, for example $r^2 = 1$, the above equation is a form of

$$\sigma^2 \Lambda_i^{-1}\mathbf{x}^i + \epsilon = 0, \tag{5.9}$$

Especially when all diagonal entries of Λ_i^{-1} are huge (when we pick $\mathbf{x}^i$ with large λ_i), the ϵ can be ignored as a small disturbance, and thus the following equation

$$\Lambda_i^{-1}\mathbf{x}^i = 0 \tag{5.10}$$

approximately describes the spherical local minima, which implies that almost all bad CM local minima disappear.

However, we cannot assume to r be so large. In fact, the r satisfying radial minima condition (3.30) in Chapter 3

$$r_{\min}^2 = \frac{\gamma(1 + \sigma^2 \|C^{-1}\mathbf{h}\|^2)}{\kappa_w (1 + \sigma^2 \|C^{-1}\mathbf{h}\|^2)^2 - \eta_s (1 - I_{\mathbf{h}})} \tag{5.11}$$

depends on the σ^2 and $||C^{-1}\mathbf{h}||^2$. By plugging in the $r^2_{\min}$, we have

$$4\sigma^2 \frac{(1 - I_{U^T\mathbf{x}^i})}{1 + \sigma^2||\Lambda^{-1}\mathbf{x}^i||^2} \Lambda_i^{-1}\mathbf{x}^i + \frac{\partial}{\partial \mathbf{x}^i} I_{U^T\mathbf{x}^i} = 0 \tag{5.12}$$

This equation describes the spherical location of the CMA stationary points. It also suggests that the spherical location of CMA local minima is somewhere between the minima of $||C^{-1}||_{S^{N-1}}$ and those of $I_{\mathbf{h}}|_{S^{N-1}}$. Dividing by $(1 + \sigma^2||\Lambda^{-1}\mathbf{x}^i||^2)^2$ on both sides we have

$$\begin{aligned} & 4\sigma^2 \frac{(1 - I_{U^T\mathbf{x}^i})}{(1 + \sigma^2||\Lambda^{-1}\mathbf{x}^i||^2)^3} \Lambda_i^{-1}\mathbf{x}^i + \frac{1}{(1 + \sigma^2||\Lambda^{-1}\mathbf{x}^i||^2)^2} \frac{\partial}{\partial \mathbf{x}^i} I_{U^T\mathbf{x}^i} && (5.13) \\ = \quad & -\frac{\partial}{\partial \mathbf{x}^i} \frac{(1 - I_{U^T\mathbf{x}^i})}{(1 + \sigma^2||\Lambda^{-1}\mathbf{x}^i||^2)^2} = 0 && (5.14) \end{aligned}$$

This shows the spherical location of the CMA local minima is exactly the same as the local maxima of $(1 - I_{\mathbf{h}})/(1 + \sigma^2||C^{-1}\mathbf{h}||^2)^2$. We summarize this result as a lemma.

Lemma 7 (Noise gain and ISI) *In the presence of noise, the location of a CM solution is determined by a division of the noise gain term and the ISI term. The spherical location of the CM solution on the radial minima surface is the same spherical location as that of the local maxima of*

$$\frac{(1 - I_{\mathbf{h}})}{(1 + \sigma^2||C^{-1}\mathbf{h}||^2)^2} \tag{5.15}$$

with the constraint $||\mathbf{h}|| = 1$. *Furthermore, as* $\sigma^2 \to \infty$

$$\frac{(1 - I_{\mathbf{h}})}{||C^{-1}\mathbf{h}||^4} \tag{5.16}$$

which with $||\mathbf{h}|| = 1$ *describes the asymptotic spherical location of the CM solution.*

5.1.2 Disappearance of CMA Local Minima

Intuitively, when the singular value disparity of the channel matrix is large, the change in the $||C^{-1}\mathbf{h}||$ term may absorb the change in the $I_{\mathbf{h}}$ term, and thus the local maxima of (5.16) may disappear near the maxima of $||C^{-1}\mathbf{h}||$ and appear near the minima of $||C^{-1}\mathbf{h}||$. However, the explicit analysis on the disappearance of the CM solutions is not an easy task, especially for high dimensional cases. Here, we will illustrate the mechanism of disappearance of the CM solution for the asymptotic case when $\sigma^2 \to \infty$. Since the radial minima surface deforms smoothly from $\sigma^2 = 0$ to the asymptotic case described by a polynomial function, the disappearance for the asymptotic case guarantees the disappearance for a finite σ^2 (We can treat the finite noise case as an arbitrarily small disturbance of the asymptotic case). Three low dimensional simulation examples provide insight into the size of these σ^2.

Let us suppose that $U = I$ for now though it would never happen for a $T/2$ channel. A spherical location of the CM solution is one of the local minima of $-\frac{(I_h - 1)}{||C^{-1}\mathbf{h}||^4}|_{S^{N\text{-}1}}$, and one of the solutions of these equations for $i = 0, ..., N-1$:

$$4\frac{(1 - I_{\mathbf{x}^i})}{||\Lambda^{-1}\mathbf{x}^i||^2}\Lambda_i^{-1}\mathbf{x}^i + \frac{\partial}{\partial \mathbf{x}^i} I_{\mathbf{x}^i} = 0 \tag{5.17}$$

Since

$$\frac{\partial}{\partial \mathbf{x}^i} I_{\mathbf{x}^i} = \frac{\partial}{\partial \mathbf{x}^i}\left\{2(1 - \sum_{j\neq i} x_j^2)\sum_{j\neq i} x_j^2 + \sum_{k,j\neq i} x_k^2 x_j^2\right\} = 4\begin{pmatrix} (x_i^2 - x_0^2)x_0 \\ \vdots \\ (x_i^2 - x_{N\text{-}1}^2)x_{N\text{-}1} \end{pmatrix} \tag{5.18}$$

(5.17) yields

$$\frac{(1-I_{\mathbf{x}^i})}{\lambda_i^{-2}+\sum_{k\neq i}(\lambda_k^{-2}-\lambda_i^{-2})x_k^2}\begin{pmatrix}(\lambda_0^{-2}-\lambda_i^{-2})x_0\\ \vdots \\ (\lambda_{N-1}^{-2}-\lambda_i^{-2})x_{N-1}\end{pmatrix}+\begin{pmatrix}(x_i^2-x_0^2)x_0\\ \vdots \\ (x_i^2-x_{N-1}^2)x_{N-1}\end{pmatrix}=0 \quad (5.19)$$

where x_i denotes $1-\sum_{k\neq i}x_k^2$. A solution of (5.17) must be a solution of the k-th equation of the above equation set, i.e. for fixed $x_0,..,x_{k-1},x_{k+1},..,x_{N-1}$,

$$\frac{(1-I_{\mathbf{x}^i})}{\lambda_i^{-2}+a_k+(\lambda_k^{-2}-\lambda_i^{-2})x_k^2}(\lambda_k^{-2}-\lambda_i^{-2})x_k+(1-b_k-2x_k^2)x_k=0 \quad (5.20)$$

where

$$a_k = \sum_{j\neq k,i}(\lambda_j^{-2}-\lambda_i^{-2})x_k^j \quad (5.21)$$
$$b_k = \sum_{j\neq k,j}x_j^2. \quad (5.22)$$

Notice that $x_k\in(-\sqrt{1-b_k}\ ,\ \sqrt{1-b_k})$. Equation (5.20) can be viewed as

$$(1-I_{\mathbf{x}^i})f(x_k)=g(x_k) \quad (5.23)$$

with

$$f(x_k) = \frac{(\lambda_k^{-2}-\lambda_i^{-2})x_k}{\lambda_i^{-2}+a_k+(\lambda_k^{-2}-\lambda_i^{-2})x_k^2} \quad (5.24)$$
$$g(x_k) = -(1-b_k-2x_k^2)x_k \quad (5.25)$$

$g(x_k)$ is a third order polynomial (Figure 5.2-c)), while $f(x_k)$ is a rational function with a special structure depending on the value of λ_i and λ_k.

a) If $\lambda_i^{-2}\ll\lambda_k^{-2}$, $f(x_k)$ is a single big wave with a maximum slope $\frac{(\lambda_k^{-2}-\lambda_i^{-2})}{\lambda_i^{-2}+a_k}\approx\lambda_k^{-2}$ at $x_k=0$ (Figure 5.2-a)).

b) If $\lambda_i^{-2}\gg\lambda_k^{-2}$, $f(x_k)$ is a (tangent like) monotonically decreasing function with maximum slope $\frac{(\lambda_k^{-2}-\lambda_i^{-2})}{\lambda_i^{-2}+a_k}\approx-1$ at $x_k=0$ (Figure 5.2-b)).

c) If $\lambda_i^{-2} \approx \lambda_k^{-2}$, $f(x_k) \approx 0$.

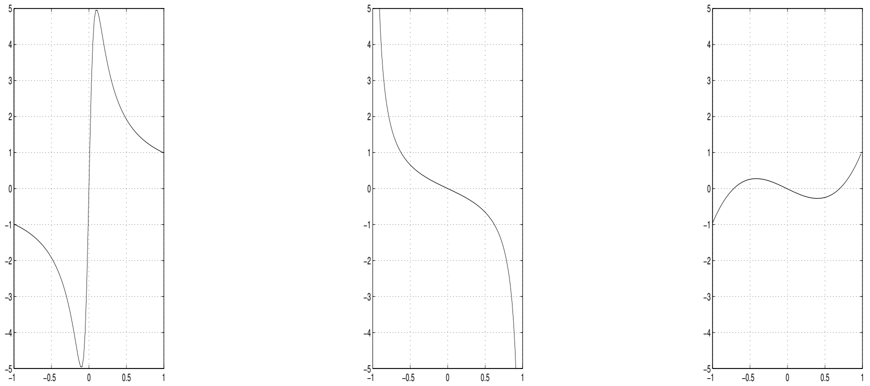

a) $f(x_k)$ with $\lambda_i^{-2} \ll \lambda_k^{-2}$ b) $f(x_k)$ with $\lambda_i^{-2} \gg \lambda_k^{-2}$ c) $g(x_k)$

Figure 5.2: g and f

Because half of the $\{\lambda_i\}$ are small, for i with small λ_i we have half of type a) $f(x_k)$ and half of type c), and for i with large λ_i we have half of type b) $f(x_k)$ and half of type c). Any solution of (5.23), say x, is one of the points where $(1 - I_{\mathbf{x}^i})f(x_k)$ meets $g(x_k)$. Furthermore, the way they meet determines whether x is a local minima or local maxima in x_k direction. Figure 5.3-a) shows the case

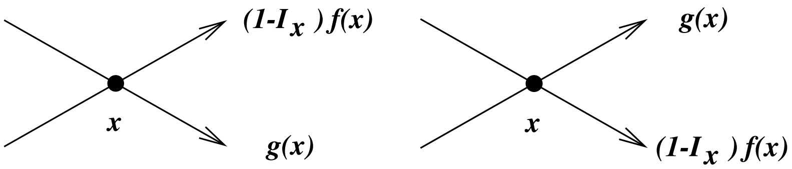

a) x is a local minima b) x is a local maxima

Figure 5.3: Cross section of $(1 - I_{\mathbf{x}^i})f(x_k)$ and $g(x_k)$

when x is a local minima and b) shows when x is a local maxima.

To count all CM solutions, we need to examine all possible $(1 - I_{\mathbf{x}^i})f(x_k)$ and

$g(x_k)$ focusing on where they meet and how they meet for all i and k under the effect of non-trivial U. However, this is a virtually impossible job. Since our primary goal is to reveal the mechanism of disappearance of the CM solutions, we make the following assumption.

- We ignore $1 - I_{\mathbf{x}^i}$ term: Since $0 < 1 - I_{\mathbf{x}} \leq 1$, $(1 - I_{\mathbf{x}^i})f(x_k)$ is a deformed version of $f(x_k)$. After the deformation, $f(x_k)$ still falls into three cases. It might be possible this deformation causes a new cross section with $g(x_k)$. However, we ignore that effect.

- When U is non-trivial (which is the typical case), strictly speaking, $g(x)$ is not a third order polynomial, since we have the $\sqrt{1 - b_i - x_k}$ terms. However, we consider it as a third order polynomial bounded by $|g(x_k)| \leq 1$.

Now let us consider the case where U is not an identity. Here is the mechanism of the CM solution disappearance

CM solution disappearance

A) For the index i with a large λ_i, there is an index set $\{k\}$ such that $\lambda_i^{-2} \ll \lambda_k^{-2}$ (in fact, the half of $\{0, .., i-1, , i+1, ...N\text{-}1\}$). For those $\{k\}$, $f(x_k)$ is type a) in Figure 5.2. Since $|g(x)| \leq 1$, $f(x_k)$ meets $g(x_k)$ at only one point near the origin and the point must be a minima from the argument of Figure 5.3-a (refer to Figure 5.4-a). For the other half indices such that $\lambda_i^{-2} \approx \lambda_k^{-2}$, $f(x_k) \approx 0$, and thus $g(x_k)$ determines the minima in the x_k direction. Therefore, the minimum of $\frac{(I_h - 1)}{\|C^{-1}\mathbf{h}\|^4}|_{S^{N\text{-}1}}$ on $\mathbf{x}^i$ with large λ_i is less than those of $I_{\mathbf{h}}|_{S^{N\text{-}1}}$ (refer to Figure 5.4-a').

B) For i with small λ_i, there is an index set $\{k\}$ such that $\lambda_i^{-2} \ll \lambda_k^{-2}$. For those $\{k\}$, $f(x_k)$ is type b) in Figure 5.2. $f(x_k)$ meets $g(x_k)$ at only one point near the origin and the point might be a minimum from the argument of Figure 5.3-a (refer to Figure 5.4-b).

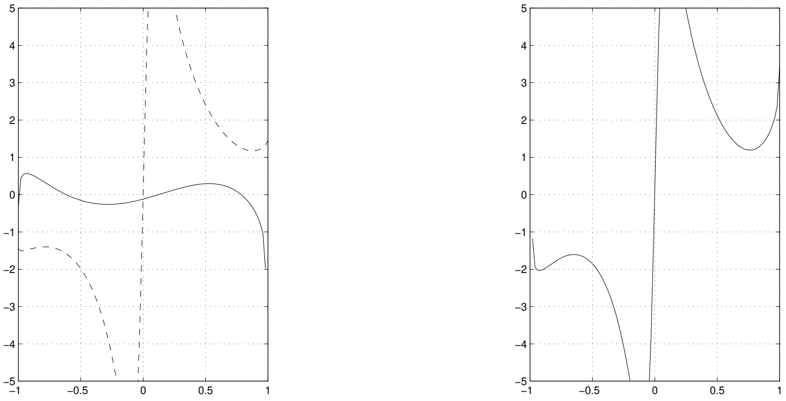

a) $(1 - I_{\mathbf{x}^0})f(x_k),\ g(x_k)$ a') $(1 - I_{\mathbf{x}^0})f(x_k) - g(x_k)$

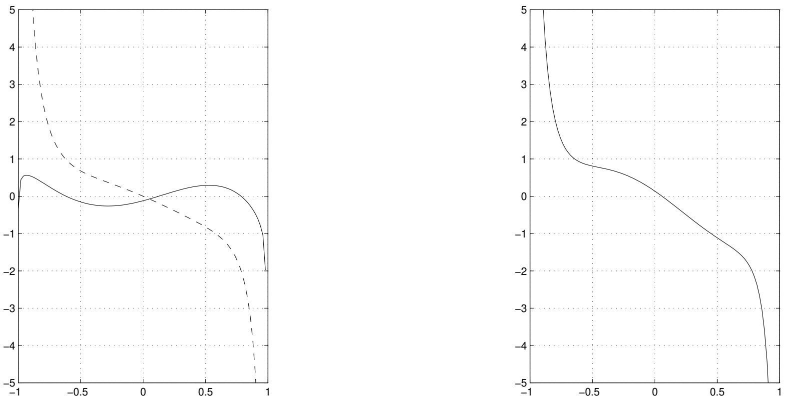

b) $(1 - I_{\mathbf{x}^1})f(x_k),\ g(x_k)$ b') $(1 - I_{\mathbf{x}^1})f(x_k) - g(x_k)$

Figure 5.4: Two dimensional example of $(1 - I_{\mathbf{x}^i})f(x_k) - g(x_k) = 0$

Example 7 Let us consider an artificial $T/2$ channel $\mathbf{c} = [-0.05,\ 1,\ 0.1,\ 0.5]^T$. Then the channel convolution matrix and its singular value decomposition are as follows

$$C = \begin{pmatrix} 1 & -0.05 \\ 0.5 & 0.1 \end{pmatrix} = \begin{pmatrix} 0.8944 & -0.4472 \\ 0.4472 & 0.8944 \end{pmatrix} \begin{pmatrix} 1.1180 & 0 \\ 0 & 0.1118 \end{pmatrix} \begin{pmatrix} 1 & 0 \\ 0 & 1 \end{pmatrix} \tag{5.26}$$

We have $\lambda_0^{-2} = 0.8$ and $\lambda_1^{-2} = 80$ with the corresponding eigenvector of $C^{-T}C^{-1}$, $\mathbf{u}_0 = [0.8944 \quad 0.4472]^T$ and $\mathbf{u}_1 = [-0.4472 \quad 0.8944]^T$. Figure 5.5 a) shows that asymptotically there are only two local minima in this channel as noise increases (the x coordinate represents the angle θ with $\mathbf{h} = (\cos(\theta), \sin(\theta))$). Figure 5.5 b) shows the radial minima surfaces for various noise powers along with the CM solutions and the LMS solutions. The radial minima surface Φ deforms from a clover shape(I_h) to an elliptic shape ($\|C^{-1}\mathbf{h}\|$) as noise power increases. Corresponding to this change, the simulation result of the FSE-CMA (the '$*$' marks) shows that the local minima move continuously toward the $\mathbf{u}_0$ direction, and two of them disappear at about -17 dB SNR. Thereafter with less than -17 dB SNR, we can have only 2 local minima near the minima of $\|C^{-1}\mathbf{h}\|$. Furthermore, the simulation shows that the LMS solutions locate near the CM solutions as mentioned in Chapter 2.

Example 8 Let us consider $\mathbf{c} = [-0.024, 0.8827, -0.1978, -0.223, 0.0104]^T$. The singular value decomposition of the channel convolution matrix is given as

$$C = U\Lambda V^T \tag{5.27}$$

where

$$U = \begin{pmatrix} 0.577 & -0.814 & -0.058 \\ -0.800 & -0.550 & -0.235 \\ 0.159 & 0.182 & -0.970 \end{pmatrix} \tag{5.28}$$

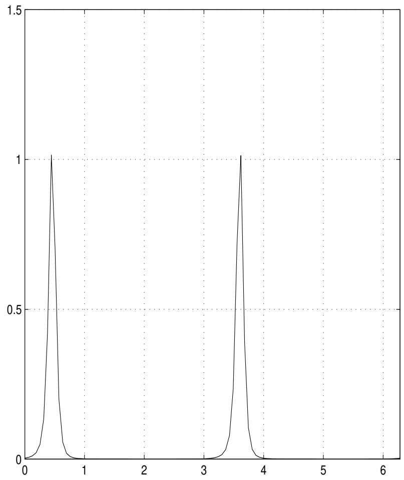

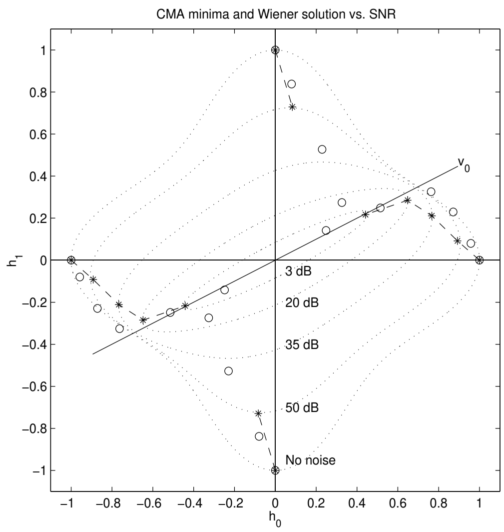

Dotted curves	:	Φ surface
$*$	:	CM solution
$\circ$	:	LMS Solution

a) $\frac{(I_h - 1)}{\|C^{-1}\mathbf{h}\|^4}\Big|_{S^{N-1}}$

Figure 5.5: A 2-dim. local minima relocation

$$\Lambda = \begin{pmatrix} 1.022 & 0 & 0 \\ 0 & 0.806 & 0 \\ 0 & 0 & 0.038 \end{pmatrix} \tag{5.29}$$

$$V^T = \begin{pmatrix} 0.672 & -0.739 & 0.024 \\ 0.142 & 0.161 & 0.976 \\ -0.725 & -0.653 & 0.214 \end{pmatrix} \tag{5.30}$$

The singular values are such that:

$$\begin{aligned} \lambda_0^{-2} &= 0.96, \\ \lambda_1^{-2} &= 1.53, \\ \lambda_2^{-2} &= 662.9, \end{aligned} \tag{5.31}$$

i.e. we have $\lambda_0^{-2} \approx \lambda_1^{-2} \ll \lambda_2^{-2}$ and the column vectors of U, $U = [\mathbf{u}_1 \ \ u_2 \ \mathbf{u}_3]$, are

$$\begin{aligned} \mathbf{u}_0 &= [0.577 \ -0.800 \ 0.159]^T \\ \mathbf{u}_1 &= [-0.814 \ -0.550 \ 0.182]^T \\ \mathbf{u}_2 &= [-0.058 \ -0.235 \ -0.970]^T \end{aligned} \tag{5.32}$$

In Figure 5.6, a) and a′) show the radial minima surface and $(1 - I_{\mathbf{h}})/(1 + \sigma\|C^{-1}\mathbf{h}\|^2)^2$ respectively, when $\sigma^2 = 0$. In a′), the x coordinate represents $\theta \in (-\pi, \pi)$ and the y coordinate represents the radius $r \in [0, 1)$ so that $\mathbf{h}^i = r(\cos(\theta), \sin(\theta))$. As the noise gain increases to -20dB, two local minima disappear near the $\mathbf{u}_3$ direction (Figure b). Since $\lambda_0^{-2} \approx \lambda_1^{-2} \ll \lambda_2^{-2}$, even in the asymptotic case as $\sigma^2 \to \infty$ only two local minima disappear (Figure b′).

Example 9 In this example, we manipulate the singular values in Example 8 so that we have $\lambda_0^{-2} \ll \lambda_1^{-2} \ll \lambda_2^{-2}$. Let $\lambda_0 = 1$, $\lambda_1 = 0.02$, and $\lambda_2 = 0.01$ with the

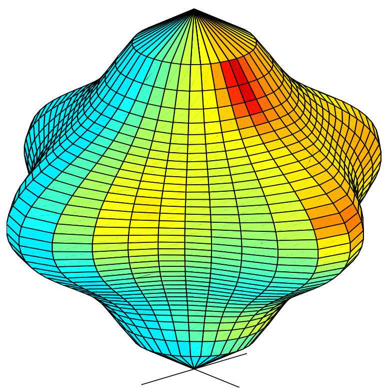

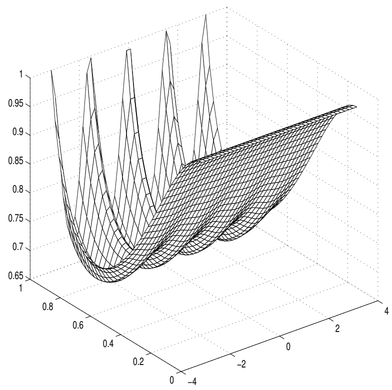

a) radial minima surface   a′) $(1 - I_{\mathbf{h}})/(1 + \sigma\|C^{-1}\mathbf{h}\|^2)^2$

Case I: When $\sigma^2 = -\infty$dB

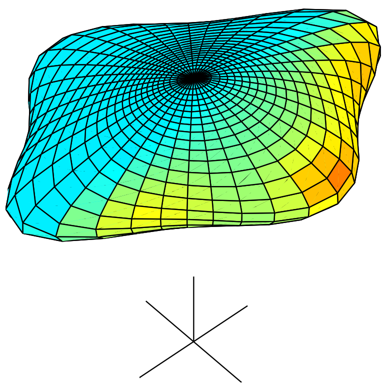

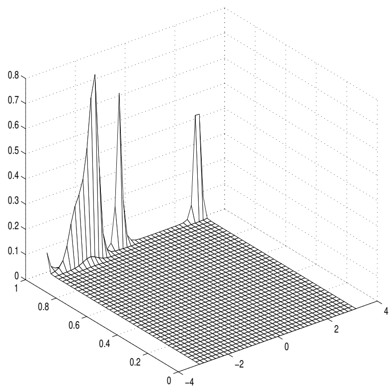

b) radial minima surface   b′) $(1 - I_{\mathbf{h}})/(1 + \sigma\|C^{-1}\mathbf{h}\|^2)^2$

Case II: When $\sigma^2 = -20$dB

Figure 5.6: Disappearance of CM solutions in Example 8

same U and V. Then

$$\begin{aligned} \lambda_0^{-2} &= \quad 1, \\ \lambda_1^{-2} &= \quad 2500, \\ \lambda_2^{-2} &= \quad 10000. \end{aligned} \tag{5.33}$$

At the -40dB noise level two CM solutions near the $\mathbf{u}_3$ direction disappear first (Figure 5.7-a). As the noise level approaches -30dB another two CM solutions near the $\mathbf{u}_2$ direction disappear, and only two CM solutions exist near the $\mathbf{u}_1$ direction (Figure b). This example illustrates that noise can wash out all the bad local minima.

5.2 Single Spike Initialization

Initialization affects the convergent performance of the CM receiver. A widely used initialization technique is called the single (or double) spike initialization, which sets the equalizer as a spike with a constrained norm:

$$\begin{aligned} \mathbf{f}_{ini} &= [0 \cdots 0 \ 1 \ 0 \cdots 0]^T \qquad (SingleSpike) \\ \mathbf{f}_{ini} &= [0 \cdots 0 \ \tfrac{1}{\sqrt{2}} \ \tfrac{1}{\sqrt{2}} \ 0 \cdots 0]^T \quad (DoubleSpike) \end{aligned} \tag{5.34}$$

It has been observed [16] that these initialization techniques tend to achieve one of the good local minima regardless of the peak position. This fact can be explained partly by the disappearance of the bad CM minima, and partly by the contraction of the regions of convergence of the bad local minima near their origin. In this section, we provide some simulation results suggesting the relation between the structure of regions of convergence and the performance of spike initialization. In the absence of noise, when the initial equalizer norm is constrained to 1 (near the origin), the CM solutions with small equalizer norm are achieved, while those with

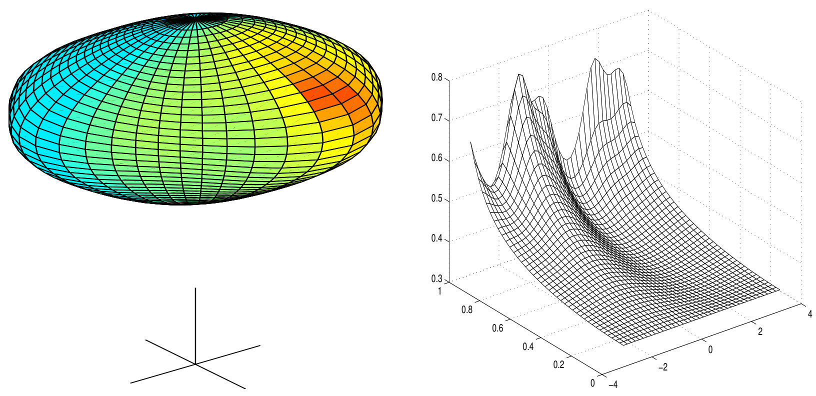

a) radial minima surface a′) $(1 - I_{\mathbf{h}})/(1 + \sigma\|C^{-1}\mathbf{h}\|^2)^2$

Case I: When $\sigma^2 = -40$dB

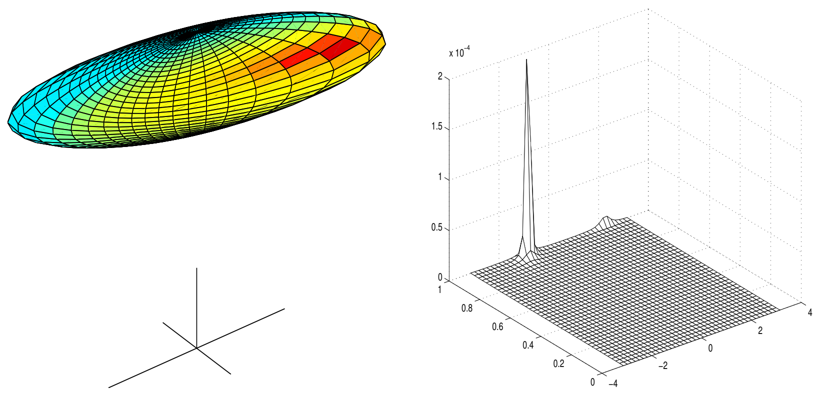

b) radial minima surface b′) $(1 - I_{\mathbf{h}})/(1 + \sigma\|C^{-1}\mathbf{h}\|^2)^2$

Case II: When $\sigma^2 = -30$dB

Figure 5.7: Disappearance of CM solutions in Example 9

large equalizer norm are achieved when the initial equalizer norm is set to a large value(far from the origin).

Example 10 We examine the performance of the spike initialization for a truncated version of the channel used in Example 6 in Chapter 4. Figure 5.8-a) shows the channel response in the time domain and b) shows the equalizer norm in dB scale for each system delay. The local minima inside the dotted box have been achieved by both single and double spike initializations. The relation between achieved system delay and the spike position is plotted in c) and d). In both cases, the system delays from 3 to 16, corresponding to good local minima, are achieved whatever initial spike location is used. In particular, for the double spike initialization, we can observe that the spike position is directly related to the achieved system delay. We can explain this by the conic structure of ROC near the origin.

Example 11 In this example we consider a small channel (length 11), truncated from chan3 introduced in Example 6 in Chapter 4. Figure 5.9 a) and b) shows the channel response and the norm of the CM solutions corresponding to their system delays respectively. In c) and d), single (and double) spike initialization with $\|\mathbf{f}_{ini}\| = 1$ is used. With this initialization the system delays of 2-6 are achieved (the dotted box in Figure b)). When we initialize the equalizer with $\|\mathbf{f}_{ini}\| = 60$, the achieved system delays are mostly 1, 7, 8, where the equalizer norm is large. This simulation result reminds us of the result in Chapter 4 that the regions of convergence of bad local minima expand far from the origin.

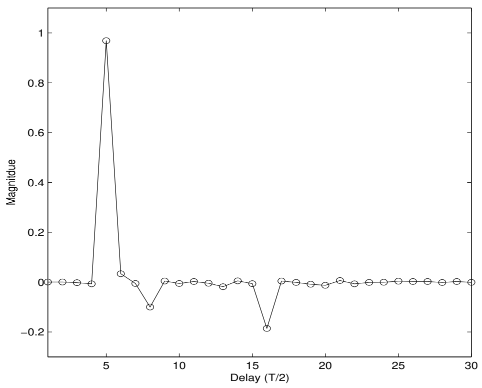

a) channel response

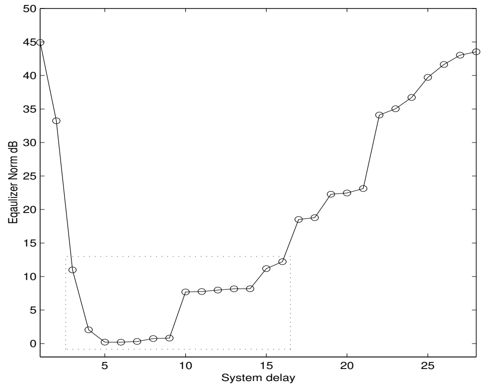

b) Equalizer norm vs system delay

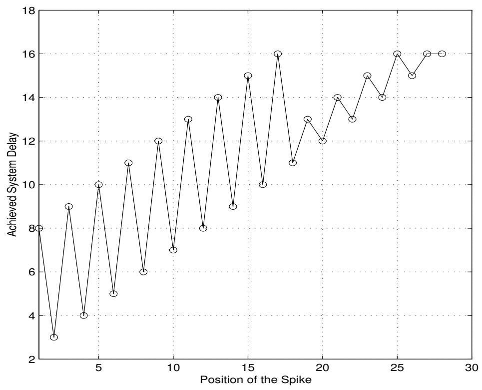

c) system delay by single spike

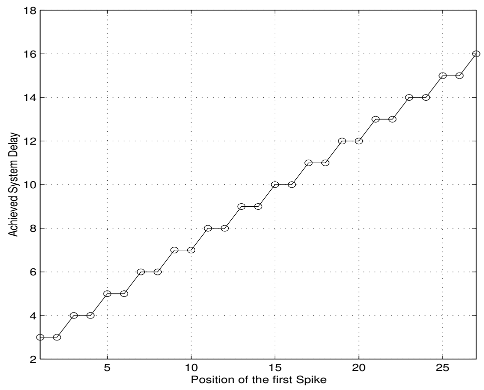

d) system delay by double spike

Figure 5.8: Spike Initialization in Example 10

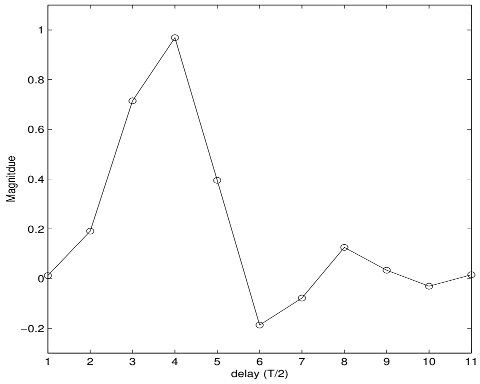

a) channel response

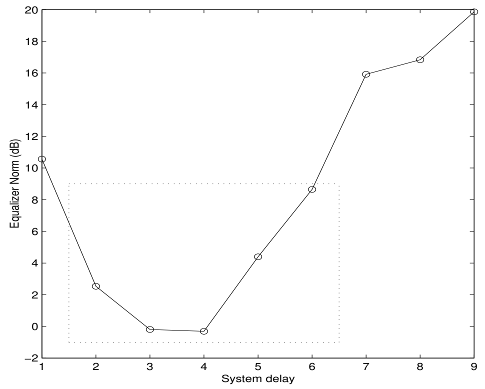

b) Equalizer norm vs system delay

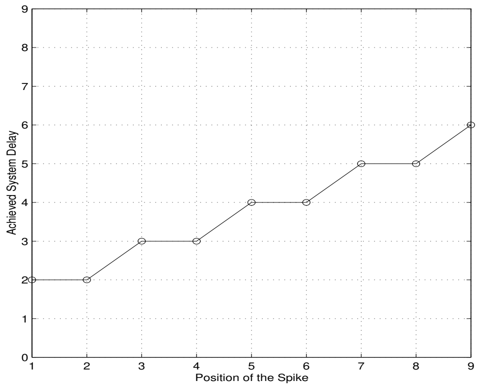

c) by single spike norm 1

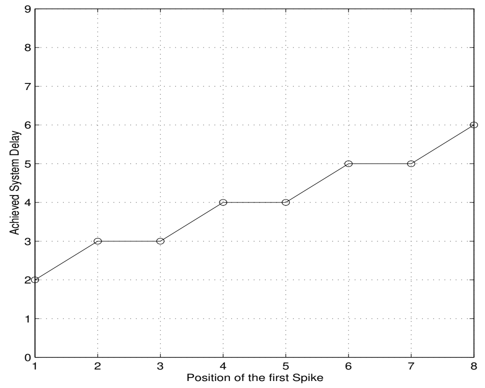

d) by double spike norm 1

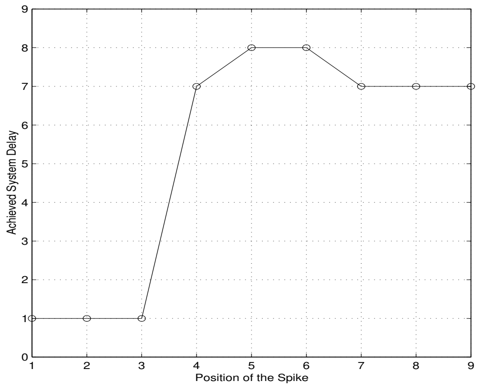

e) by single spike norm 60

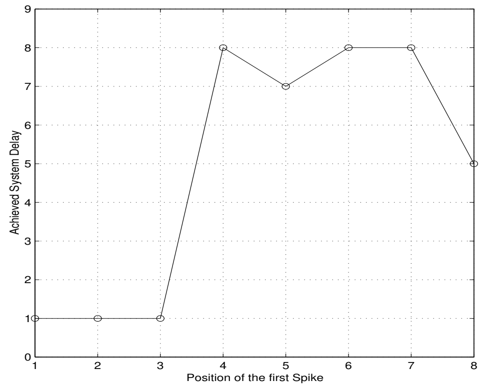

f) by double spike norm 60

Figure 5.9: Spike Initialization in Example 11

Chapter 6

Blind Cross Polarized Source Separation using FS-CMA

CMA can also be applied to a blind source separation problem in digital communication systems [33,35,5]. In this chapter we investigate the linear Cross Pole Interference (CPI) canceller using CMA.

6.1 Linear Cross Pole Interference Equalization

In modern communication systems, the demand for transmitting extensive information through channels of limited bandwidth has encouraged the search for an efficient transmission scheme exploiting both spectral and spatial resources. Especially in digital microwave radio systems, such an efficient system can be realized by frequency reuse of two orthogonally polarized carrier waves at the same frequency. Two mutually independent source sequences $\mathbf{s}_1$ and $\mathbf{s}_2$ are transmitted simultaneously on the vertical and the horizontal polarizations at the same nominal carrier frequency and received by two appropriately polarized antennas. Armed with this technique, theoretically, one can transmit twice the amount of information through a fixed bandwidth channel. However, it has been observed that in practice the performance of the system tends to be degraded due to interference (including cross-pole) when signals pass through physical channels.

Interference is caused by not only the bandwidth of the channel (inter symbol interference (ISI)) but also by the structure of orthogonal polarization: refraction and reflection of carrier waves during propagation allow only mixed signals to reach the receiver antennas. The structural interference is referred to as *cross-polarization interference* (CPI) and modeled as a linear addition of two source sequences [29]. Recovering signals despite CPI, as well as ISI, is essentially a source separation problem. One may apply conventional dual finite impulse response (FIR) filter equalization techniques based on second order statistics estimation or training sequence adaptation [24,29], or blind adaptation using CMA [33].

6.1.1 System model

Figure 6.1 models cross-polarization interference in a communication system using vertically and horizontally polarized antennas. Two independent source sequences $\mathbf{s}_1$ and $\mathbf{s}_2$ are transmitted on the horizontally and the vertically polarized carrier waves, respectively. FIR filters $\mathbf{c}_{11}$ and $\mathbf{c}_{22}$ represent the direct path between horizontal and vertical polarization antennas, respectively, while $\mathbf{c}_{12}$ and $\mathbf{c}_{21}$ represent the cross-coupling terms.

The received signal of a fractionally spaced receiver is sampled at a fraction of the baud rate. This way, additional channel information from the fractional sampling can be utilized for equalization. We consider a $T/2$-spaced receiver (i.e., the sampling interval is half of the baud interval T). A $T/2$-spaced CPI equalizer

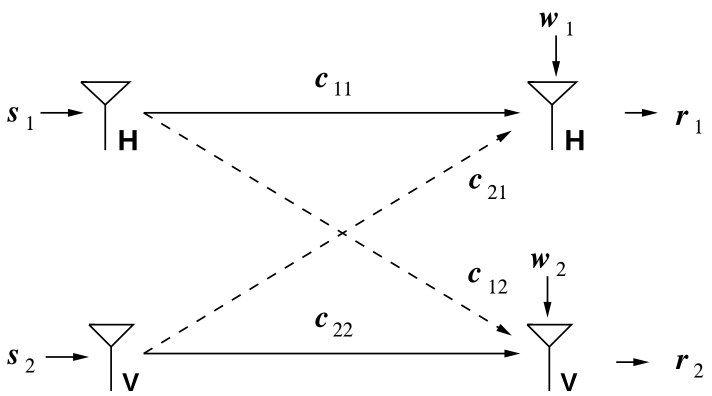

Figure 6.1: Cross Polarization Interference

intended to extract one of the transmitted signals is illustrated in Figure 6.2.

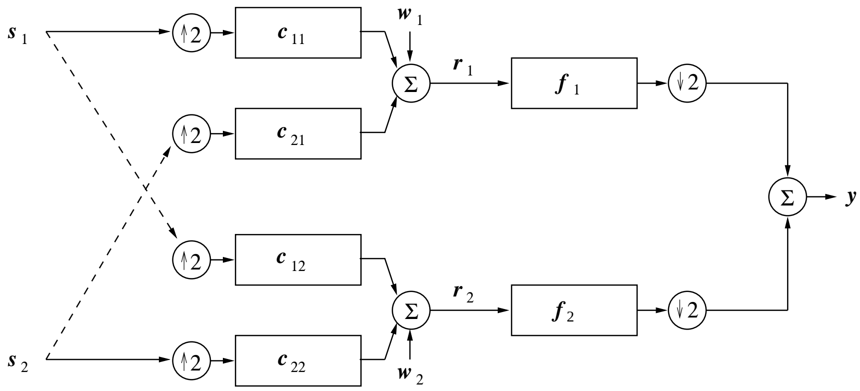

Figure 6.2: FS CPI equalizer for a desired signal

For now, we assume that there is no channel noise $\mathbf{w}_1$ or $\mathbf{w}_2$. Then, for channel paths $\mathbf{c}_{ij}$ and equalizers $\mathbf{f}_k$, the combined baud spaced response can be written as a linear combination of channel convolution matrices C_{ij} and equalizer vectors $\mathbf{f}_i$, i.e., $C_{ij}\mathbf{f}_k$. Thus in the absence of noise, the output y of the model in Figure 6.2 is given by

$$y = \mathbf{s}_1^T(C_{11}\mathbf{f}_1 + C_{12}\mathbf{f}_2) + \mathbf{s}_2^T(C_{21}\mathbf{f}_1 + C_{22}\mathbf{f}_2) \tag{6.1}$$

where C_{11}, C_{12}, C_{21}, and C_{22} are the convolution matrices of $\mathbf{c}_{11}, \mathbf{c}_{12}, \mathbf{c}_{21}$ and $\mathbf{c}_{22}$ respectively. We define

$$\mathbf{q}_1 \quad := \quad C_{11}\mathbf{f}_1 + C_{12}\mathbf{f}_2 \tag{6.2}$$

$$\mathbf{q}_2 \quad := \quad C_{21}\mathbf{f}_1 + C_{22}\mathbf{f}_2 \tag{6.3}$$

as the system responses of the FS CPI equalizer for sources $\mathbf{s}_1$ and $\mathbf{s}_2$, and we have the following linear relation:

$$\begin{bmatrix} \mathbf{q}_1 \\ \mathbf{q}_2 \end{bmatrix} = \begin{bmatrix} C_{11} & C_{12} \\ C_{21} & C_{22} \end{bmatrix} \begin{bmatrix} \mathbf{f}_1 \\ \mathbf{f}_2 \end{bmatrix} \tag{6.4}$$

Define

$$C := \begin{bmatrix} C_{11} & C_{12} \\ C_{21} & C_{22} \end{bmatrix} \tag{6.5}$$

as an analogy of the channel convolution matrix for an FS equalizer. C is invertible when the *Schur complement of* C_{11} in C, i.e, $C_{22} - C_{21}C_{11}^{-1}C_{12}$, is non singular [19].

6.1.2 Assumptions

We make the following assumptions on the source, the channels, and the equalizers in addition to Assumption 1 in Chapter 3.

A1. The source sequences $\{s_1\}$ and $\{s_2\}$ are mutually independent i.i.d.

A2. The $T/2$-channel models $\{\mathbf{c}_{ij}\}$ are all the same length and satisfy the sub-channel disparity condition by having no common roots among its sub-channels.

A3. The length of $\{\mathbf{f}_i\}$ satisfies the length condition of perfect equalization for $T/2$-spaced equalization, i.e. the length of equalizer $N_{f_i} = N_c - 2$.

From these assumptions we have the invertible channel convolution matrices C_{11}, C_{12}, C_{21}, and C_{22}. Denote $A := C_{21}C_{11}^{-1}$ and $B := C_{22}C_{12}^{-1}$. The non-singularity of the Schur complement of C_{11}, i.e. $C_{22} - C_{21}C_{11}^{-1}C_{12}$, is equivalent to the non-singularity of $A - B$. We assume that our cross-pole channels have diversity such that

A4. $A - B$ is a non-singular matrix, which guarantees that C is invertible.

6.2 ZF and MMSE solutions of the CPI Equalizer

6.2.1 Zero-Forcing Solutions

In the absence of noise, the output of the CPI equalizer is given by

$$y = \mathbf{s}_1^T\mathbf{q}_1 + \mathbf{s}_2^T\mathbf{q}_2 \tag{6.6}$$

To equate y to (a delayed version of) $\mathbf{s}_1$, we have two equations

$$\begin{cases} \mathbf{q}_1 = \delta_i \\ \mathbf{q}_2 = 0 \end{cases} \text{or equivalently,} \begin{bmatrix} \delta_i \\ 0 \end{bmatrix} = \begin{bmatrix} C_{11} & C_{12} \\ C_{21} & C_{22} \end{bmatrix} \begin{bmatrix} \mathbf{f}_1 \\ \mathbf{f}_2 \end{bmatrix} \tag{6.7}$$

Since we assume that C is invertible, (6.7) yields a unique solution depending on the chosen delay $\delta_i := [0 \cdots 0\ 1(i-th)\ 0 \cdots 0]^T$.

$$\begin{cases} \mathbf{f}_1^* = C_{11}^{-1}(B-A)^{-1}B\delta_i \\ \mathbf{f}_2^* = -C_{12}^{-1}B^{-1}AC_{11}\mathbf{f}_1^* \end{cases} \tag{6.8}$$

The derivation of $\mathbf{f}_i^*$ can be found in [19].

6.2.2 MMSE solution

In this subsection, we now consider the noisy case. Suppose the noise $\{w_1\}$ and $\{w_2\}$ are mutually independent, identically distributed with the same variance σ_w^2, and uncorrelated to the sources s_1 and s_2. The output in the presence of noise is

$$y = \mathbf{s}_1^T \mathbf{q}_1 + \mathbf{s}_2^T \mathbf{q}_2 + \mathbf{w}_1^T \mathbf{f}_1 + \mathbf{w}_2^T \mathbf{f}_2 \tag{6.9}$$

The minimum mean squared error (MMSE) equalizers $(\mathbf{f}_1^*, \mathbf{f}_2^*)$ of delay i are defined as

$$(\mathbf{f}_1^*, \mathbf{f}_2^*) = \arg\min_{\mathbf{f}_1, \mathbf{f}_2} E\left\{\|y - (s_1)_i\|^2\right\}, \tag{6.10}$$

where $(s_1)_i$ denotes the i-th delayed source s_1. Let $\mathbf{f} := [\mathbf{f}_1^T \ \mathbf{f}_2^T]^T$. Since $\mathbf{s}_1$ and $\mathbf{s}_2$ are mutually independent, we treat $\mathbf{s} := [\mathbf{s}_1^T \ \mathbf{s}_2^T]^T$ as an i.i.d. source, and the same for the noise $\mathbf{w} := [\mathbf{w}_1^T \ \mathbf{w}_2^T]^T$. Now we have simplified the expression of y into a form which is similar to that for FS-MMSE in Chapter 2.

$$y = \mathbf{s}^T C \mathbf{f} + \mathbf{w}^T \mathbf{f} \tag{6.11}$$

The MMSE solution $\mathbf{f}^*$ is given by

$$\mathbf{f}^* = (C^H C + \lambda I)^{-1} C^H \delta_i \tag{6.12}$$

where $\lambda = \sigma_{\mathbf{w}}^2 / \sigma_{\mathbf{s}}^2$. The derivation of (6.12) is identical to that of the FS-MMSE solution. We can obtain a more explicit expression in terms of C_{ij} by considering:

$$MSE = E\left\{\|y - (s_1)_i\|^2\right\} = \sigma_s^2(\|\mathbf{q}_1 - \delta_i\|^2 + \|\mathbf{q}_2\|^2) + \sigma_w^2(\|\mathbf{f}_1\|^2 + \|\mathbf{f}_2\|^2) \tag{6.13}$$

By setting $\frac{\partial}{\partial \mathbf{f}_1} MSE$ and $\frac{\partial}{\partial \mathbf{f}_2} MSE$ to zero, we obtain

$$\mathbf{f}_1^* = C_{11}^{-1} \frac{I - (I + A^H A + \lambda C_{11}^{-H} C_{11})^{-1}}{(I + A^H A + \lambda C_{11}^{-H} C_{11})^{-1} - (I + B^H B + \lambda C_{12}^{-H} C_{12}^{-1})^{-1} (I + A^H B)} \delta_i \tag{6.14}$$

$$\mathbf{f}_2^* = C_{12}^{-1} \frac{A^H A - B^H A + \lambda C_{11}^{-H} C_{11}^{-1}}{B^H B - A^H B + \lambda C_{12}^{-H} C_{12}^{-1}} C_{11} \mathbf{f}_1^* \tag{6.15}$$

where the fraction denotes left inversion (i.e. $\frac{P}{Q} := Q^{-1} P$). Because of the non symmetric terms $A^T B$ and $B^T A$, the solutions cannot be expressed in a simple form. Note that the MMSE solutions in (6.14) and (6.15) agree with the ZF solutions in (6.8) in the absence of noise (i.e. $\lambda = 0$).

If a communication system allows training signals, the MMSE solutions shown above can be obtained via the LMS algorithm:

$$\mathbf{f}_1^{(n+1)} = \mathbf{f}_1^{(n)} - \mu(y - s_1)\mathbf{r}_1^* \tag{6.16}$$

$$\mathbf{f}_2^{(n+1)} = \mathbf{f}_2^{(n)} - \mu(y - s_1)\mathbf{r}_2^* \tag{6.17}$$

where μ is a step size and $\mathbf{r}_i^*$ is the complex conjugated regressor vector of equalizer $\mathbf{f}_i$. Notice that the desired signal is determined by the training sequence, i.e. $\mathbf{s}_1$ could be replaced by $\mathbf{s}_2$.

6.3 CM solutions of CPI equalizer and Initialization

6.3.1 CM solutions

We apply CMA to the CPI equalizer in order to obtain the CM solution as shown in Figure 6.3. This model was introduced by Treichler and Larimore first [33], and recently implemented by Applied Signal Technology [35].

The constant modulus algorithm for CPI uses two stochastic gradient updates: one each for $\mathbf{f}_1$ and $\mathbf{f}_2$.

$$\mathbf{f}_1^{(n+1)} = \mathbf{f}_1^{(n)} - \mu\frac{\partial}{\partial \mathbf{f}_1}J(\mathbf{f}_1, \mathbf{f}_2)|_{\mathbf{f}_1=\mathbf{f}_1^{(n)},\mathbf{f}_2=\mathbf{f}_2^{(n)}} = \mathbf{f}_1^{(n)} - \mu y(|y(n)|^2 - \gamma)\mathbf{r}_1^* \tag{6.18}$$

$$\mathbf{f}_2^{(n+1)} = \mathbf{f}_2^{(n)} - \mu\frac{\partial}{\partial \mathbf{f}_2}J(\mathbf{f}_1, \mathbf{f}_2)|_{\mathbf{f}_1=\mathbf{f}_1^{(n)},\mathbf{f}_2=\mathbf{f}_2^{(n)}} = \mathbf{f}_2^{(n)} - \mu y(|y(n)|^2 - \gamma)\mathbf{r}_2^* \tag{6.19}$$

where the cost function J is the same as the conventional CMA cost function defined in Chapter 2, and $\mathbf{r}_1$ and $\mathbf{r}_2$ denote the regressors of $\mathbf{f}_1$ and $\mathbf{f}_2$ respectively.

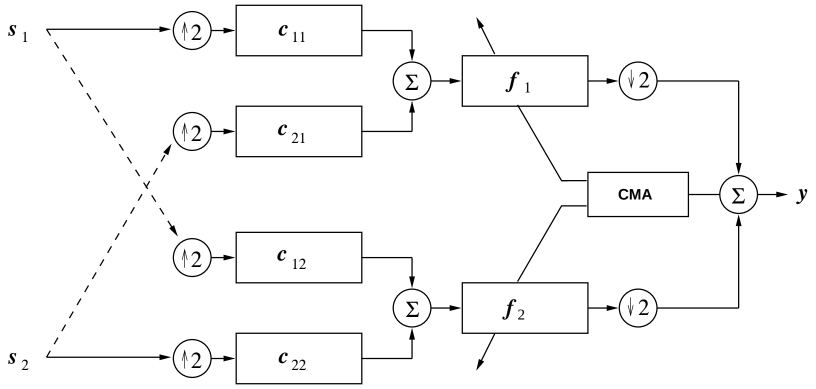

Figure 6.3: FS CPI cancellation using CMA

The two update equations (6.18),(6.19) for CMA CPI can be expressed by a single equation by employing the following notations

$$\mathbf{r} := [\mathbf{r}_1^T \ \mathbf{r}_2^T]^T \tag{6.20}$$

$$\mathbf{f} := [\mathbf{f}_1^T \ \mathbf{f}_2^T]^T \tag{6.21}$$

$$\mathbf{f}^{(n+1)} = \mathbf{f}^{(n)} - \mu \frac{\partial}{\partial \mathbf{f}} J(\mathbf{f})|_{\mathbf{f}=\mathbf{f}_1^{(n)}} = \mathbf{f}^{(n)} - \mu y(|y(n)|^2 - \gamma)\mathbf{r}^* \tag{6.22}$$

where $\mathbf{r} = [\mathbf{r}_1^T \ \mathbf{r}_2^T]^T$ and $\mathbf{f} = [\mathbf{f}_1^T \ \mathbf{f}_2^T]^T$. Furthermore, by defining

$$\mathbf{q} := [\mathbf{q}_1^T \ \mathbf{q}_2^T]^T \tag{6.23}$$

$$\mathbf{s} := [\mathbf{s}_1^T \ \mathbf{s}_2^T]^T \tag{6.24}$$

we have $\mathbf{q} = C\mathbf{f}$ and

$$y = \mathbf{s}^T \mathbf{q} \tag{6.25}$$

The update equation (6.22) with the expression (6.25) yields a conventional CMA cost function of $\mathbf{q}$.

$$J(\mathbf{q}) = (\|\mathbf{q}\|^2 - \gamma)^2 + \eta_s + \gamma^2 - m_4 \tag{6.26}$$

In the absence of noise, depending on the initialization of the equalizer $\mathbf{f}_1$ and $\mathbf{f}_2$, we have $\mathbf{q}_1 = \delta_i$ and $\mathbf{q}_2 = 0$ or vice versa. In short, the CM solutions match the ZF solutions in the absence of noise.

The cost function of the CPI equalizer in the system space can be expressed in term of $\mathbf{q}_1$ and $\mathbf{q}_2$, and this form provides intuitive interpretation of the CMA cross pole cancellation.

Lemma 8 *The FS-CMA CPI cost function can be expressed in terms of* $\mathbf{q}_1$ *and* $\mathbf{q}_2$*:*

$$J = \left(||\mathbf{q}_1||^2 + ||\mathbf{q}_2||^2 - 1\right)^2 + \eta_s I_{[||\mathbf{q}_1||,||\mathbf{q}_2||]} + \eta_s I_{\mathbf{q}_1} + \eta_s I_{\mathbf{q}_2} + \gamma^2 - m_4 \quad (6.27)$$

Proof: Recall that

$$J(\mathbf{q}) = (||\mathbf{q}||^2 - \gamma)^2 + \eta_s + \gamma^2 - m_4 \quad (6.28)$$

On the other hand,

$$||\mathbf{q}||^2 = \sum \mathbf{q}_i^2 = \sum {\mathbf{q}_1}_i^2 + \sum {\mathbf{q}_2}_i^2 = ||\mathbf{q}_1||^2 + ||\mathbf{q}_2||^2 \quad (6.29)$$

$$I_{\mathbf{q}} = ||\mathbf{q}||^4 - \sum \mathbf{q}_i^4 = (||\mathbf{q}_1||^2 + ||\mathbf{q}_2||^2)^2 - \sum {\mathbf{q}_1}_i^4 - \sum {\mathbf{q}_2}_i^4 \quad (6.30)$$

$$= 2||\mathbf{q}_1||^2||\mathbf{q}_2||^2 + ||\mathbf{q}_1||^4 - \sum {\mathbf{q}_1}_i^4 + ||\mathbf{q}_2||^4 - \sum {\mathbf{q}_2}_i^4 \quad (6.31)$$

$$= I_{[||\mathbf{q}_1||,||\mathbf{q}_2||]} + I_{\mathbf{q}_1} + I_{\mathbf{q}_2} \quad (6.32)$$

■

(6.27) can be interpreted as follows:

1) Ignoring $\eta_s I_{\mathbf{q}_1} + \eta_s I_{\mathbf{q}_2}$ terms, J is a CM cost function of $||\mathbf{q}_1||$ and $||\mathbf{q}_2||$. This implies

$$\begin{array}{l} ||\mathbf{q}_1|| = 1 \text{ and } ||\mathbf{q}_2|| = 0 \text{ or} \\ ||\mathbf{q}_1|| = 0 \text{ and } ||\mathbf{q}_2|| = 1 \end{array} \quad (6.33)$$

2) For $\mathbf{q}_2 = 0$ ($\mathbf{q}_1 = 0$), J is a conventional CMA cost function for $\mathbf{q}_1$ ($\mathbf{q}_2$). Thus we have $\mathbf{q}_1 = \delta_i$ and $\mathbf{q}_2 = 0$ or vice versa.

This interpretation indicates that the norms of $\mathbf{q}_1$ and $\mathbf{q}_2$ would be of primary concern in the initialization of CPI CMA, which reduces a multi-dimensional problem into a two dimensional problem.

6.3.2 Initialization Issue

From (6.26) we can conclude that the fractionally spaced CMA CPI equalizer inherits the robustness properties of the conventional FS-CM receiver. However, for the blind CPI equalizer the reliability of the acquisition of the desired signal is a new important issue: how one can acquire the desired signal, and how reliable (or robust) is the acquisition technique.

For the CMA CPI equalizer, the acquisition problem is reduced to the choice of a system delay from the system response $\mathbf{q} = [\mathbf{q}_1^T \ \mathbf{q}_2^T]^T$. A conventionally used acquisition method is the generalized version of the single spike initialization, i.e, $\mathbf{f}_1$ is set to a spike and $\mathbf{f}_2$ is set to zero in order to obtain $\mathbf{s}_1$. This method seems reasonable especially when the cross channel magnitude is small, i.e., the singular values of C_{12} and C_{21} are small. For such C with small C_{12} and C_{21}, the regions of convergence can be approximated by the exponential hyper-cone rotated in $\mathbf{q}_1$ space and $\mathbf{q}_2$ space separately. However, the analytical approach to the reliability of this initialization technique requires detailed information on the channel structure when the cross channel power increases. For this reason the reliability of the spike initialization of CMA CPI has not been resolved and remains an open question. We conclude this section by providing an example suggesting that under certain conditions the spike initialization is quite robust.

Example 12 Let us consider the simplest model of CPI.

$$C = \begin{pmatrix} 1 & \alpha \\ \alpha & 1 \end{pmatrix} \tag{6.34}$$

where $\alpha < 1$. Then we have

$$\begin{pmatrix} \mathbf{q}_1 \\ \mathbf{q}_2 \end{pmatrix} = \begin{pmatrix} 1 & \alpha \\ \alpha & 1 \end{pmatrix} \begin{pmatrix} \mathbf{f}_1 \\ \mathbf{f}_2 \end{pmatrix} \tag{6.35}$$

Notice that α roughly represents the cross-pole interference power. Since $\det C = 1-\alpha^2$, as $\alpha \to 1$ (as cross-pole interference power increases) the condition number of C increases. We will examine the ROCs for the single spike initialization as $\alpha \to 1$.

The regions of convergence of CMA for $\mathbf{q}_1$ and $\mathbf{q}_2$ are equally divided hyper-cones (Figure 6.4-a) and those for $\mathbf{f}_1$ and $\mathbf{f}_2$ are characterized by the singular decomposition of $\bar{C}^{-1}$

$$\begin{pmatrix} 1 & \alpha \\ \alpha & 1 \end{pmatrix}^{-1} = \begin{pmatrix} \cos(\frac{\pi}{4}) & \sin(\frac{\pi}{4}) \\ -\sin(\frac{\pi}{4}) & \cos(\frac{\pi}{4}) \end{pmatrix} \begin{pmatrix} \frac{1}{1+\alpha} & 0 \\ 0 & \frac{1}{1-\alpha} \end{pmatrix} \begin{pmatrix} \cos(\frac{\pi}{4}) & -\sin(\frac{\pi}{4}) \\ \sin(\frac{\pi}{4}) & \cos(\frac{\pi}{4}) \end{pmatrix} \tag{6.36}$$

The cost function is stretched by $\frac{1}{1-\alpha}$ in the $x+y$ direction and shrunk by $\frac{1}{1+\alpha}$ in the $x-y$ direction, and thus the noise gain of the equalizer ($\mathbf{f}_k$) increases. However, the symmetry of $\bar{C}^{-1}$ keeps the regions of convergence unchanged (Figure 6.4). This result implies that the single spike initialization ($\mathbf{f}_1 = 1$ and $\mathbf{f}_2 = 0$) is still reliable, as the cross-pole interference power increases. Furthermore, from the behavior of $\frac{1}{1-\alpha}$ as $\alpha \to 1$, the FS-CMA CPI equalizer shows remarkable robustness in terms of bit error rate (BER) performance. Notice that in Figure 6.5 the BER is uniformly under 10^{-5} until about 10dB cross power ratio. Although our analysis

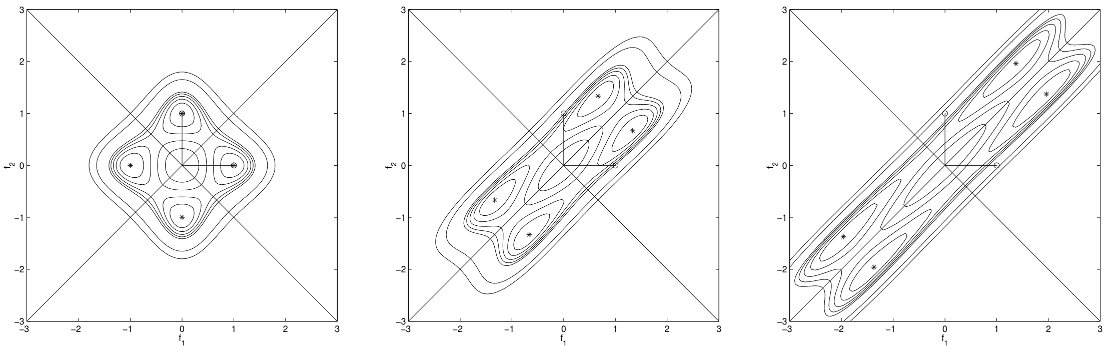

a) $\alpha = 0$ b) $\alpha = 0.5$ c) $\alpha = 0.7$

Figure 6.4: Regions of convergence for $\mathbf{f}_1$ and $\mathbf{f}_2$

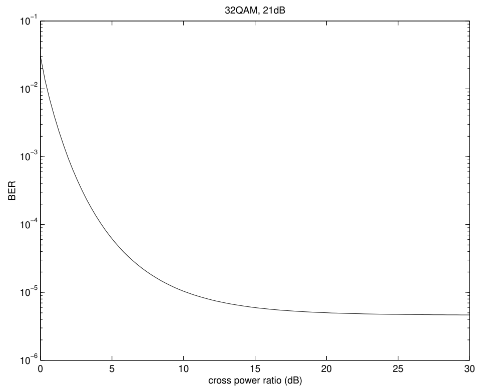

Figure 6.5: BER and cross power ratio α (32 QAM at 21 dB noise) from (6.35)

was performed under the assumption of a noise-free channel, the above plot can be used to explain the experimentally obtained result in [35]

Chapter 7

Conclusion

In this thesis we have investigated the multimodal structure of the Constant Modulus Algorithm applied to blind equalization and blind cross-pole interference rejection. First, we have characterized the regions of convergence of the CM solutions in the absence of noise by using a differential geometrical approach. Second, the location of the CM solutions in the presence of noise has been studied. We have presented the trade-off relation between noise gain and ISI reduction, and shown that most of the bad CM solutions can disappear. This analysis is made possible by decoupling the CMA cost function into a function of parameter norm and a measure of ISI in the system space. Finally, we have formulated the cross-pole interference cancellation problem in the fractionally spaced setting, and developed the ZF and the MMSE solutions as well as the CM solutions.

Bibliography

[1] P. A. Bello, "Characterization of Randomly Time-Invariant Linear Channels," *IEEE Transactions on Communications Systems*, vol. CS-11, pp. 360-393, Dec. 1963.

[2] A. Benveniste, M. Goursat, and G. Ruget, "Robust Identification of a Non-minimum Phase System: Blind Adjustment of a Linear Equalizer in Data Communications," *IEEE Trans. on Automat. Contr.*, vol. AC-25, no. 3, Jun. 1980.

[3] W. M. Boothby, *An Introduction to Differentiable Manifolds and Riemanian Geometry*, Academic Press, Inc., 1986.

[4] W. Chung and J. P. LeBlanc, "The local minima of fractionally-spaced CMA blind equalizer cost function in the presence of channel noise," *International Conference on Acoustics, Speech and Signal Processing*, Seattle, WA, pp3345-3350, May 1998.

[5] W. Chung, J. R. Treicher, and C. R. Johnson, Jr., "Blind Adaptive Cross-Pole Interference Cancellation Using Fractionally-Spaced CMA," *Allerton Conference*, Monticello, IL, 23-25 Sep 1998.

[6] W. Chung and C. R. Johnson, Jr., "Characterization of the Regions of Convergence of CMA Adaptive Blind Fractionally Spaced Equalizer," *Asilomar Conference on Signals, Systems and Computers*, Pacific Grove, CA, Nov. 1998.

[7] I. Fijalkow, A. Touzni, and J. R. Treichler, "Fractionally spaced equalization using CMA: robustness to channel noise and lack of disparity," *IEEE transactions on Signal Processing*, vol. 45, no.1 pp. 55-66, Jan. 1997.

[8] R. D. Giltin and S. B. Weinstein, "On the Required Tap Weight Precision for Digitally-Implemented Adaptive Equalizers," *Bell Systems Technical Journal*, Vol. 58, No 2, pp.302-321, Feb. 1979.

[9] R. D. Giltin and S. B. Weinstein, "Fractionally-Spaced Equalization: An improved Digital Transversal Equalizer," *Bell Systems Technical Journal*, Vol. 60, No 2, pp.275-296, Feb. 1981.

[10] R. D. Giltin, J. F. Hays, and S. B. Weinstein, *Data Communication Principles*, New York: Plenum Press, 1992.

[11] D. N. Godard, "Self-Recovering Equalization and Carrier Tracking in Two-Dimensional Data Communication Systems," *IEEE Transactions on Communications*, vol. 28, no. 11, pp. 1867-1875, Oct. 1980.

[12] M. Gu and L. Tong, "Geometrical characterization of Constant Modulus Receivers," *In Proc. 30th Conf. Information Sciences and Systems*, Princeton, NJ., Mar. 1998.

[13] S. Haykin, *Adaptive Filter Theory*, Prentice Hall, third edition, 1991.

[14] C. R. Johnson, Jr., H. J. Lee, J. P. LeBlanc, T. J. Endres, et al., "On Fractionally-Spaced Equalizer Design for Digital Microwave Radio Channels," *Proc. Asilomar Conference on Signals, Systems and Computers*, Pacific Grove, CA, pp. 290-294, Oct. 1995.

[15] C. R. Johnson, Jr. and B. D. O. Anderson, "Godard Blind Equalizer Error Surface Characteristics: White, Zero-Mean, Binary Case," *International Journal of Adaptive Control & Signal Processing*, vol. 9, pp. 301-324, July-August 1995.

[16] C. R. Johnson, Jr., P. .B. Schniter, T. S. Endres, J. M. Behm, D. R. Brown, and R. A. Casas, "Blind Equalization Using the Constant Modulus Criterion: A Review," *Proc. IEEE*, vol.86 no 10. Oct. 1998.

[17] T. Kailath, *Linear Systems*, Prentice Hall, 1980.

[18] S. Lambotharan, J. Chambers, and C. R. Johnson, Jr., "Attraction of Saddles and Slow Convergence in CMA Adaptation," *Signal Processing*, vol. 55, no.2, pp 335-340, June 1997.

[19] P. Lancaster and M. Tismenetsky, *The Theory of Matrices*, Academic Press, 1985.

[20] J. P. LeBlanc, "Effects of Source Distributions and Correlation on Fractionally Spaced Blind Constant Modulus Algorithm Equalizers," *Ph.D. Dissertation*, Cornell University, Ithaca, NY, August 1995.

[21] J. P. Leblanc and C. R. Johnson, Jr., "Global CMA Error Surface Characteristics, Source Statistics Effects: Polytopes and Manifolds," 13^{th} *Int. Conf. on DSP*, (Santorini, Greece) Jul. 1997.

[22] E. A. Lee and D. G. Messerschmitt, *Digital Communication*, Kluwer Academic Publishers, 1994.

[23] Y. Li and Z. Ding, "Global Convergence of fractionally spaced godard (CMA) adaptive equalizers," *IEEE transactions on Signal Processing*, vol. 44, no.4 pp. 818-26, Apr. 1996.

[24] J. Namiki and S. Takahara, "Adaptive receiver for cross-polarized digital transmission," *Proc. ICC*, June 1982, pp.46.31-46.35.

[25] L. Perko, *Differential Equations and Dynamical Systems*, Springer-Verlag, 1996.

[26] P. Schniter and C. Richard Johnson, Jr., "Minimum-Entropy Blind Acquisition/Equalization for Uplink DS-CDMA," *Allerton Conference*, 1998 - Monticello, IL, 23-25 Sep 1998.

[27] J. G. Proakis, *Digital Communications*, McGraw Hill, second edition, 1989.

[28] Z. Reznic, C. R. Johnson, Jr., and F. L. Victoria, "Frequency Domain Interpretation of LMS Convergence of a Fractionally Spaced Equalizer," *IEEE Signal Processng Letters*, vol. 3. No. 7 July 1996, pp. 206-208.

[29] J. Salz, "Data transmission over cross-coupled linear channels," *AT&T Technical Journal*, vol. 64, No. 6. July-August 1985, pp. 1147-1160.

[30] G. B. Thomas Jr. and R. L. Finney, *Calculus and Analytic Geometry*, Addison-Wesley, 1988.

[31] L. Tong, G. Xu, and T. Kailath, "A New Approach to Blind Identification and Equalization of Multipath Channels," *Proc. Asilomar Conference on Signals, Systems and Computers*, Pacific Grove, CA, pp. 856-860, Nov. 1991.

[32] J.R. Treichler and B. G. Agee, "A New Approach to Multipath Correction of Constant Modulus Signals," *IEEE Transactions on Acoustics, Speech, and Signal Processing*, vol. ASSP-31, no. 2, pp. 459-472, April 1983.

[33] J.R. Treichler and M.G. Larimore, "New processing techniques based on the constant modulus adaptive alogrithm," *IEEE Transactions on Acoustics, Speech, and Signal Processing*, vol. ASSP-33, No. 2, April 1985, pp. 420-431.

[34] J. R. Treichler, I. Fijalkow, and C. R. Johnson, Jr., "Fractionally spaced equalizers: How long should they be?," in *IEEE Signal Processing Mag.*, vol. 13, no. 3, pp. 65-81, May 1996.

[35] J.R. Treichler, J. Bohanon, M. Larimore, G. Collins, V. Wolff, C.R. Johnson Jr., and S.L. Wood, "Blind separation and combination of high-rate digital QAM radio signals," *Proc. 8th IEEE Digital Signal Processing Workshop*, Bryce, UT, August 1998.

[36] G. Ungerboeck, "Fractional Tap-Spacing Equalizer and Consequences for Clock Recovery in Data Modems," *IEEE Transactions on Communications*, vol. COM-24, no. 8, pp. 856-864, Aug. 1976.

[37] H.H. Zeng, L. Tong, and C. R. Johnson, Jr., "Relationships between the constant modulus and Wiener receivers," *IEEE Trans. Info. Theory*vol. 44, no. 4, pp 1523-38, July 1998